Excitations in Quantum Crystals
(A Survey of NMR Experiments in Solid Helium)

R. A. GUYER

Department of Physics and Astronomy, University of Massachusetts, Amherst, Massachusetts 01002

R. C. RICHARDSON*

Department of Physics, Cornell University, Ithaca, New York 14850

L. I. ZANE

Department of Physics, Duke University, Durham, North Carolina 27706

This article gives a systematic review of the many NMR experiments in solid helium to date, emphasizing the viewpoint that the results may be interpreted primarily in terms of the effects of three fundamental excitations in the solid: the vacancy waves; the ^{3}He tunneling interaction or exchange; and the ^{3}He–^{4}He tunneling interaction or mass fluctuation waves.

CONTENTS

* Present Address, Physics Department Colorado State Univ., Ft. Collins, Colorado.

1. INTRODUCTION

A quantum solid is one in which the zero-point motion of the atoms about the equilibrium lattice sites is a large fraction of the near-neighbor distance. This large zero-point motion has three important consequences (e.g., Guyer, 1969):

(a) Neighboring atoms in the lattice encounter one another away from their respective lattice sites at distances comparable with the hard core radius.

(b) An atom visits a large region of space in the vicinity of its lattice site. The small parameter of conventional lattice dynamics (rms displacement/near-neighbor distance) is not small so that there is large anharmonicity.

(c) Neighboring atoms tunnel around one another and exchange lattice sites.

The difficulties caused by an atom's visit to a relatively large region of space near its lattice site or its encounters with its near neighbors at the hard-core radius have a significant effect on how one does a theory of quantum crystals. But, the aggregate of conventional thermostatic and thermodynamic experiments on the quantum crystals exhibit few remarkable or unusual features that are a consequence of large anharmonicity or close approach (Guyer, 1969).

However, the third consequence of the large zero-point motion of the atoms in a quantum crystal has important experimental implications. There is a finite overlap between the wavefunction of an atom localized near lattice site 1 and the wavefunction for an atom localized near lattice site 2, a near neighbor site of 1. Because of this overlap, the atoms can tunnel about one another and change place. In solid ^{3}He, the atoms are fermions (there is one unpaired nuclear spin) so there is a nuclear exchange process due to the finite overlap. The energies associated with the exchange process are on the order of 1 mK. Thus this process is unimportant

to the ground state properties that are seen in most of the thermostatic and thermodynamic measurements at 1 K. But the particles which make up the solid have mobility through it, by virtue of quantum mechanical tunneling, on a time scale that is easily observable. These particle motions give rise to a wide variety of phenomena, e.g. (a) the tunneling excitations, (b) vacancy wave excitations, (c) mass fluctuation waves, (d) the coupling of the particle motions manifested in these excitations to one another and to the phonons, etc. Because ^{3}He atoms are tagged by their nuclear spin, it is possible to observe the particle motion phenomena in nuclear magnetic resonance (NMR) experiments on the quantum crystals.

The purpose of this paper is to present a careful survey of (a) the theory of particle motion phenomena in quantum crystals, (b) the NMR experiments on these systems which see particle motion phenomena, and (c) the correlation of theory and experiment. We will deal with pure ^{3}He, ^{3}He with small concentrations of ^{4}He, ^{4}He with small concentrations of ^{3}He, and nondilute mixtures. Our approach to the theory of these systems will be principally phenomenological. For those phenomena whose description is new in this paper we will go into somewhat greater detail although we will maintain a phenomenological posture throughout. It is our intention here to explicate the physics of particle motion phenomena as seen in NMR experiments, and to suggest the direction of further theoretical and experimental work.

This paper is organized as shown in the Table of Contents. A word about that organization. For each kind of system (pure ^{3}He, dilute mixtures, and nondilute mixtures) we discuss in order: (a) the excitations in the system, (b) the expectations for NMR experiments on the system, and (c) the results of NMR experiments on the system. A serious attempt is made to be descriptive in dealing with most of the presentation. Therefore, the major portion of the detailed calculations that are called for are found in the Appendices. We treat new and old topics with uniform depth so that this article will serve as more than a guide to the literature.

The physical picture of the tunneling motions that interest us emerges toward the end of the substantial progress that has been made in the theory of quantum crystals in the past six years. Let us recount that progress. The theoretical description of a quantum crystal must account for:

(a) the short-range correlations in the relative motion of a pair of neighboring particles that approach one another at hard core distances; and

(b) the motion of the particles over a large region of space in the vicinity of their lattice site where they see many derivatives of the interaction potential.

The short-range correlation problem has been dealt with by Nosanow and co-workers (Nosanow, 1966; Hetherington, 1967), Brueckner and co-workers (1965, 1969), and Krumhansl and Wu (1968) using a Jastrow wavefunction within the framework of a variational calculation of the ground-state energy; and by Hansen and Levesque (1968) using molecular dynamics. The outcome of these calculations is that a pair of atoms in a quantum crystal interact with one another through an effective interaction which is the product of the bare interaction and correlation function for the pair, i.e., approximately the t-matrix result. This effective interaction has a softened hard core for which short-range correlations are relatively unimportant.

The long-range correlation problem (phonons) has been dealt with by Koehler (1966, 1967), Horner (1967) and others (see the review b, Werthamer, 1969) using "self-consistent" phonons; and by Brenig (1963) and Fredkin and Werthamer (1965) as the RPA response of a driven Hartree system. The outcome of these calculations is that for the purpose of finding the phonons, the spring constant of the interaction between a pair of particles in a quantum solid is given by the second derivative of the *bare interaction* between the pair, averaged over their relative motion. The phonons in the solid are the collective modes for particles coupled by these springs. Finally, in detailed numerical calculations for the phonons in a quantum solid, the *bare interaction* called for in the phonon theories is replaced by the t matrix. The phonons are taken to be the collective modes for pairs of particles coupled by springs whose spring constant is the second derivative of the t matrix averaged over the relative motion of the pair.

A large body of computational results (principally on solid helium) have been generated by Nosanow and co-workers (Nosanow, 1966; Hetherington, 1967), Werthamer and co-workers (de Wette, 1967; Gillis, 1968), and Koehler (1966, 1967) for the ground state thermostatic properties [energy, E; pressure, P; bulk modulus, β; phonon spectrum, $\omega(q)$, etc]. These results are in reasonable qualitative agreement with experiment.

Recently Iwamoto and Namaizawa (1966), Sarkissian (1969), and Guyer (1968b) have developed a theory of quantum solids using what are essentially the techniques of the theory of nuclear matter. This approach has the advantage of yielding the t matrix and phonons within the same computational framework. Detailed calculations of the ground state properties of solid helium within the framework of this theory yield lowering of the ground state from 3 K/particle to 1 K/particle, and a pressure dependence of E and β in excellent agreement with experiment. Aside from conceptual problems which are clarified by this approach, its most important contribution is to show that a simple but careful treatment of the short-range correlation part of the problem yields substantial improvement in the quantitative features of the theory.

Guyer and Zane (1969) have extended the treatment

of the ground state problem due to Guyer (1968b) and Sarkissian (1969) to include the exchange process. Calculations with their theory of exchange yields results in good qualitative agreement with experiment. See also Hetherington, Mullin, and Nosanow (1967) and Nosanow and Varma (1968). More important than this agreement between theory and experiment, is the physical picture which results from this theory. Guyer and Zane show that the particle motions which lead to the nuclear exchange process are embodied in the tunneling motions that are represented by a Hubbard Hamiltonian[1] (Herring, 1966). It is with regard to these tunneling motions that the quantum crystals (solid ^{3}He, ^{4}He, and mixtures) are truly unique. The physics we are discussing in this paper is a consequence of the tunneling motion.

2. BACKGROUND (NMR)

A nuclear magnetic resonance experiment on a sample containing nuclear spins begins by placing it in an external magnetic field $\mathbf{H}_0$.[2] Each of the spins in the sample precesses about the magnetic field with the Larmor frequency

$$\omega_0 = \gamma H_0, \qquad (2.1)$$

where $\gamma = 2.04 \times 10^4$ rad/G·sec for ^{3}He. After the spins have come to thermal equilibrium in the Larmor field (i.e., for spin 1/2 the population of the two spin states is $P_+/P_- = \exp +\beta\hbar\gamma H_0$, where $\beta^{-1} = k_B T$, and T is the ambient temperature of the sample) a radio frequency magnetic field, $\mathbf{H}_1(t)$, in the plane perpendicular to $\mathbf{H}_0$ is turned on at frequency $\omega = \omega_0$ for a short period of time. Energy is dumped into the spin system by the rf field, and the spin system is driven away from equilibrium; $P_+/P_- < \exp +\beta\hbar\gamma H_0$. The rf field is turned off, and as the spin system returns to equilibrium various experiments are done to observe it.

In a T_1 *measurement*, the z component of the magnetization is studied as a function of time. If the spins come to equilibrium among themselves in a time short compared to the time required for the excess energy in the spin system to decay away, then, as the spin system returns to equilibrium, it can be described by a spin temperature, and decay of the excess energy or magnetization corresponds to a decay of the spin temperature. At $\beta_S^{-1} = k_B T_S \gg \hbar\gamma H_0$, we have

$$M_z = \sum_{i=1}^N \langle\mu_i\rangle \approx N\mu^2 H_0 \beta_S$$

and

$$(d/dt)M_z(t) = N\mu^2 H_0 (d\beta_S/dt). \qquad (2.2)$$

Thus a T_1 measurement is a measurement of the inverse temperature β_S as a function of time.

More precisely, a T_1 measurement is a measurement of the motion of the total spin of the system among the manifold of energy levels due to $\mathbf{H}_0$; this motion is described by a temperature. The Hamiltonian describing the spins in $\mathbf{H}_0$ is the Zeeman Hamiltonian given by

$$\mathcal{H}_z = -\mathbf{H}_0 \cdot \sum_{i=1}^N \boldsymbol{\mu}_i. \qquad (2.3)$$

The manifold of energy levels for N spins 1/2 in $\mathbf{H}_0$ is the manifold of Zeeman energy levels or the Zeeman system. The temperature of the Zeeman system changes as M_z changes. The spins which add up to give M_z are precessing at the Larmor frequency ω_0. One of these spins will flip, contributing to the decay of M_z, if it sees a local magnetic field which is varying at the Larmor frequency ω_0. By local field we mean a field of microscopic origin at the site of the spin in question, $\mathbf{H}_l(\mathbf{R})$, where $\mathbf{R}$ is the lattice site of the spin.

A local field occurs because of the dipolar interaction between the spin at $\mathbf{R}$ and its neighbors, i.e., because of $\mathbf{H}_l(\mathbf{R}, t)$

$$= \sum_{R' \neq R} \left(\frac{\boldsymbol{\mu}_{R'}(t)}{|\mathbf{R} - \mathbf{R}'|^3} - \frac{3(\mathbf{R} - \mathbf{R}')[\boldsymbol{\mu}_{R'}(t) \cdot (\mathbf{R} - \mathbf{R}')]}{|\mathbf{R} - \mathbf{R}'|^5} \right), \qquad (2.4)$$

where the $\mathbf{R}'$ are the positions of the *field particles*. See Fig. 1. We refer to the neighbors of the spin at $\mathbf{R}$ as the field particles of $\mathbf{R}$, they are the particles which cause the local field seen by the spin at $\mathbf{R}$. We write this local field as a Fourier transform

$$\mathbf{H}_l(\mathbf{R}, t) = \int d\omega \mathbf{H}_l(\mathbf{R}, \omega) \exp(-i\omega t). \qquad (2.5)$$

If this local field has a Fourier component in the transverse plane at frequency ω_0, the spin at $\mathbf{R}$ (which is precessing at ω_0) sees this component of the local field precessing with it. The spin sees $\mathbf{H}_l(\mathbf{R}, \omega_0)$ as a static field and it undergoes an additional precession about this field just as it precessed about the rf field above which was tuned to look to it like a static field. The spin at $\mathbf{R}$ "flips" due to the motion of the field particles at ω_0 manifested in $\mathbf{H}_l(\mathbf{R}, \omega_0)$, and contributes to the decay of M_z.

We have made this qualitative argument to suggest the physics we are going to see in a T_1 measurement. *Those motions of the particles in the system which give rise to fluctuations in $\mathbf{H}_l(R, t)$ at frequency ω_0 will be observable in a T_1 measurement.*

Suppose a system of excitations exists in a solid which gives rise to the motions of the field particles which lead to the decay of M_z and an attendant energy loss from the Zeeman system. The energy which the Zeeman system is losing is transferred from it to the system of excitations. The dipolar field is the agency by which this

---

[1] A cell model Hamiltonian was first used to look at solid helium by Gersch and co-workers (Fernandez, 1966). Subsequently Hamiltonians of this kind have come to be called Hubbard Hamiltonians.

[2] We discuss NMR from a pulse point of view in this section. A more general discussion is found in the excellent book by Abragam (1961).

transfer is accomplished. The energy dumped from the Zeeman system into the excitation system will raise the temperature of the excitation system unless the excitation system is tightly coupled to the reservoir in which the experimental sample sits. In the typical NMR experiment, the excitation system is tightly coupled to the reservoir by some means. However, it can happen that at low temperatures the excitation system will become uncoupled from the reservoir. The energy dumped from the Zeeman system to the excitation system will bring the two systems to a common equilibrium temperature above the reservoir temperature.
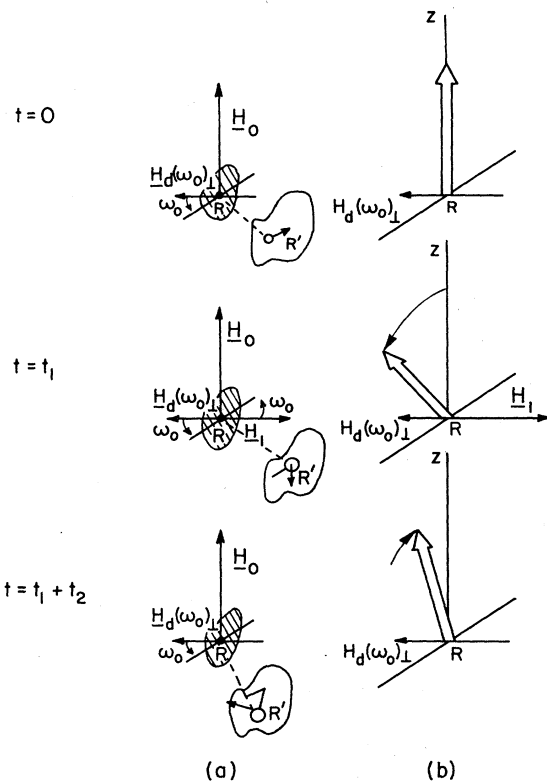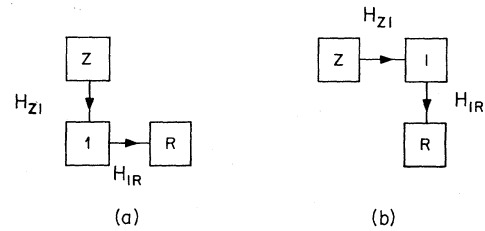

(a) (b)

FIG. 2. Relaxation topologies. In the simplest case, relaxation of the rf energy put into the Zeeman system is accomplished by coupling the Zeeman system to the particle motions, the 1-system, and having the excitations which represent the particle motions be tightly coupled to the reservoir, (a). If it happens that the particle motions are weakly coupled to the reservoir, then, they and the Zeeman system will come to mutual equilibrium on a fast time scale and decay together to the reservoir through a mechanism which couples the 1-system to the reservoir.

Then, on a longer time scale, the coupled systems will decay together to the temperature of the reservoir. See Fig. 2. The mechanism of this long time decay will be the coupling of the excitation system to the reservoir. For example, if the field particle motion is due to the vacancy wave excitations, then, the vacancy waves couple to the phonons which in turn easily transfer the energy from the sample to the reservoir. The topology of energy relaxation corresponds to Fig. 2(b). The long time which characterizes the decay of the coupled Zeeman–excitation systems may depend upon the characteristic time for the excitation systems to couple to one another or to the reservoir (e.g. the vacancy wave–phonon coupling) and on the relative specific heats of the excitation systems. Thus we expect that at low temperatures, a T_1 measurement will contain information about (a) the specific heat of the excitation systems giving rise to the particle motion, and (b) the characteristic time for the coupling of these excitations to one another and to the reservoir.

In a T_2 *measurement*, the transverse (x, y) component of the magnetization is studied as a function of time. The characteristic time for the decay of the transverse magnetization is a measure of the time required for the spins to come to equilibrium among themselves. The magnetization vector can be tipped from along H_0 into the transverse plane by application of an rf magnetic field of appropriate duration; i.e. a 90° pulse. See Fig. 3. Once in the transverse plane (for example, along the x axis at $t=0$) the individual spins move in the plane relative to one another due to (a) precession about the $\omega=0$ Fourier component of the z component of the local field, $H_l(R, \omega=0)_z$, and (b) precession about the $\omega=\omega_0$ component of the local field in the transverse direction, $H_l(R, \omega_0)_\perp$. If the local field at R is time independent, the motion of the spin at R is reversible. This reversibility is demonstrated by the observation of the recovery of M at time $2t_1$ to its value at time 0 after the application of a 180° pulse at time t_1. See Fig. 3. If the time evolution of the local field is reversible after turning all of the spins by 180° at t_1,

(a) (b)

FIG. 1. A T_1 Experiment. In Column (a) we show the magnetic fields seen in the laboratory by the spins in the region of space R at various times in a T_1 experiment. In Column (b) we show the response of the magnetization of the spins in R to the various magnetic fields shown in Column (a). In Column (b) we are in a frame of reference rotating at ω_0 so that the rotating fields in Column (a) have become static fields. At $t=0$, the spins see H_0 which they precess around at frequency $\omega_0=\gamma H_0$. At $t=0$ they also see a relatively weak dipolar field due to the motion of the field particles of R, e.g., the particles in the region of space R'; $\gamma H_0 \gg \gamma H_1 \gg \gamma H_d(\omega_0)$. At $t=t_1$, an rf field, H_1, is turned on. This field is perpendicular to H_0 and precesses in the laboratory frame at frequency ω_0. The spins precessing about H_0 at frequency ω_0 see H_1 as a static field and precess about it. If H_1 is on for a time t_{90} given by $\gamma H_1 t_{90}=\pi/2$, the spins precess into the transverse plane, $M_z(t_1+t_{90})=0$. After the rf field is turned off, e.g. at $t=t_1+t_2$, $t_2>t_{90}$, the spins, precessing at frequency ω_0, see only the transverse component of the dipolar field at frequency ω_0, This internal magnetic field drives the spins back toward the z axis. (In this figure we have used regions of space instead of individual lattice sites so that we could use a classical picture of the motion of the magnetization.)
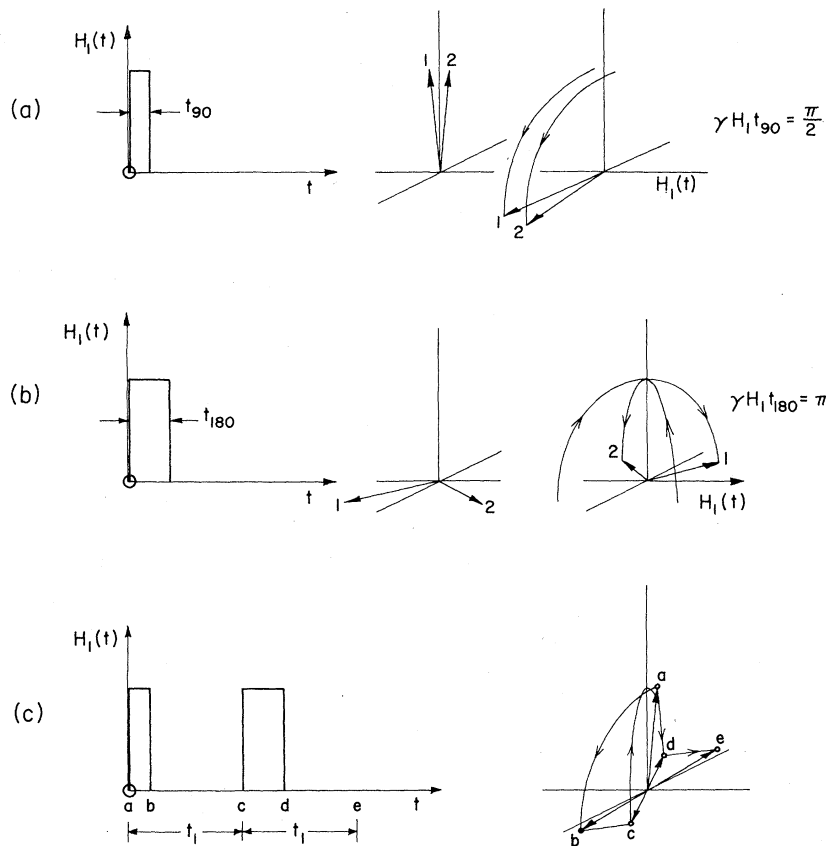
FIG. 3. A T_2 experiment. A 90° pulse is an rf field of sufficient duration that the z component of the magnetization goes to zero as shown in (a). When the magnetization is in the transverse plane, following a 90° pulse, a 180° pulse is an rf field of sufficient duration to flip the component of the magnetization perpendicular to H_1 by 180° as shown in (b). The full pulse sequence for a T_2 experiment is shown in (c). For a classical spin: at $t=0$ the spin points upward, at an application of a 90° pulse it turns into the transverse plane, $a{\to}b$; the motion from b to c is due to the local field, e.g., $H_1(0)_z$; at t_1 a 180° pulse flips the spin by 180°, $c{\to}d$; if the local field flips by 180° when the spin flips by 180°, then the spin returns to e at time $2t_1$ to form an echo.

we have $M(2t_1)$ equal to $M(0)$. The spin motion is reversible; there is no thermalization of the spins. The transverse component of the magnetization will not return to $M(0)$ at time $2t_1$ following a 180° pulse at t_1 if the local field on each particle does not reverse its motion in time when all of the spins are turned by 180°. See Fig. 4. Those motions of the field particles around R which give rise to an irreversible time evolution of the local field at R, and consequently an irreversible precession of the spin at R, are motions which transfer energy between the field particles and the spin at R. Such motions bring about thermal equilibrium among the spins. Both the motions of the field particles at $\omega=\omega_0$, as well as their motions at $\omega\ll\omega_0$, contribute to the irreversible precession of the spin at R. Thus a T_2 measurement is a probe of (a) the low-frequency motion of the field particles, as well as (b) their motions at ω_0 which also appear in T_1.

In a conventional *diffusion* experiment, the Zeeman system of spins is examined by a T_2 pulse sequence (e.g., a 90° pulse at $t=0$ followed by a 180° pulse at time t_1) while sitting in an externally applied magnetic field gradient. If the particles are free to move from place to place in the field gradient due to a particle motion process, the transverse component of the magnetization will undergo an additional irreversible motion due to the diffusion of particles in the field gradient. Thus a diffusion experiment is a T_2 experiment in an externally applied magnetic field gradient. Such an experiment directly measures the diffusion constant of the spins. See Fig. 5.

In addition to the conventional diffusion experiments, there are energy diffusion experiments. In an *energy diffusion* experiment, the diffusion of the z component of magnetization is studied as a function of time. Such an experiment begins by placing the Zeeman system in a weak field gradient. This gradient is used only to see the spins in different parts of the sample; the Larmor frequency will be a function of position in the sample. Energy may be dumped into the spins at the center of the sample by turning on an rf field of frequency ω_0. Energy may be dumped into the spins on the left or right of the sample by using rf fields at $\omega_0\pm\Delta\omega$. Let us assume that the energy is put into the spins at the center of the sample and that this energy is strongly coupled to a particle motion excitation (e.g., the tunneling motion of the particles) on a time scale fast compared to T_1. Thus the Zeeman system and the excitation system in the vicinity of the center of the sample will share the rf energy and be "hot" compared

FIG. 4. Reversibility and irreversibility. In (a) we show: (1) the configuration of the local magnetic fields at the lattice site of five spins at the times t_{90}, t_1, t_1+t_{180}, and $2t_1$ (cf. Fig. 3) and, (2) the orientation in the transverse plane of each spin. Between $t=t_{90}$ and t_1, the spins "fan out" in response to their local field. At t_1+t_{90}, the spins have been flipped by 180°; so has the local field. At time $2t_1$, the local fields have returned to their configurations at $t=0$, except for a reversal of all signs. The motion of the local fields and spins is reversible in time. In (b) we show (1) the configuration of local magnetic fields and (2) the orientation of the spins as in (a). We note that the local magnetic fields do not return at $t=2t_1$ to the negative of their value at $t=0$. The local magnetic fields do not reverse their motion in time when the spins are turned over by 180°. Thus the spins do not reverse their motion in time. The component of the magnetization along the $-x$ axis is less at $2t_1$ when the motion of the spins is irreversible.
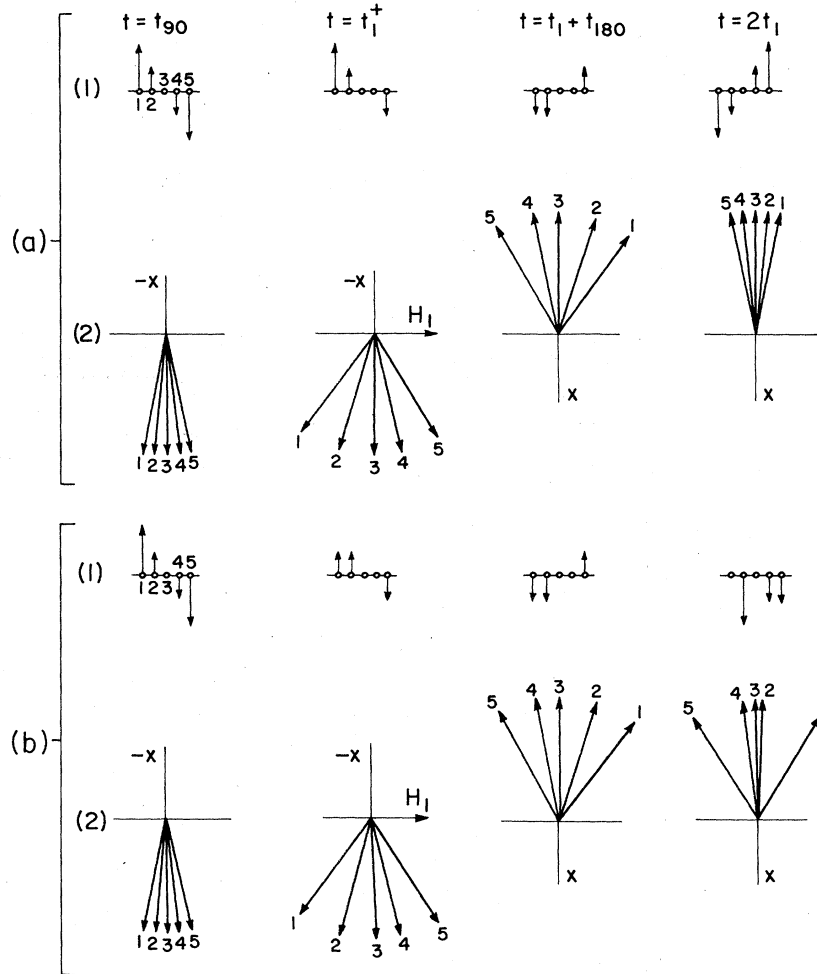
to the reservoir. Both the hot spins (Zeeman system) and the hot excitation system will diffuse through the sample. As they do so they keep up with one another because of their strong coupling. The diffusion of these coupled systems through the sample corresponds to a diffusion of the temperature or energy. It is measured by measuring $M_z(x, t)$. See Fig. 6.

3. EXCITATIONS IN PURE ³He

3.1 Excitations

Our understanding of the results of an NMR experiment on solid ³He will depend upon our understanding of the excitations that exist in the solid and the interactions which occur between them. This section is devoted to a discussion of the three kinds of excitations that are important in pure ³He. These excitations are the phonons, vacancy waves, and tunneling excitations.

Phonons. The phonons are the excitations in the solid which describe the small displacement motions of particles about their equilibrium lattice sites. These displacement motions are too small to contribute significantly to the motion of the field particles which are seen in a T_1 experiment (Abragam, 1961). However, the phonons play a crucial role in transferring energy from the other excitations (e.g., vacancy waves) to the reservoir. We do not discuss the phonons here in any detail[3]; the energy of the phonons, their specific heat, and energy constant are tabulated in Appendix D. When we have need to calculate the properties of the phonons we will use the formulae from this Appendix and the experimentally determined Debye temperature from Sec. 4. We will discuss the coupling between the various excitations after we have discussed each excitation in the necessary detail, thus we go on to the vacancy waves and the tunneling excitations.

---

[3] The theory of phonons in quantum crystals, a subject of considerable interest in its own right, has been recently reviewed by Werthamer (1969).
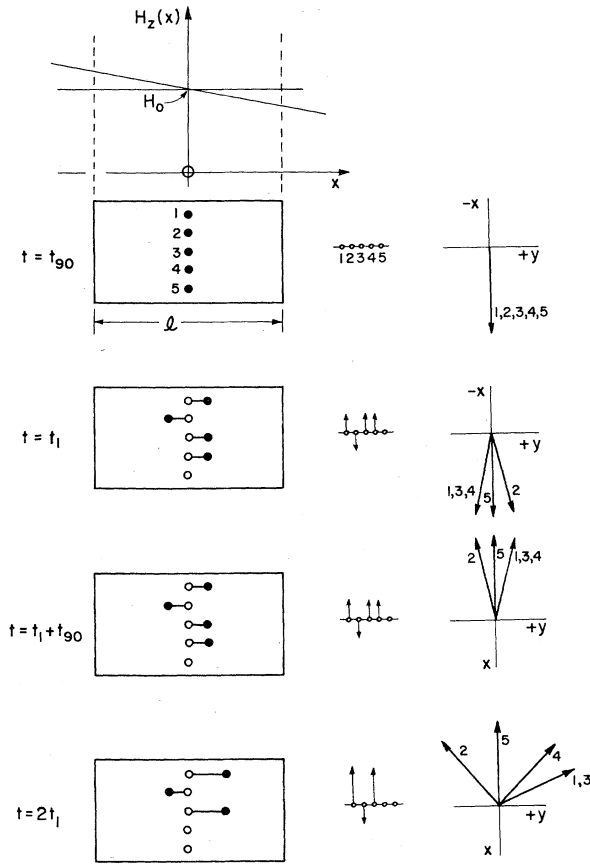
FIG. 5. A diffusion experiment. A gradient of the z component of the external field is placed on the system, $H_z(x) = H_0 - Gx$. Here we show the time evolution of five particles in the sample, and the time evolution of the spin of each particle. At $t = t_{90}$ the five particles are taken to be at the center of the sample. Their transverse magnetization in a co-ordinate system rotating at ω_0 is $5\mu_N$. Due to the particle motion excitations, the particles diffuse in space. Each particle sees a local field which is unique to its motion through the sample. Its spin moves relative to the $+x$ axis in a way which depends on the time averaged local field. If on the average the particle is to the left of $x=0$, it has seen a slightly higher field than H_0; it has precessed in the transverse plane slightly faster than the particle that remains at $x=0$. Its spin precesses to the right. See particle 2 at t_1. When the 180° pulse occurs, the local field reverses, but the gradient which is responsible for the motion we exhibit here does not. The particles continue to move by diffusion (irreversibly) in the gradient, and at $2t_1$ the magnetization along the $-x$ axis is considerably less than $5\mu_N$. Here we have shown only the degradation of $M_x(2t_1)$ due to motion in the external gradient. There is superposed on this decay an additional loss of magnetization that is due to the irreversibility of the time evolution of the local fields shown in Fig. 4.

The particle motions which are more drastic than those described by the phonons and which are observable in a T_1 measurement are embodied in the model particle motion Hamiltonian used by Gersch and Fernandez (1966), Guyer and Zane (1970), and Mullin (1971)

$$\mathcal{H}_{PM} = \sum_{R,\sigma} \epsilon(R) b_{R\sigma}{}^+ b_{R\sigma} + \sum_{RR',\sigma} t(RR') b_{R\sigma}{}^+ b_{R'\sigma}$$
$$+ \frac{1}{2} \sum_{R,\sigma\sigma'} \phi_0(R) b_{R\sigma}{}^+ b_{R\sigma'}{}^+ b_{R\sigma'} b_{R\sigma}, \quad (3.1)$$

where the operator $b_{R\sigma}{}^+$ creates a particle at R of spin σ in the ground state of a complete set of Wannier states. The energy $\epsilon(R)$ is a Hartree single-particle energy

$$\epsilon(R) = K(RR) + \frac{1}{2} \sum_{R''\sigma' \neq (R)\sigma'} V(RR, R''R'') \langle b_{R''\sigma'}{}^+ b_{R''\sigma'} \rangle, \quad (3.2)$$

where $K(RR)$ is the diagonal matrix element of the kinetic energy operator

$$K(RR') = \int d\mathbf{x}\, \phi_R{}^*(x) T(x) \phi_{R'}(x) \quad (3.3)$$

$[\phi_R(x)$ is the ground state Wannier function at lattice site $\mathbf{R}]$, $v(RR, R''R'')$ is the diagonal matrix element of the potential energy

$$v(RR', R''R''')$$
$$= \int d\mathbf{x}\int d\mathbf{x}'\, \phi_R{}^*(x) \phi_{R''}{}^*(x') v(x-x') \phi_{R'''}(x') \phi_{R'}(x),$$
$$(3.4)$$

$$t(RR') = K(RR') + \frac{1}{2} \sum_{R'',\sigma'} v(RR', R''R'') \langle b_{R''\sigma'}{}^+ b_{R''\sigma'} \rangle, \quad (3.5)$$
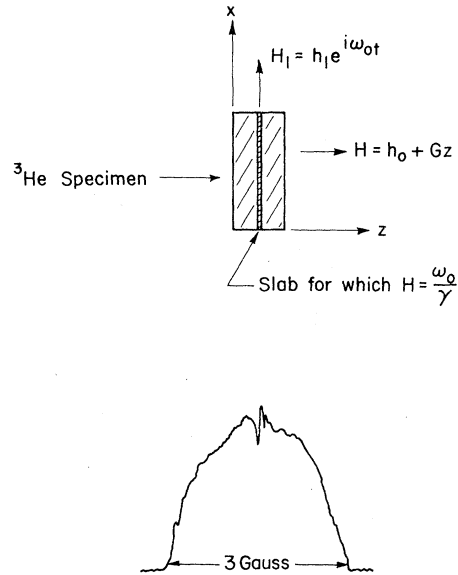
FIG. 6. Energy diffusion measurement. The specimen of solid ³He is placed in a static magnetic field H_0 with a uniform gradient $G = dH/dz$ in the z direction. Application of a strong rf signal, $h_1 \exp(i\omega_0 t)$, with the polarization of h_1 lying in the plane perpendicular to H_0, heats the spins in the thin slab of the specimen over which $H(z) = \omega_0/\gamma$. The energy of the Zeeman system is quickly transferred locally to the tunneling energy reservoir. The subsequent measurement of the resonance absorption signal using a much weaker rotating rf field h_1, reveals a resonance line with a "hole burned in it" corresponding to the signal from the portion of the specimen with locally higher spin temperatures. The specimen returns to thermal equilibrium through spatial diffusion of the energy in the tunneling reservoir. The rate of the energy diffusion is determined through studies of the time evolution of the hole in the absorption signal. [Hunt and Thompson (1968)].

FIG. 7. Vacancy wave excitations. The ground state of the lattice has one particle at each lattice site (a). A vacancy state is created by $b_R{}^+b_{R'}\times(1-\delta_{RR'})$ which removes a particle from R', and doubly occupies the lattice site at R (b). This vacancy state has two components, a hole at R' and a particle at R. Both components propagate due to $\mathfrak{IC}_{PM}$, as shown in (c) and (d).
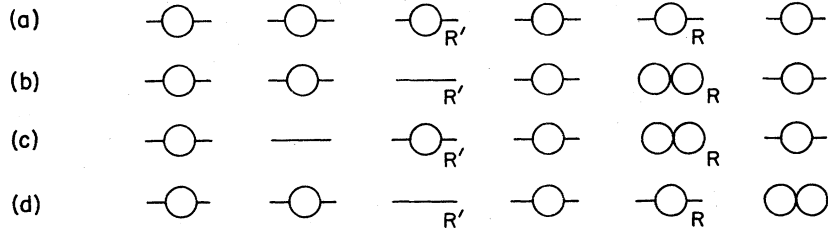
and $\phi_0(R)$ is a hard-core energy associated with the double occupation of a lattice site, $\phi_0(R) = v(RR, RR)$. It requires more than one state per lattice site to describe the small displacement motions at a lattice site which are manifested in the phonons.[4] Here we are interested only in the large displacements embodied in $\mathfrak{IC}_{PM}$. The first term in Eq. (3.1) gives the Hartree energy for the system, $E_H = N\epsilon_0(R)$. The second term in Eq. (3.1), called the tunneling term, leads to particle motion from lattice site R to R', and the third term is the hard core repulsion which works to inhibit this motion. There are two kinds of simple excitations in the system of particles described by $\mathfrak{IC}_{PM}$. These are the vacancy wave excitations and the tunneling excitations.

Vacancy Waves. We take the ground state of the system to be the state $|0\rangle$ corresponding to having one particle at each lattice site. Then, a vacancy is created by operating on the ground state with the vacancy creation operator $C_V{}^+(RR')$ given by

$$C_V{}^+(RR') = b_R{}^+b_{R'}(1-\delta_{RR'}), \qquad (3.6)$$

where for the purpose of discussing vacancies we ignore the spin index. This vacancy state has two components, a doubly occupied lattice site at R, and an empty lattice site at R'. See Fig. 7. It is conventional to put the doubly occupied lattice site on the surface and to look at the "hole" only (Hetherington, 1968). Both components of this vacancy state propagate through the crystal because of the tunneling term in $\mathfrak{IC}_{PM}$. We construct an operator for creation of a vacancy wave state thus

$$C_V{}^+(\mathbf{k}, \mathbf{k}')$$
$$= \sum_{RR'} \exp{(i\mathbf{k}\cdot\mathbf{R})} \exp{(-i\mathbf{k}'\cdot\mathbf{R}')}b_R{}^+b_{R'}(1-\delta_{RR'}).$$
$$(3.7)$$

Using the equation of motion method, we find

$$ih(\partial/\partial t)C_V{}^+(\mathbf{k}, \mathbf{k}') = [\phi_0+t(\mathbf{k})-t(\mathbf{k}')]C_V{}^+(k, k'),$$
$$(3.8)$$

where $t(\mathbf{k}) = \sum_{R'} t(RR') \exp{[i\mathbf{k}\cdot(\mathbf{R}-\mathbf{R}')]}$. The term $t(\mathbf{k})$ in Eq. (3.8) is due to the propagation of the doubly occupied lattice site, the "particle," and the term $t(\mathbf{k}')$ is due to the propagation of the empty side, the "hole." Now we take $t(RR') = -t$ for R' a near neighbor of R and zero otherwise; then for simple cubic geometry we have

$$t(k) = -2t(\cos{k_x\Delta} + \cos{k_y\Delta} + \cos{k_z\Delta}), \quad (3.9)$$

where Δ is the near neighbor distance. For simplicity we assume that the "particle" does not propagate, then the vacancy wave dispersion relation is simply

$$\hbar\omega_V(k) = \phi_0 + 2t(\cos{k_x\Delta} + \cos{k_y\Delta} + \cos{k_z\Delta}) \quad (3.10)$$

which is shown in Fig. 8. From the discussion in Sec. 4, Fig. 29(b), we have the estimate $t = 0.4$ K at $V = 20.0$ cm³/mole. At $V = 20.0$ cm³/mole, the crystal structure is bcc with each lattice site having eight near neighbors. The bandwidth for the vacancy waves is $\Delta\epsilon_V = 2z|t| = 6$ K. At the edge of the Brillouin zone we have $\hbar\omega(k_D) = \phi_0 - z|t|$, and at the zone center $\hbar\omega(0) = \phi_0 + z|t|$.[5] From the discussion in Sec. 4 we have the estimate $\phi \equiv \phi_0 - z|t| \approx 14.5$ K or $\phi_0 \approx 18$ K. Throughout this paper we use experimentally determined values of ϕ and we take the vacancy energy, specific heat, concentration etc., to be given in terms of these experimental constants. For example, the vacancy concentration is given by

$$x_V = \exp{(-\beta\phi)}. \qquad (3.11)$$

Formulae for other quantities of interest for the vacancies are found in Appendix D.

Tunneling Excitations. By the tunneling excitations we mean the excitations of the system associated with the particle motions which are usually referred to as exchange (Herring, 1968). We use the phrase tunneling excitations because the word exchange is ambiguous;

---

[4] A fundamental question in the theory of quantum crystals is that of the coupling between the phonons (small displacement motions) and the particle motions embodied in Eq. (3.1). The description of displacement motion in the vicinity of a lattice site requires more than one state per lattice site (Nosanow, 1965; Guyer, 1968a). The coupling of motion among low-lying states at a lattice site, to motion among states at different lattice sites gives rise to phonon–particle motion interactions. Recently McMahan and Nosanow (1970) produced a proof that these motions are independent. The earlier work of Nosanow and Varma (1968) also pertains to this point.

[5] The vacancy waves of our model are propagating in a homogeneous background like ⁴He. In ³He, the vacancy waves propagate in a spin disordered medium. The fact that the vacancy waves must disorder the ³He medium to move through it leads to a slight modification of the structure of the band; it leads to a major modification of the mobility and diffusion constant of the vacancies. These points are explicitly illustrated in the recent work of Brinkman and Rice (1970). We argue for the qualitative structure of the energy band, $\omega(k_D) < \omega(0)$, by noting that a vacancy wave excitation at $k \approx k_D$ corresponds to removal of a short-wave length density fluctuation. Mullin (1971) has pointed out that a vacancy is dressed by lattice distortion and may carry an effective positive mass along with itself. See also Footnote 8.
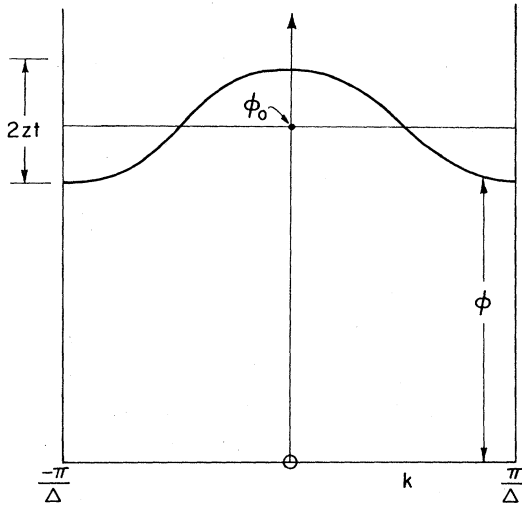
FIG. 8. Vacancy wave excitation spectrum. The vacancy wave excitation spectrum is like a "hole" spectrum in a semiconductor. The band edge is at $\phi_0 - zt$. This energy is identified with the experimentally measured excitation temperature, ϕ. The bandwidth is $2zt \approx 6K$, whereas the typical experiment is done at 2K. Thus the experimentally observed vacancy waves are near the band edge.

it suggests a process associated with antisymmetrizing wavefunctions for Fermions; it does not suggest the physical process involved as picturesquely as the word tunneling nor that the process may involve two ^{3}He atoms, a ^{3}He and a ^{4}He atom, or two ^{4}He atoms (Guyer and Zane, 1969; 1970).

In pure solid ^{3}He, the tunneling excitations are associated with the creation of a virtual vacancy state. They are given by the Hamiltonian

$$\mathcal{H}_T = \sum_{RR',\sigma\sigma'} [-t(RR')^2/\phi_0] b_{R\sigma}{}^+ b_{R'\sigma} b_{R'\sigma'}{}^+ b_{R\sigma'} \quad (3.12)$$

which describes the elemental tunneling motion shown in Fig. 9. The steps to this process are: (a) the system starts in the ground state $|0\rangle$ and the particle at R with spin σ tunnels to R' (this is the beginning of a vacancy), (b) instead of the particle and hole propagating away from one another to become a full fledged vacancy, one of the two particles at R' returns to R, and the system returns to the ground state. In the intermediate state, the virtual vacancy state, the energy of the system is $E_0 + \phi_0$ so that the matrix element for this process,

$$t(RR')(E_0 - \mathcal{H}_{PM})^{-1}t(R'R) \quad (3.13)$$

is equal to $-t(RR')^2/\phi_0$.

We may convert $\mathcal{H}_T$ into a *pseudospin* Hamiltonian by carrying out the transformation discussed at length by Anderson (1963). We write

$$\sum_{\sigma} \sum_{\sigma'} b_{R\sigma}{}^+ b_{R'\sigma} b_{R'\sigma'}{}^+ b_{R\sigma'}$$

$$= b_{R\uparrow}{}^+ b_{R'\uparrow} b_{R'\uparrow}{}^+ b_{R\uparrow} + b_{R\downarrow}{}^+ b_{R'\downarrow} b_{R'\downarrow}{}^+ b_{R\downarrow}$$

$$+ b_{R\uparrow}{}^+ b_{R'\uparrow} b_{R'\downarrow}{}^+ b_{R\downarrow} + b_{R\downarrow}{}^+ b_{R'\downarrow} b_{R'\uparrow}{}^+ b_{R\uparrow} \quad (3.14)$$

and make the identifications $b_{R\uparrow}{}^+ b_{R\downarrow} = \sigma_R{}^+$, $b_{R\downarrow}{}^+ b_{R\uparrow} = \sigma_R{}^-$, and $\Delta n_R = n_{R\uparrow} - n_{R\downarrow} = \sigma_R{}^z$, where $n_R = \sum_\sigma b_{R\sigma}{}^+ b_{R\sigma}$. Then it is possible to rewrite Eq. (3.12) in the form

$$\mathcal{H}_T = -\sum_{RR'} m(RR')(\tfrac{1}{2} + 2\sigma_R \cdot \sigma_{R'}), \quad (3.15)$$

where $m(RR') = t(RR')^2/\phi_0$, and σ_R is the unitless angular momentum of the spin at R. The part of this Hamiltonian of interest is the part associated with particle dynamics; this is

$$\mathcal{H}_T = -2\sum_{RR'} |J(RR')| \sigma_R \cdot \sigma_R, \quad (3.16)$$

where

$$J = |J(RR')| = t(RR')^2/\phi_0. \quad (3.17)$$

We use Eq. (3.16) as the fundamental definition of J. As such the values of J quoted in this work are taken from our Fig. 32; they will differ from the J used in many of the NMR papers. The primary justification for the use of Eq. (3.16) to define J is the use of this definition in almost all nonNMR work on Heisenberg systems.[6] At $V = 20.0$ cm^3/mole, we have $J = 0.35$ MHz $= 1.6 \times 10^{-5}$ K from the discussion in Sec. 4, Fig. 32, thus using $\phi_0 \approx 18$ K in Eq. (3.17), we have $|t| \approx 0.02$ K. This result is in poor agreement with our theoretical estimate of 0.14 K made in Appendix A.[7]

We will refer to the pseudospin Hamiltonian given by Eq. (3.16) as the tunneling Hamiltonian. This Hamiltonian is a Heisenberg Hamiltonian and the tunneling excitations, energy, specific heat, etc., which follow from $\mathcal{H}_T$ are those of a Heisenberg antiferromagnet (Baker, 1967). The energy, specific heat, etc., for $\mathcal{H}_T$ are tabulated in Appendix D.
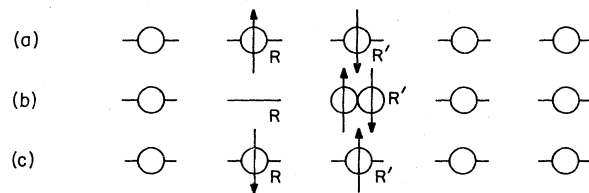

FIG. 9. Tunneling excitations. Due to the tunneling term in $\mathcal{H}_{PM}$, a particle moves to double occupy the lattice site R'. Because of the hard-core repulsion between pairs of particles, this double occupation is energetically expensive. One of the doubly occupying particles returns to lattice site R. If the particles are tagged, e.g. by their spin or mass, this kind of motion is detectable and gives rise to a system of excitations.

---

[6] A secondary justification for this definition of J is the near unanimous vote of the participants in the First Quantum Crystals Conference, Aspen, Colorado, (1969), which overrode a veto by J. C. Wheatley.

[7] This estimate of t is not in good agreement with those in Sec. 4. The problem of course is that ϕ_0 should be much larger than 18 K. Our indentification of ϕ_0 with the vacancy excitation temperature was prompted by an interest in pushing the model as far as possible. From a quantitative point of view, we have pushed it too far. We may invert the calculation here and conclude $\phi_0 \approx 10^3$ K. Certainly the model vacancy is not the real vacancy.

3.2 Interactions

Now let us turn to the question of interactions among the excitations which exist in the solid.

Phonon–Vacancy Wave Interactions. The phonons couple strongly to the vacancy waves in the solid because they see a vacancy wave as a *dynamic* mass fluctuation. If a vacancy were static, a phonon would scatter off of it due to the perturbation

$$\tfrac{1}{2}\Delta m_R \dot{\mathbf{u}}_R{}^2 = \tfrac{1}{2}(m_R - m_3)\dot{\mathbf{u}}_R{}^2 \qquad (3.18)$$

without change in energy. Here $\mathbf{u}_R$ is the displacement of the atom at lattice site R (Carruthers, 1961). This is the perturbation which gives the isotopic impurity contribution to the thermal conductivity. See Fig. 10. But a vacancy wave is a dynamic mass fluctuation which can exchange energy with the phonons. The phonons see a vacancy wave through the time-dependent perturbation

$$\tfrac{1}{2}\Delta m_R(t)\dot{\mathbf{u}}_R{}^2 = \tfrac{1}{2}[m_R(t) - m_3]\dot{\mathbf{u}}_R{}^2. \qquad (3.19)$$

The rate of change of the energy of the phonons due to interaction, via the perturbation

$$\mathfrak{IC}_{VP} = \tfrac{1}{2}\sum_R \Delta m_R(t)\dot{\mathbf{u}}_R{}^2, \qquad (3.20)$$

with the vacancy waves has been calculated. Appendix A.4 quotes the result of that calculation which is similar in its details to that in Appendix A.6. As an illustration of the basic definitions of relaxation times and of the physical content of the phonon scattering from dynamic mass fluctuations we discuss the phonon–vacancy wave relaxation process here at some length.

The vacancy system (the aggregate of vacancy wave excitations) has energy (Eq. D10)

$$E_V = (\phi_0 + \tfrac{1}{2}k_B T)n_V, \qquad (3.21)$$

where $n_V = Nx_V = N \exp(-\beta\phi)$; the phonon system (the aggregate of phonon excitations) has energy
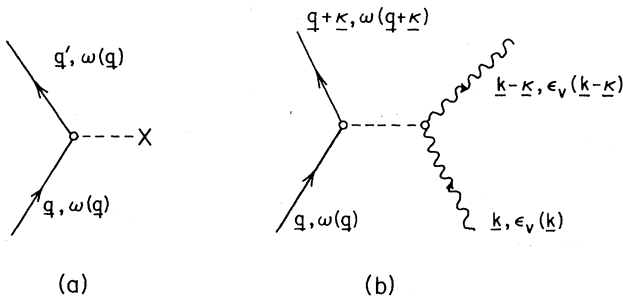

FIG. 10. Vacancy wave–phonon interaction. If a vacancy is static, it appears to a phonon as a scattering center. The phonon scatters from the vacancy with a change in momentum but no change is energy (a). If a vacancy is dynamic, it appears to the photon as a moving scattering center, a vacancy wave. The photon scatters from the vacancy wave with a change in energy and momentum (b). In this latter process, energy is transferred between the phonons and the vacancy waves.
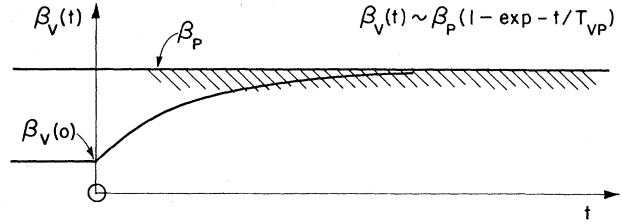

FIG. 11. Definition of T_{12}. The time which describes the relaxation of the 1-system to the 2-system is called T_{12}, e.g. vacancy wave–photon coupling, T_{VP}. This time is defined as characterizing the behavior of the temperature of the 1-system in the limit that the temperature of the 1-system is asymptotically approaching that of the 2-system due to the coupling $\mathfrak{IC}_{12}$ between the systems. As their process occurs the 1-system is completely isolated except for its link to the 2-system, and the 2-system is tightly coupled to a reservoir. Even though the 2-system receives energy from the 1-system, the 2-system does not change temperature.

(Eq. D18)

$$E_P = (NA_P/V)k_B T(T/\theta)^3 = NB_P\beta^{-4}/V, \qquad (3.22)$$

where $A_P = 3(\pi)^4/5$, and $B_P = A_P/(k_B\theta_D)^3$. The vacancy wave system and phonon system are assumed to come to equilibrium among themselves on a short time scale. Thus each system is characterized by its own temperature; we write

$$E_V = N(\phi_0 + \tfrac{1}{2}k_B T_V) \exp(-\beta_V\phi) \qquad (3.23)$$

and

$$E_P = (N/V)B_P\beta_P{}^{-4}, \qquad (3.24)$$

where $(k_B\beta_V)^{-1} = T_V$, $(k_B\beta_P)^{-1} = T_P$, and T_V and T_P are the respective temperatures of the vacancy wave system and the phonon system. The fundamental relaxation time which governs the coupling of the vacancy waves and the phonons is T_{VP} defined by the set of equations:

$$(dE_V/dt)\,|_{VP} = k_V(d\beta_V/dt)\,|_{VP} \qquad (3.25)$$

and

$$(d\beta_V/dt)\,|_{VP} = -(T_{VP})^{-1}(\beta_V - \beta_P), \qquad (3.26)$$

where $k_V = (d/d\beta_V)E_V(\beta_V)$ is the energy constant for the vacancy system. By $(dE_V/dt)\,|_{VP}$, we mean the rate of change of E_V due to $\mathfrak{IC}_{VP}$. We regard these defining equations as meaningful only for $\beta_V \approx \beta_P$, i.e., asymptotically as the hotter vacancy system approaches the phonon system or vice versa. Thus $T_{VP}{}^{-1}$ is understood to be the rate at which the inverse temperature of the vacancy system decays when (a) the vacancy system is infinitesmally hotter than the phonon system, (b) the coupling of the two systems is by $\mathfrak{IC}_{VP}$, and (c) the phonon system remains throughout strongly coupled to a reservoir which maintains its temperature at β_P. See Fig. 11.

The intrinsic rate for coupling energy from the vacancy system to the phonon system is given by Eq.

(A4.4)

$$T_{VP}^{-1} = \frac{400z^2}{\pi} \left(\frac{\Delta m}{m_3}\right)^2 \frac{\hbar \omega_V(3,3)^2}{k_B T} \left(\frac{T}{\theta_D}\right)^6, \quad (3.27)$$

where in this case $\Delta m = -m_3$, θ_D is the Debye temperature which characterizes the phonon spectrum; $\omega_V(3,3)$ is the frequency which characterizes the vacancy tunneling motion, $t = \hbar \omega_V(3,3)$. We may understand the general features of Eq. (3.27) by outlining a variation of the calculation detailed in Appendix A.6.

(a) The phonons see the vacancy waves through the perturbation $\mathcal{H}_{VP}$ which we regard as a noise source. We write

$$\mathcal{H}_{VP} = F_V(t) = \sum_R \tfrac{1}{2}[m_R(t) - m_3]\dot{u}_R^2, \quad (3.28)$$

where $m_R(t)$ is a time-dependent number.

(b) The rate of change of the energy of the phonons due to their coupling to this noise source is given by

$$dE_P/dt = \sum_{\lambda q, \lambda' q'} [\hbar \omega_\lambda(q) - \hbar \omega_{\lambda'}(q')]W(\lambda q, \lambda' q'), \quad (3.29)$$

where $W(\lambda q, \lambda' q')$ is the rate at which phonons of wavevector $\mathbf{q}$ are scattered to wavevector $\mathbf{q}'$ by $F_V(t)$. In second-order perturbation theory, we have

$$W(\lambda \mathbf{q}, \lambda' \mathbf{q}')$$
$$= \frac{1}{\hbar^2} t^{-1} \int_0^t dt' \int_0^t dt'' \langle h(t')_{qq'} h(t'')_{qq'}\rangle_{Av} n_q(n_{q'}+1), \quad (3.30)$$

where $h(t)_{qq'}$ is the qq' component of $F_V(t)$ and n_q is the phonon occupation number. The bracket in this equation means that $h(t)h(t)$ is averaged over an ensemble of noise sources.

(c) From Eq. (3.28) for $F_V(t)$ and the definition of $\mathbf{u}_R$ from Eq. (A6.4), we have

$$F_V(t) = \sum_{q\lambda, q'\lambda'} h(t)_{\lambda q, \lambda' q'}$$
$$= \sum_{q\lambda, q'\lambda'} (\hbar/4m_3 N)[\omega_\lambda(q)\omega_{\lambda'}(q')]^{1/2}$$
$$\times \mathbf{e}_\lambda(q)\cdot\mathbf{e}_{\lambda'}(\mathbf{q}')[n_q(n_{q'}+1)]^{1/2}f_V(t)_{qq'}, \quad (3.31)$$

where

$$f_V(t)_{qq'} = \sum_R f_V(\mathbf{R}, t) \exp[i(\mathbf{q}-\mathbf{q}')\cdot\mathbf{R}], \quad (3.32)$$

and

$$f_V(\mathbf{R}, t) = m_R(t) - m_3. \quad (3.33)$$

Thus we may write Eq. (3.30) in the form

$$W(\lambda q, \lambda' q') = [(4m_3 N)^2]^{-1}\omega_\lambda(q)\omega_{\lambda'}(q')$$
$$\times [\mathbf{e}_\lambda(q)\cdot\mathbf{e}_{\lambda'}(q')]^2 n_q(n_{q'}+1)g_V(\omega_{qq'})_{qq'}, \quad (3.34)$$

where

$$g_V(\omega_{qq'})_{qq'}$$
$$= \sum_{RR'} \int_0^\infty dt\Delta m_R(0)_{qq'}\Delta m_{R'}(t)_{qq'} \exp(i\omega_{qq'}t), \quad (3.35)$$

and $\omega_{qq'} = \omega(q) - \omega(q')$.

(d) We make several plausible assumptions which simplify $g_V(\omega_{qq'})_{qq'}$. These are

1. $\Delta m_R(0)$ and $\Delta m_{R'}(t)$ are uncorrelated for $R \neq R'$.
2. $\Delta m_R(t) = \Delta m_R(0)a(t)$.
3. $\langle \Delta m_R(0)\Delta m_R(0)\rangle_{Av} = \Delta m_R(0)^2 k_B T(\beta_V - \beta_P)$.

Using 1–3 and Eqs. (3.34) and (3.35), we obtain Eq. (3.29) in the form

$$dE_P/dt = [1/(4N)^2] \sum_{qq',\lambda\lambda'} [\hbar\omega_\lambda(q) - \hbar\omega_{\lambda'}(q)]$$
$$\times \omega_\lambda(q)\omega_{\lambda'}(q')A(\omega_{qq'})n_q(n_{q'}+1)\Gamma k_B T(\beta_V - \beta_P),$$
$$(3.36)$$

where

$$\Gamma = \sum_R (|\Delta m_R(0)|^2/m_3^2) \quad (3.37)$$

and

$$A(\omega) = \int_0^\infty dt a(0)a(t) \exp(i\omega t). \quad (3.38)$$

(e) We assume $a(t)$ has a simple time dependence, e.g.,

$$a(t) = a(0) \exp -(zt/\tau)^2, \quad a(0) = 1, \quad (3.39)$$

where $\tau^{-1} = \omega_V(3,3)$. We replace the q sums in Eq. (3.36) by integrals. Then, upon ignoring the λ dependence of $\omega_\lambda(q)$ and using the acoustic approximation, $\hbar\omega_\lambda(q) = \hbar cq$, we find

$$\overset{①}{dE_P/dt} = 1200\overset{②}{z^2(\hbar\tau^{-1})}\overset{③}{\tau^{-1}}\overset{④}{(T/\theta_D)^6}\Gamma k_B T(\beta_P - \beta_V), \quad (3.40)$$

where $k_B\theta_D = \hbar cq_D$.

The various factors in this result are:

① the typical energy available in the vacancy system to be transferred to the phonons;
② the rate at which this energy is transferred;
③ a measure of the phase space available for the 2-phonon process;
④ the strength of the noise source.

Although the calculation we have outlined here is rather complicated in its details the result is a simple dependence on the basic quantities which enter the problem.

The fundamental time which measures the rate of transfer of energy from the vacancy waves to the phonons is defined in terms of the rate of change of the inverse temperature of the vacancy system as in Eqs. (3.25) and (3.26). Thus, using the definition of T_{VP}^{-1}
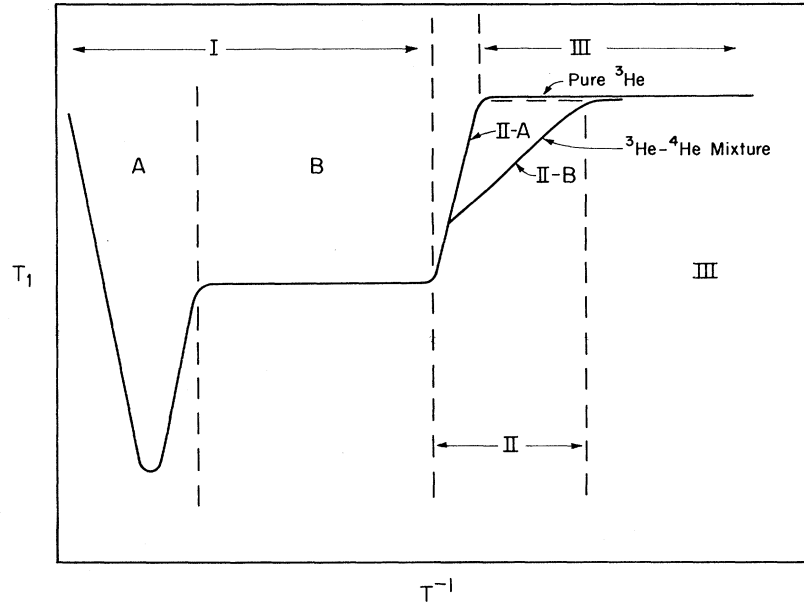
FIG. 12. T_1 vs T^{-1}. There are three qualitatively different mechanisms which determine T_1 in Regions I, II, and III of a T_1 vs T^{-1} plot. In Region I, T_1 is determined by the direct coupling of the Zeeman energy to a particle motion excitation, e.g., the vacancy waves, I-A, the tunneling excitations, I-B, etc. In Region II, T_1 is determined by the coupling between excitations in the system, e.g., tunneling–vacancy. In Region III, T_1 is determined by the spatial diffusion of the excitations.

and Eq. (3.40), we have

$$(dE_V/dt) \, |_{VP} = k_V (d\beta_V/dt) \, |_{VP}$$
$$= k_V T_{VP}^{-1} (\beta_V - \beta_P) = -(dE_P/dt) \, |_{VP}$$

or

$$T_{VP}^{-1} = -(dE_P/dt) \, |_{VP} [k_V(\beta_V - \beta_P)]^{-1}$$

and finally

$$T_{VP}^{-1} = -(1200z^2/k_V)(\hbar/\tau)\tau^{-1}(T/\theta_D)^6 k_B T\Gamma \quad (3.41)$$

as quoted in Eq. (3.27). Once again this is a deceptively simple result.

Tunneling–Vacancy Interactions. The tunneling excitations are strongly coupled to the vacancy wave excitations because they see the vacancy waves as dynamic spin fluctuations. If a vacancy were static a tunneling excitation would see it through the static perturbation

$$J(RR') \Delta\alpha(RR', 0)\sigma_R \cdot \sigma_{R'} \quad (3.42)$$

and be scattered without change in energy. But the tunneling excitations see the vacancy waves through

$$\mathcal{H}_{TV} = \sum_{RR'} J(\mathbf{RR'}) \Delta\alpha(RR', t)\sigma_R \cdot \sigma_{R'}, \quad (3.43)$$

where $\Delta\alpha(\mathbf{RR'}, t) = \alpha(RR', t) - \langle \alpha(\mathbf{RR'}) \rangle$ and $\alpha(\mathbf{RR'}, t)$ is zero unless there is a ^{3}He particle at $\mathbf{R}$ and $\mathbf{R'}$.

The rate of change of the energy of the tunneling excitations through coupling to the vacancies by $\mathcal{H}_{TV}$ has been calculated by Garwin and Landesman (Garwin, 1964b) and Richards (1965). The treatment of this problem in Appendix A leads to a decay of the energy in the tunneling system at the rate

$$(T_{TV})^{-1} = 2(z-1)\omega_3(V, 3)x_V, \quad (3.44)$$

where x_V is the concentration of vacancies at the lattice temperature, z is the number of near neighbors, and $\omega_3(V, 3)$ is the rate at which a ^{3}He particle will tunnel into a vacancy site. This relaxation rate is worked out in detail in Appendix A.3. For our discussion here we want the result of that calculation, Eq. (3.44), and a physical idea of its meaning. In Appendix A.3 we show that the rate at which the tunneling system loses energy is given by the rate at which the motion of a ^{3}He vacancy pair is uncorrelated. See Eq. (A3.8) and the accompanying discussion. This rate is given by the product of the probability that a ^{3}He vacancy pair occurs and the frequency with which the vacancy component of the pair tunnels. The first factor is $x_V^2(z-1)$ and the second is $\omega_3(V, 3)$.[8]

The Tunneling–Phonon Interaction. There is no evidence in any experiment on ^{3}He to date that a tunneling–phonon interaction occurs at an observable rate. A phenomenological theory of the tunneling–phonon interaction has been developed by Nosanow and Varma (1968). See also McMahan and Nosanow (1970).

4. RELAXATION IN PURE ^{3}He EXPERIMENTAL

4.1 T_1 Relaxation, Theory

There are three kinds of excitations in solid ^{3}He which are responsible for the results observed in NMR experiments. These excitations and their coupling to one another are described above. In this section we discuss the interpretation of NMR experiments on pure

---

[8] The treatment of this problem by P. M. Richards (1965) gets the correct answer. That treatment is incorrect in its details; the important pairs are 3–V pairs (Zane, 1970). See Appendix A.3.
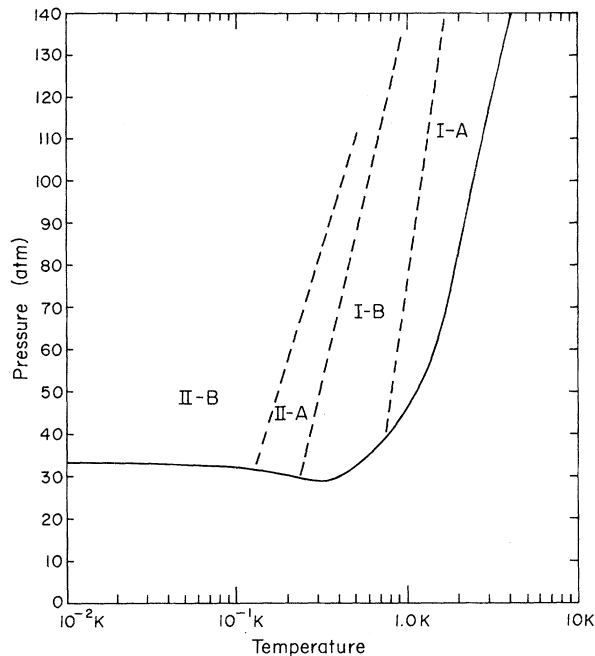
Fig. 13. Relaxation mechanisms vs temperature and pressure. On a phase diagram, we show the boundaries between the various relaxation regions for $\omega_0 \rightarrow 0$. The boundary between Region I-A and Region I-B is found by equating Eq. (A7.11) and Eq. (A7.18). The boundary between Region I-B and Region II-A is found by equating Eq. (A7.18) and Eq. (A7.20). The boundary between Region II-A and II-B is found by equating Eq. (A7.20) and Eq. (A7.36). We do not show the boundary to Region III since it is size dependent.

³He in terms of these excitations, and the extensive experimental explorations that have been conducted on the ³He system. We discuss T_1, T_2, and diffusion experiments.

The result of a typical T_1 experiment on pure ³He is as shown in Fig. 12. The data is ordered into three regions designated by I, II, and III by the temperature. In Region I, the high-temperature region, the energy in the Zeeman system is transferred to one of the particle motion excitation systems inhabiting the solid. The excitation system in turn is tightly coupled to the reservoir and the experiment gives evidence about the nature of the excitation system. In Region II, the intermediate-temperature region, the excitation system which takes the energy from the Zeeman system is not tightly coupled to the reservoir, and the experiment gives evidence about the coupling between the excitation systems in the solid. In Region III, the low-temperature region, the energy taken from the Zeeman system by the excitation system in the solid is delivered to the reservoir by spatial motion of the excitations, e.g., by diffusion. Regions I and II are characterized by energy flow in time among the excitation systems in the solid, e.g., from the Zeeman system to the tunneling system to the vacancy wave system, etc. Region III is char-

acterized by energy flow in space, e.g., from the Zeeman system to the tunneling system where it diffuses across the sample.

We show in Fig. 13 a P-T phase diagram on which we map the temperature and pressure corresponding to Regions I, II, and III. In Table I we have listed the T_1 experiments that have been done on pure ³He. The various regions on the T_1 vs T^{-1} plot are further subdivided to indicate that changes in the details of the relaxation process in each region occur although the qualitative features remain the same, e.g., Regions I-A and I-B on Fig. 12. On Fig. 13 we have also indicated this further subdivision.

Region I. Energy is dumped into the Zeeman system by the rf field. This energy is transferred to one of the particle motion excitations through the agency of the dipolar field as explained in Sec. 3. In Region I-A the vacancy waves are the important particle motion excitations which cause fluctuations in the dipolar field.[9] As the temperature is lowered, the vacancy concentration goes toward zero as

$$x_V(\beta) = \exp\left(-\beta\phi\right),$$

and the attendant motions of the magnetic moments disappear leaving only the motions due to the tunneling excitations to cause fluctuations in the dipolar field, Region I-B (Garwin, 1966; Hartmann, 1964).

Region I-A. The energy dumped into the Zeeman system by the rf field is delivered to the vacancy wave excitations. In Fig. 14 we show the topology of the energy flow process. The relaxation time which characterizes this process is derived in Appendix A.1 and will be discussed in some detail below. Throughout Region I-A (and Region I-B) the vacancy waves are tightly coupled to the reservoir through the vacancy wave-phonon coupling discussed above.

From Eq. (A1.20) the T_1 for relaxation of energy
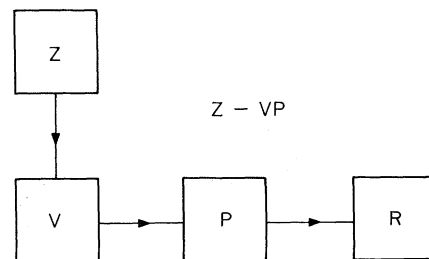
Fig. 14. Topology Z-VP.

---

[9] In Region I-A, the energy in the Zeeman system is transferred to the vacancy waves through the agency of the dipolar field. For this to be a correct physical picture we must have the vacancy wave dressed by spin fluctuation excitations (magnons at low temperature), i.e., the vacancy wave is not a bare particle. The Zeeman system is coupled through the dipolar field to the spin fluctuations in the wake of the vacancy.

TABLE I. Summary of NMR relaxation experiments.

Reference	Summary of Experiment
	Pure ^{3}He
Goodkind and Fairbank (1959, 1960)	Measurement of T_1 and T_2 at $V=20$ cm^3/mole at temperatures above 1 K. (Region IA). Observed minimum in T_1 and showed temperature dependence of vacancy concentration.
Reich (1963)	Measurement of T_1, T_2, and D in the volume range $18.4<V<22.5$ cm^3/mole down to 0.5 K (Regions IA, IB, and IIA). Observed "plateau" in T_1 and decoupling of the tunneling bath from the lattice in Region IIA.
Garwin and Landesman (1964)	Measurement of T_1 and T_2 for volumes $16.5<V<19.3$ cm^3/mole. Described the physics involved in the relaxation processes in the various regions (IA, IB, and IIA) in terms of the three-bath model.
Beal, Giffard, Hatton, Richards, and Richards (1964); and Richards, Hatton, and Giffard (1965)	Investigated T_1 for volumes $18.5<V<24.0$ cm^3/mole down to 0.1 K (Regions IA, IB, IIA, IIB, III). Systematic measurements of frequency dependence of T_1 in regions IB, IIA, and IIB. Measurements of the heat capacity of the tunneling bath.
Richardson, Hunt and Meyer (1965); and Richardson, Landesman, Hunt, and Meyer (1966)	T_1 and T_2 measurements for $19.5<V<24.5$ cm /mole down to 0.35 K (Regions IA, IB, IIA, and IIB). Study of frequency dependence of T_1 and T_2 in Region IB. Measurement of 10/3 effect in T_2, and discussion of spectral function for relaxation.
Thompson, Hunt, and Meyer (1967)	Measurement of diffusion coefficient D_z at low temperatures, down to 0.05 K. Correlation of D_z with J for volumes in the range $20<V<24$ cm^3/mole.
Hunt and Thompson (1968)	Measurement of energy diffusion rate D_E in "hole burning" experiment.
Senghaphan and Zimmerman (1968)	Measurements of T_1 in Regions IA and II for volumes $20<V<24$ cm^3/mole. Studies of phonon interaction with relaxation rates.
	Dilute mixtures of ^{4}He in He
Garwin and Reich (1964)	Measured anomalously long T_1 in Region II for specimen at 19 cm^3/mole with $x_4=0.01$. Measured large heat capacity of "tunneling reservoir."
Giffard and Hatton (1967); Giffard (1968); and Giffard, Hatton and Truscott (1971)	Studies of T_1 on Regions II and III. Observed the concentration dependence of T_1 at $V=20$ cm^3/mole with various concentration of ^{4}He in the range $5\times10^{-7}<x_4<3\times10^{-4}$. In low-temperature measurements, Region III, observed the diffusion limited "plateau" and the increase of T_1 with temperature below 0.1 K.
Hunt, Richardson, Thompson, Guyer, and Meyer (1967)	Studies of T_1 in Region III for $20<V<23$ cm^3/mole. Observed specimen size limitation for T_1 in Region III, the diffusion limited "plateau," ($x_4=2\times10^{-4}$).
Bernier and Landesman (1969); Bernier (1970); and Landesman and Bernier (1970)	Measurements of T_1 in Region II, and T_2 in Region I for $V=20$, 21 cm^3/mole and $10^{-4}<x_4<10^{-2}$. Interpretation of the concentration dependence of T_1 and heat capacity in terms of mass fluctuation wave excitations.
Yu and Reich (1969)	Measurements of frequency and concentration dependence of T_1 in Region II for $18.3<V<20.8$ cm^3/mole and with $5\times10^{-6}<x_4<1.5\times10^{-3}$.
	Nondilute mixtures of He in ^{4}He
Miyoshi, Cotts, Greenberg, and Richardson (1970)	Measurements of frequency and concentration dependence of T_1, T_2, and D in Region I for $19<V<21$ cm^3/mole and for ^{3}He concentrations in the range $0.02<x_3<1.0$.

from the Zeeman system to the vacancy wave system is

$$T_1^{-1}\big|_{ZV}=(T_{ZV})^{-1}=\tfrac{2}{3}(M_2/\omega_0)g(\eta),\qquad(4.1)$$

where

$$g(\eta)=g(\omega_0\tau_V)$$
$$=\{\omega_0\tau_V/[1+(\omega_0\tau_V)^2]\}+\{4\omega_0\tau_V/[1+4(\omega_0\tau_V)^2]\},$$
$$(4.2)$$

$$\tau_V^{-1}=x_Vz\omega_3(V,3),\qquad(4.3)$$

and $\omega_3(V,3)$ is the frequency for tunneling of a ^{3}He

particle into a neighboring vacancy site; $\omega_3(V,3)$ is calculated at the end of Appendix A.1 and discussed in some detail below. Here also $\omega_0=\gamma H_0$ is the Larmor frequency, and M_2 is the Van Vleck second moment; see Appendices A.1 and B.1. We may understand the physical content of this result upon looking at the $\omega_0\tau_V\ll1$ limit. In this limit the "looking" frequency of a spin, ω_0, is much less than the frequency which characterizes the fluctuations in its local field. For Eq. (4.1) we have

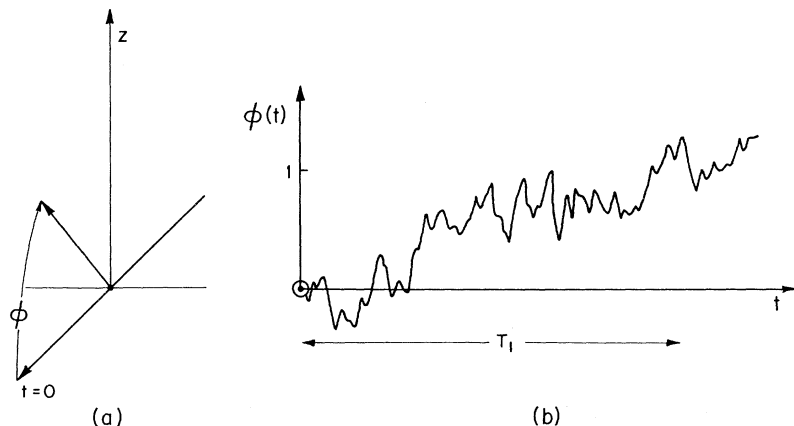$$T_1^{-1}=(10/3)M_2\tau_V\approx\omega_d^2\tau_V,\qquad(4.4)$$

Fig. 15. Time evolution of $\phi(t)$. At $t=0$, i.e., after a $90°$ pulse, a classical spin lies in the x, y plane. At the site of the spin, the fluctuating local field, $H_l(\omega_0)\perp$, causes the spin to random walk back toward the z axis. The angle ϕ also random walks and might evolve in time as shown in (b).

(a)　　　　　　　　　　(b)

where $\omega_d \approx \mu^2 z/(\hbar\Delta^3)$ is the frequency of precession of a spin in the dipolar field of z near neighbors at distance Δ. A spin at R sees a local field of average strength H_d fluctuating between $+H_d$ and $-H_d$ at frequency τ_V^{-1}. If precessing at frequency ω_0 in the horizontal plane (the rf field has just been turned off) the spins orientation with respect to the z axis as measured by ϕ will random walk, in response to the fluctuating transverse local field, a distance $\Delta\phi=1$ in a time given by

$$T_1 \approx (\Delta\phi/\omega_d\tau_V)^2 \tau_V \approx [(\Delta\phi)^2/\omega_d^2\tau_V]. \qquad (4.5)$$

Here the typical step the spin takes is of length $\omega_d\tau_V$; $n=\Delta\phi/(\omega_d\tau_V)$ steps are required to walk directly the distance $\Delta\phi$, n^2 step are required to random walk $\Delta\phi$, τ_V is the time per step. See Fig. 15. For $\Delta\phi=1$, the spin has effectively recovered to its original orientation along the external field and Eq. (4.5) agrees with Eq. (4.4). In the limit $\omega_0 \gg \tau_V^{-1}$, the physical argument is the same as above but now the "looking" frequency of a spin is much faster than the frequency with which the local field is fluctuating. Then, the amplitude of the local field at frequency ω_0 enters Eq. (4.5) in place of the low-frequency local field ω_d; i.e., we replace ω_d by $\omega_d(\omega_0)=\omega_d(\omega_0\tau_V)^{-1}$ in Eq. (4.5). Then, the spin random walks a distance $\Delta\phi=1$ taking steps of duration τ_V and length $\omega_d(\omega_0)\tau_V$, i.e.,

$$T_1 \approx [\Delta\phi/\omega_d(\omega_0)\tau_V]^2\tau_V = (\Delta\phi^2/\omega_d^2)(\tau_V/\omega_0^2).$$

Equations (4.1) and (4.2) are the analytic expression of this physics.

Now let us consider the behavior of T_1 as the temperature is lowered. We choose a particular Larmor frequency with which to look at the system. See Fig. 16a. The frequency which characterizes the particle motion which cause the fluctuations in the local field becomes smaller and smaller as the temperature is lowered

$$\tau_V^{-1} = z\omega_3(V, 3)x_V = z\omega_3(V, 3) \exp(-\beta\phi).$$

At high temperature, $\omega_0\tau_V \ll 1$, the spin relaxes in time

$$T_1^{-1} \approx \omega_d^2\tau_V$$

which becomes shorter as the temperature is lowered, and is independent of the Larmor frequency. At the resonance temperature, $\omega_0\tau_V \approx 1$, the spin looks at precisely the frequency of the fluctuations of the local field, and the local field fluctuations are most effective in turning the spin up; T_1 is as short as it can be. At low temperatures, $\omega_0\tau_V \gg 1$, the spin looks for what is a fast component of the local field,

$$T_1^{-1} \approx \omega_d^2(\omega_0^2\tau_V)^{-1}.$$

T_1 becomes longer as the temperature is lowered, and τ_V becomes longer. At fixed temperature T_1 becomes longer as the frequency is raised, and the spin goes further out of synchronism with the fluctuation in the local field. See Fig. 16a, b.

Region I-B. The energy dumped into the Zeeman system by the rf field is delivered to the tunneling excitations. In Fig. 17, we show the topology of the energy flow process. The onset of Region B occurs as the temperature is lowered and the particle motion due to vacancy waves is frozen out; i.e. at point B on Fig. 16(a). In the limit of low Larmor frequency, we would estimate C to be at $x_V\omega_3(V, 3) \approx J$ or

$$x_V(T_C) = J/\omega_3(V, 3).$$

From the results at the end of this section at 20.0 cm³/mole, we have $J \approx 0.4\times10^6$ Hz, and $\omega_3(V, 3) \approx 10^{11}$, for ϕ in $x_V(\beta)$ equal to 14.5 K we have $x_V(\beta) = J/\omega_3(V, 3)$ at $T \approx 1.5$ K. The transition from Region I-A to Region I-B is at $T = 1.5$ K for $v = 20.0$ cm³/mole.

From Eq. (A2.17), we find the rate for relaxation of energy from the Zeeman system to the tunneling excitations is

$$T_1^{-1}|_{ZT} = J_1(\omega_0/\omega_T) + 4J_1(2\omega_0/\omega_T), \qquad (4.7)$$

where

$$J_1(\omega_0/\omega_T) = [\tfrac{1}{2}\pi(M_2/3\omega_T)]^{1/2} \exp\ (-\omega_0^2/2\omega_T^2)$$

$$\text{(Gaussian),} \quad (4.8)$$

$$J_1(\omega_0/\omega_T) = (\pi M_2/6\omega_T) \exp\ -(\omega_0/\omega_T) \quad \text{(Lorentzian),}$$

$$(4.9)$$

and ω_T is proportional to J, $\omega_T = bJ$; the magnitude of b depends on the choice of a Gaussian or a Lorentzian correlation function. See the discussion in Appendices A.2 for further details leading to $J(\omega_0/\omega_T)$. The dependence of T_1 and b on the correlation function is taken up below. The function $J_1(\omega_0/\omega_T)$ has the same qualita-
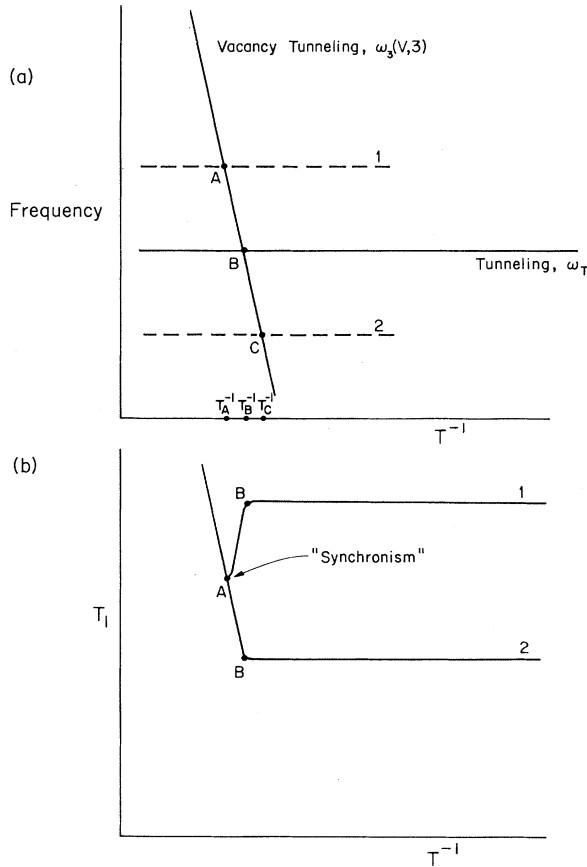

FIG. 17. Topology Z–TVP.

tive dependence upon ω_0/ω_T as the function $g(\omega_0 \tau_V)$ above. When the looking frequency is slow compared to J, $\omega_0/\omega_T \rightarrow 0$ we have the shortest T_1,

$$T_1^{-1} \approx (\omega_d^2/\omega_T)$$

in analogy with Eq. (4.5). When the looking frequency is fast compared to J, $\omega_0/\omega_T \rightarrow + \infty$, the ω_0 Fourier component of the fluctuating local field goes to zero as

$$\omega_d(\omega_0) = \omega_d \exp\ [-\tfrac{1}{4}(\omega_0^2/\omega_T)]$$

and we get a very long T_1,

$$T_1^{-1} \approx \omega_d(\omega_0)^2/\omega_T \approx (\omega_d^2/\omega_T)\ \exp\ [-\tfrac{1}{2}(\omega_0/\omega_T)^2].$$

In this region, the fundamental microscopic time, J, and hence ω_T, is temperature independent, but very volume dependent. For a sample prepared at a particular molar volume, ω_T is fixed, and ω_0/ω_T is varied by changing H_0. At fixed H_0 or ω_0, samples prepared at differing molar volumes yield a variation in ω_T (e.g., a factor of 50 over the bcc phase) which permit one to explore a wide range of ω_0/ω_T.

The frequency dependence of T_1 in Region I-A differs from that in Region I-B because of the time dependence of the correlations in the dipolar field brought about by the two kinds of particle motion excitations.

4.2 T_1 Experiments, Results

There have been measurements of T_1 in pure ^{3}He in Region I by many experimenters. The accumulated body of the work extends over a wide range of: (a) molar volume, 16 cm^3/mole to 24.5 cm^3/mole; (b) temperature, $0.003K < T < T_M$, and (c) Larmor frequency, with parameter ω_0/ω_T being varied from 10^{-2} to 30.

Before characterizing these results, we must give a qualification statement for the expression pure ^{3}He. Most of the experiments were performed prior to the knowledge that traces of ^{4}He could play a major role in some of the relaxation processes. Thus most of the experiments to be discussed were performed with gas samples containing unknown amounts of ^{4}He impurity at the level of about 100 ppm, the best gas then available from the supplier (Monsanto Corporation, Moundsville, Ohio). Subsequent work revealed that the

FIG. 16. Frequencies. The qualitative behavior of T_1 vs T^{-1} is determined by the comparison of the "looking" frequency, ω_0, and the frequencies that characterize H_l. In (a) we show $\omega_3(V, 3)$ and ω_T, the frequencies which characterize H_l, as a function of T^{-1}. At $T^{-1} > T_B^{-1}$, $\omega_3(V, 3) \gg \omega_T$, and the dipolar field is characterized by $\omega \approx \omega_3(V, 3)$. At $T^{-1} < T_B^{-1}$, $\omega_3(V, 3) \ll \omega_T$, and the dipolar field is characterized by $\omega \approx \omega_T$. For the two choices of the Larmor frequency, 1 and 2, indicated by dashed lines, there are two different kinds of behavior for T_1 vs T^{-1} as shown in (b). For dashed line 1, $\omega_0 = \omega_3(V, 3)$ at T_A^{-1}, and $\omega_0 > \omega_T$ everywhere. The spin sees the dipolar field in synchronism with itself at T_A^{-1}; hence, the minimum value of T_1 occurs at T_A^{-1}. For dashed line 2, it is not possible to satisfy the synchronism condition, $\omega_0 = \omega_3(V, 3)$.
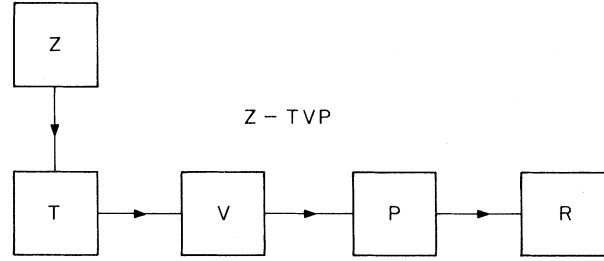
T_1 behavior at lower temperatures, in Regions II and III on Fig. 12, is profoundly affected by the quantity of isotopic impurity. However, the properties of solid ^{3}He which depend upon the vacancy waves and the tunneling excitations do not seem to be seriously affected by traces of isotopic impurity of less than approximately 0.5%. We shall therefore discuss the quantitative results of T_1 experiments in Region I, and the T_2 and spin diffusion coefficient measurements at all temperatures as being properties of pure ^{3}He even though the actual experiments used somewhat contaminated gas samples. A discussion of T_1 in Regions II and III will be deferred to Sec. 6 and 7 where we discuss systems with isotopic impurities.

In all of the relaxation experiments, the samples were formed at "constant volume" using the "blocked capillary technique" in which a plug forms in the filling capillary when the liquid under pressure is cooled to the freezing point on the melting curve. It is then usually assumed that the plug stays fixed as the experimental sample chamber is cooled through the melting point to fill the chamber with solid. In the solidification process, the pressure in the chamber typically drops by 10%, and it is common for the plug to slip as the solid is being formed. This introduces an error in the volume determination of order 0.1 cm³/mole which depends upon the relative volume of the sample cell and the fill capillary. In some recent work, a strain gauge measurement of the pressure in the sample chamber was used to determine the molar volume of the experimental sample. The standard PVT data used for molar volume determination is that given by Mills, Grilly, and Sydoriak (1961), and by Grilly and Mills (1959). An accurate determination of the bcc–hcp phase boundary has been made by Straty and Adams (1966).

Finally, before discussing the results we comment on the quality of the crystals that are formed in a typical experiment. Because of the simplifications that result in the theoretical analysis, the most desirable form of solid in the NMR experiments is a powder of crystallites so that anisotropy associated with crystal orientation relative to the field H_0 is averaged out (e.g. Abragam, 1961). In practice, this circumstance is not always achieved. Workers who are interested in the formation of single crystals for transport measurements of solid helium have found it rather easy to form single crystals (Ackerman and Guyer, 1968; Mueller, 1970). Variations in T_1 in Region I-B of about 10% due to anisotropy for solids formed even by rapid cooling from liquid to solid have been observed (Giffard, Hatton, and Truscott 1971).

The earliest measurements of T_1 in solid ^{3}He were by Goodkind and Fairbank (1959, 1960) who identified the liquidlike behavior of Region I-A as being due to vacancies. Their work was extended to lower temperatures by Reich (1963) who observed the plateau in Region I-B due to tunneling. Figure 18 shows the

measurements of Reich over the temperature range $0.5 < T^{-1} < 3$ for various molar volumes of the solid at a constant Larmor frequency of 5.24 MHz. We note that in Region I-A, where the relaxation rate is characterized by vacancy motion, the relaxation time first decreases with temperature as τ_V decreases as expected from Eq. (4.4), then passes through a minimum at $\omega_0\tau_V \approx 1$, and finally increases as τ_V^{-1} with further decrease in temperature. As the volume is increased, the temperature at which the minimum occurs decreases, reflecting the fact that the vacancy excitation temperature decreases with increasing molar volume. We note also that in the high-temperature region, I-A, the magnitude of T_1 shows only a mild decrease with increasing volume since the frequency of the vacancy motion, $\omega_3(V, 3)$ is apparently not a strong function of the volume. Further discussion of the quantitative determination of ϕ and $\omega_3(V, 3)$ will be delayed until after the discussion of the T_2 and diffusion experiments.

At temperatures below that of the minimum of T_1, where $\omega_0\tau_V \gg 1$, we enter the region described by Eq. (4.6) and, provided that the Larmor frequency is sufficiently large, the relaxation time increases as the temperature is lowered until there are so few vacancies present in the system that the tunneling motion becomes relatively more important. The frequency dependence of T_1 throughout Region I has been investigated by
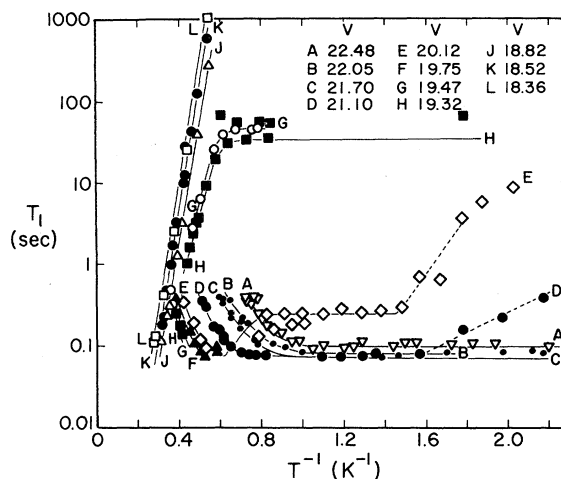

FIG. 18. T_1 vs T^{-1} for various molar volumes. The figure shows the T_1 data of Reich (1963) for various molar volumes measured at a fixed precession frequency of 5.24 MHz. Curve E for $V = 20.12$ cm³/mole displays all of the characteristics seen for T_1 in Regions I and II. The minimum at $T^{-1} \approx 0.6\mathrm{K}^{-1}$ occurs when the vacancy tunneling frequency $\omega_3(V, 3)$ is near the precession frequency; at lower temperatures the recovery is determined by the ^{3}He tunneling rate. The minima for curves H, J, K, and L would occur at higher temperatures than that at which the measurements were made. For curves A, B, C, and D there is no minimum in T_1 because the precession frequency is less than the effective frequency of the ^{3}He tunneling ω_T; the ^{3}He tunneling dominates the process when the temperature is low enough that $\mathfrak{X}V\omega_3(V, 3) < \omega_T$. [After Reich (1963)].

Richards, Hatton, and Griffard (1965), and by Richardson, Hunt, and Meyer (1965). The data of Richardson, Hunt and Meyer at various Zeeman frequencies for the volume 20.4 cm³/mole are shown in Fig. 19. In this figure we see that as the Zeeman frequency is raised from 1.05 MHz to 6.80 MHz, the behavior of T_1 for values of T^{-1} between 0.5 and 0.9 changes dramatically. It is in this temperature range, I-A, that τ_V is of the order 10^{-7} sec so that the frequency dependence of T_1 begins to be observable. The minimum in T_1 does not even appear if the Zeeman frequency is less than the tunneling rate, $\omega_0 \leq \omega_T$, because point C in Fig. 16(a) occurs at a higher temperature than that expected for the minimum, point B, the point at which $\omega_T \approx \tau_V^{-1}$.

At lower temperatures, we enter Region I-B, the "plateau" region in T_1. The magnitude of T_1 in the plateau is expected to vary with frequency as given by Eq. (4.8). It is through studies of the frequency variation of T_1 in Region I-B that we acquire detailed information about the spectral function $J(\omega_0/\omega_T)$. Figure 20 shows the T_1 data of Richardson, Hunt, and Meyer for many different molar volumes in the bcc phase plotted in a reduced form $T_1(0)/T_1(\omega_0)$ versus $(\omega_0/J)^2$. If we assume that all of the volume dependence of T_1 is contained in $T_1(\omega_0=0)$ and in $\omega_T(V)$, then the plot is essentially the function $J_1(\omega_0/\omega_T)$ vs $(\omega_0/\omega_T)^2$. From Eq. (4.8) we see that the points on such a plot are given by

$$T_1(0)/T_1(\omega_0) = J(\omega_0/\omega_T) + 4J(2\omega_0/\omega_T).$$

The solid lines represent the calculated values of T_1 assuming either of two simple analytical forms for the correlation function that governs the time evolution of the dipolar field due to tunneling motion, the Gaussian function, $J(\eta) = \exp{-\eta^2/2}$, and the Lorentzian function, $J(\eta) = \exp{(-\eta)}$, (see Appendix A for a detailed discussion of this point). It appears that in the bcc phase the function $\exp{[-(\omega_0/\omega_T)]}$ obtained from the Lorentzian approximation produces a better fit to the observed data than a Gaussian approximation. Figure 20b shows a similar plot for the data in the hcp phase. It can be seen that in the hcp phase the function $\exp{[-(\omega_0^2/2\omega_e^2)]}$ obtained from the Gaussian approximation produces a better fit to the observed data than the Lorentzian approximation. The actual correlation function for either phase is probably not exactly a pure Gaussian or a pure Lorentzian. The question of the functional form of $J_1(\omega_0/\omega_T)$ must be understood if one is to reliably use only the relaxation data to calculate the tunneling frequency J. The use of experimental evidence to straighten out this question is further complicated by uncertainty as to the validity of the powder hypothesis for experimental samples (single crystals produce anisotropic values of T_{ZT} which vary by at least 10%) and by the presence of 200 ppm ^{4}He
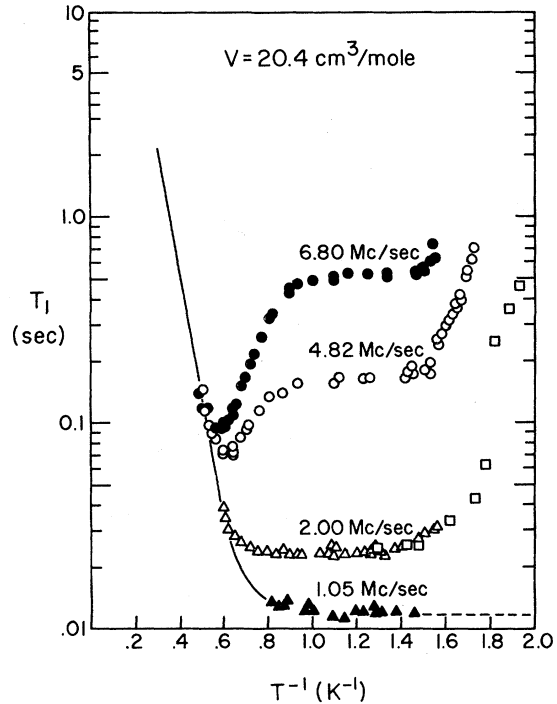

FIG. 19. T_1 vs T^{-1} at various precession frequencies. The figure displays the frequency effects on T_1 at $V = 20.4$ cm³/mole measured by Richardson, Hunt, and Meyer (1965). At high temperatures $T^{-1} < 0.6$ K^{-1}, the relaxation rate is independent of frequency and is governed by the vacancy tunneling motion. The curves for 6.8 MHz and 4.82 MHz display a minimum at $\omega_0 \tau_V \approx 1$. For this specimen $\omega_0 \tau_V/2\pi \approx 3$ MHz so that in the measurements with $\omega_0/2\pi = 2.00$ MHz and 1.05 MHz, there is no minimum in T_1. The plateau values of T_1 in Region IB $(1 < T^{-1} < 1.4)$ at various frequencies are used in the determination of the spectral function, $J(\omega_0)$, for the Zeeman–tunneling relaxation process [after Richardson, Hunt, and Meyer (1965).]

impurities in most of the experimental samples. The effects of ^{4}He motion upon relaxation will be discussed in the following sections of the paper. The crucial observation from studies of dilute ^{3}He–^{4}He mixtures is that the motion of ^{4}He impurities could lead to anomalously short values of T_1 in the limit $(\omega_0/\omega_T) \ll 1$. To resolve these questions further experiments with very pure ^{3}He single crystals should be performed. Further theoretical progress is possible by calculating the sixth moment of the line shape and by including the effects of zero-point motion in the evaluation of the moments (Harris, 1971).

4.3 T_2 Relaxation, Theory

The result of a typical T_2 experiment on pure ^{3}He is as shown in Fig. 21. The data are ordered into two regions, I-A and I-B, by the temperature. Since the process by which equilibrium is established among the spins involves energy transfer within the Zeeman system only, T_2 has a much less bizarre temperature
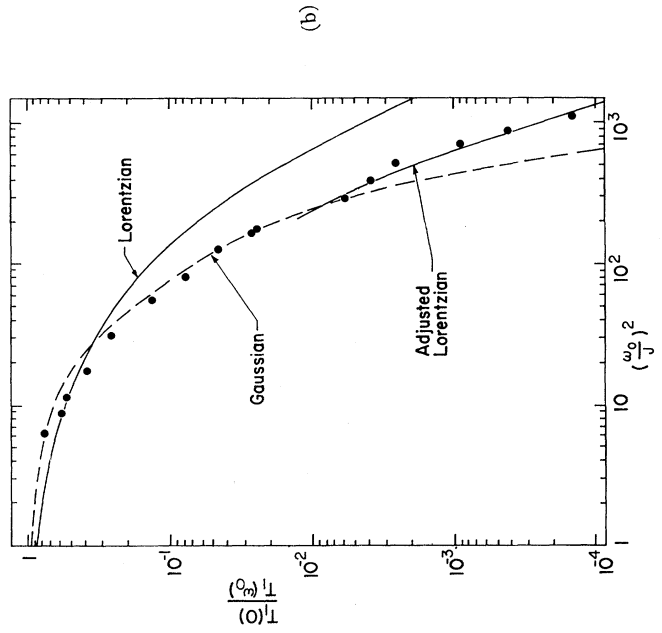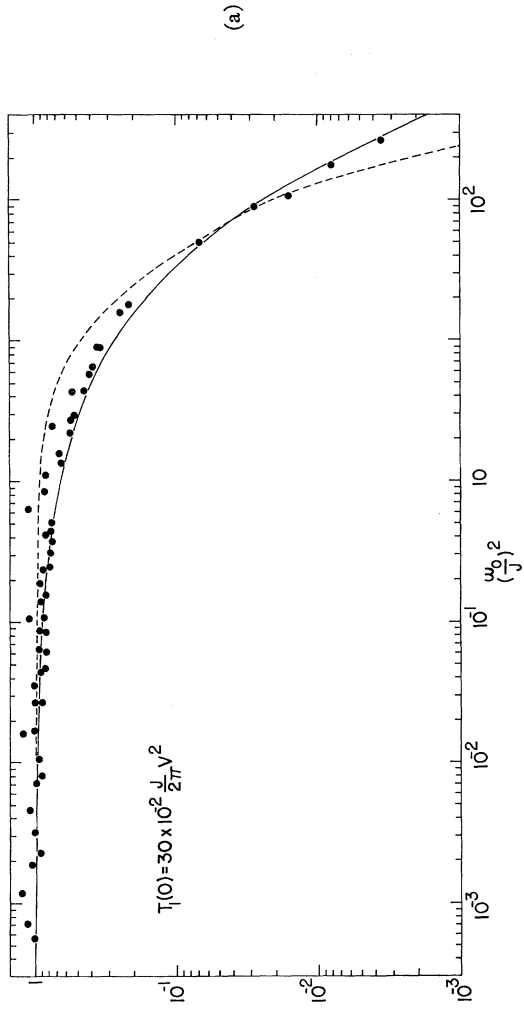
FIG. 20. (a) Reduced plot of $(T_1^{-1})|_{ZT}$ for bcc ^{3}He. The figure represents a reduced plot of all $(T_1^{-1})|_{ZT}$ points obtained in the experiment of Richardson, Hunt, and Meyer (1965). The values of J used are those obtained from a smooth curve through the data points of Panczyk and Adams (1969) for $V \geq 21$ cm^3/mole, and the values of J obtained in T_1 "heat capacity" experiments of Giffard and Hatton (1967) and Bernier and Landesman (1969) at $V=20$ cm^3/mole. The values of J obtained in these thermostatic measurements are not dependent upon the approximation used to represent the time evolution of the fluctuating dipole field (Gaussian or Lorentzian approximations). The coefficient $k=30\times10^{-12}$ in the expression $T_1(0)=k(J/2\pi)^{V^2}$ is determined from the condition that $T_1(\omega_0) \rightarrow T_1(0)$ as $\omega_0/J \rightarrow 0$. The points in the figure give a presentation of the spectral density function $J_1(\omega_0)$ in the form $T_1(0)/T_1(\omega_0)=[J_1(\omega_0)+4J_1(2\omega_0)]/5J_1(0)$. The dashed curve is that calculated from Eq. (4.8) in the text and is based upon the Guassian approximation, $\omega_T=4.76J$. The solid line is that obtained by empirically fitting the spectral function of the Lorentzian approximation, $J_1(\omega_0) \approx \exp(-\omega_0/\omega_T)$, to the data points to agree with the values of $T_1(0)/T_1(\omega_0)$ for large values of (ω_0/J). The equation of the curve is given by $T_1(0)/T_1(\omega_0)=[\exp(-\omega_0/\omega_T)+5\exp(-2\omega_0/\omega_T)]/5$ with $\omega_T=4.16J$. The apparent fit of the data to the Lorentzian approximation is compelling (Giffard, 1968; Richards, 1970). However, if the data points are adjusted to fit the exact theoretical Lorentzian expression, $(\omega_T=4.76J/\sqrt{2})$, Eq. (A2.20), by varying the parameter J for each molar volume, the values of J so determined are larger than those given in thermostatic measurements by a factor of about 2. Moreover, the coefficient 30×10^{-12} is in closer agreement with that obtained in the theoretical Gaussian expression, 31.6×10^{-12}, than the theoretical Lorentzian, 17.7×10^{-12}. Since there is no obvious theoretical reason why either approximation is to be preferred, we choose the data points of the figure to represent $J_1(\omega_0)$. Richardson, Landesman, Hunt, and Meyer (1966) have obtained an empirical expression for $J_1(\omega_0)$ for bcc ^{3}He from a set of points essentially similar to that in the figure, but obtained by a piecewise generation of the curve by varying J for each molar volume to obtain the best fit to the data of the other volumes. Their result is

$$\frac{J_1(\omega_0)}{J_1(0)} = \exp\left[\frac{-1.0(\omega_0/\omega_T)^2}{(\omega_0/\omega_T)+0.18}\right],$$

where $\omega_T=4.76J$. This relation asymptotically approaches the Lorentzian for $\omega/\omega_T \gg 0.18$. (b) Reduced plot of $T_1^{-1}|_{ZT}$ for hcp ^{3}He. The points in the figure represent a reduced plot of $T_1^{-1}|_{ZT}$ for the hcp phase for the points reported by Richardson, Landesman, Hunt, and Meyer (1966) for $V=19.55$ cm^3/mole, and by Miyoshi, Cotts, Greenberg, and Richardson (1970) for $V=18.80$ cm^3/mole. The data analysis differs from that of the bcc phase for two reasons: (1) all of the points are measured in the limit $\omega_0/J > 1$, and (2) there are no systematic thermostatic measurements of J for pure hcp ^{3}He. We therefore use the values of J determined from T_2 measurements for the same specimens. That is, the value of $T_1(0)$ used for each molar volume is $(3/10)T_2'$, where T_2' is the experimentally measured value of T_2 in the adiabatic limit, $\omega_0/J \gg 1$; and the value of J used is that given by the relation $J/2\pi=T_1(0)/[kV^2]=(3/10)T_2'/[kV^2]$. The value $k=43.1\times10^{-12}$ selected for this plot is that calculated in Eq. (4.8) for the hcp phase in the Gaussian approximation for the time evolution of the dipolar motion. The absolute magnitude of J is therefore subject to the details of the approximation we use but the ratio of the values of J for the two specimens should be correct. The dashed line is the curve calculated from Eq. (4.8), the Gaussian approximation with $\omega_T=6.48J$; and the solid line labeled "adjusted Lorentzian" passing through the data points for $(\omega_0/J)^2 > 200$ is the curve calculated from Eq. (4.9), based on the Lorentzian approximation with $\omega_T=6.48J/\sqrt{2}$. A theoretically consistent fitting of the data to the Lorentzian approximation would require that the values of J be recalculated from $J/2\pi=(3/10)T_2'/(kV^2)$ with $k=[43.1/(\pi)^{1/2}]\times10^{-12}$. In that case the abscissae of all points would be shifted by a factor of $1/\pi$, and the points would then not fit either theoretical approximation very well. In other to reflect this, we have plotted the solid line labeled Lorentzian which is the curve calculated from Eq. 4.9, with $\omega_T=6.48J/\sqrt{2}\pi$. As in the bcc phase, the adjusted Lorentzian approximation gives the better fit at the largest measured values of ω_0/J; on the other hand, the points at lower frequencies seem to fit the Gaussian approximation very much better in the hcp phase than in the bcc phase. An empirical expression for the spectral function $J_1(\omega_0)$ which has been fitted to the data for the hcp phase (Miyoshi, 1970) is

$$\frac{J_1(\omega_0)}{J_1(0)} = \frac{1}{5}\exp\left[\frac{-1.6(\omega_0/\omega_T)^2}{(\omega_0/\omega_T)+1.0}\right]$$

with $\omega_T=6.48J$, the value given by the Gaussian approximation. In the limit $\omega_0/\omega_T \ll 1$, the relation is of the Gaussian form, $\exp[-1.6(\omega_0/\omega_T)^2]$; and in the high-frequency limit it approaches the Lorentzian form, $\exp[-1.6(\omega_0/\omega_T)]$.
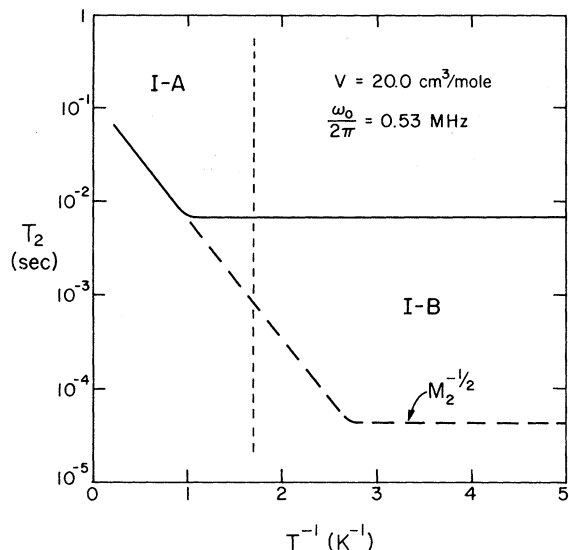
FIG. 21. T_2 vs T^{-1}. The figure shows a "typical" shape of the data curves for T_2 vs T^{-1} for $V = 20.4$ cm³ with a Larmor frequency of 0.53 MHz. The magnitude of T_2 is greatest near the melting curve, and decreases rapidly with the decrease in the vacancy population. When the characteristic vacancy tunneling frequency becomes less than the ³He tunneling frequency the ³He tunneling motion dominates the spin equilibrium process. The dashed line indicates the expected rigid lattice limit for T_2 in the absence of ³He tunneling motion for which there is no motional narrowing of the resonance line so that $T_2 \sim \gamma H_{\text{dipole}} \sim M_2^{-1/2}$, where M_2 is the Van Vleck second moment of the line.

dependence than T_1. In Region I-A we have equilibrium among the spins established by the motion of the vacancy waves; in Region I-B equilibrium is established by the tunneling motions. In Table I we have listed the T_2 experiments that have been done on pure ³He along with the parameters which describe the experiment.

Region I-A. The irreversible motion of the spins in the transverse plane occurs because of fluctuations in the local field due to the motion of vacancy waves through the field particles. The rate at which this irreversible motion takes place is given by Eq. (B1.12),

$$T_2^{-1} = \tfrac{2}{3}(M_2/\omega_0)\{\tfrac{3}{2}\eta + \tfrac{5}{2}[\eta/(1+\eta^2)] + [\eta/(1+4\eta^2)]\},$$

$$(4.10)$$

where $\eta = \omega_0 \tau_V$, M_2 is the Van Vleck second moment, and ω_0, τ_V^{-1} etc., are discussed below Eq. (4.3) and in Appendix A. The physical content of this result is much the same as that of Eq. (4.1) for T_1 in Region I-A. The irreversible motion of the spins in the transverse plane is caused by the fluctuations in the local field. The spins which are precessing about the z axis at frequency ω_0 will change motion in the transverse plane by coupling to $H_d(\omega_0) \perp$ as well as to $H_d(\omega=0)_z$. For the purposes of causing a spin flip, only $H_d(\omega_0) \perp$ will work. For causing spin motion in the transverse plane, both $H_d(\omega_0) \perp$ and $H_d(0)_z$ work. The first term in Eq. (4.10) comes from the z component of the dipolar field

$H_d(0)_z$ which causes irreversible transverse motion independent of the "looking" frequency. The second and third terms in Eq. (4.10) are the contribution to T_2^{-1} of $H_d(\omega_0) \perp$; they are essentially the same as the contribution of this field to T_1^{-1}; c.f. Eq. (4.2).

We may understand the qualitative dependence of T_2 on ω_d, ω_0, and τ_V by arguments similar to those below Eq. (4.3). In the limit $\omega_0 \to 0$, the spin sees the zero frequency component of $H_d(\omega_0 \to 0)$ as well as $H_d(0)_z$. Both fields contribute to the irreversible transverse motion and

$$1/T_2(\omega_0 \to 0) \mid_{zV} \sim (10/3)M_2\tau_V \sim (10/3)\omega_d^2\tau_V. \quad (4.11)$$

The spin random walks in the transverse plane in response to $H_d(\omega_0) \perp$ and $H_d(0)_z$. The argument below Eq. (4.5) applies. In the limit $\omega_0 \to +\infty$, the spin sees the ω_0 Fourier component of $H_d(\omega_0) \perp$ which goes to zero as $\omega_d(\omega_0 \tau_V)^{-1}$. If the spin moved in the transverse plane in response to $H_d(\omega_0) \perp$ only, then T_2 would go to $+\infty$ as $\omega_0 \to +\infty$, i.e., as the looking frequency goes out of synchronization with the fluctuating field. But the spin moves in the transverse plane in response to $H_d(0)_z$ as well as to $H_d(\omega_0) \perp$. Thus as $\omega_0 \to +\infty$ T_2 does not go to $+\infty$ but it goes to

$$1/T_2(\omega_0 \to \infty) = M_2\tau_V = (3/10)(1/T_{2(\omega_0 \to 0)}) \quad (4.12)$$

the value determined by $H_d(0)_z$ alone. At low frequencies, 30% of T_2^{-1} is due to $H_d(0)_z$, and 70% is due to $H_d(\omega_0) \perp$. As $\omega_0 \to +\infty$, the transverse component goes away because the spin can't see $H_d(\omega_0) \perp$ and only $H_d(0)_z$ remains. The result in Eq. (4.12), $T_2^{-1}(0) = (3/10)T_2^{-1}(+\infty)$, is called the ten-thirds effect. We discuss its observation in experiments below. Finally, we note that (1) the spin motions due to $H_d(0)_z$ occur entirely in the transverse plane—they are energy conserving and termed adiabatic, and (2) the spin motions due to $H_d(\omega_0) \perp$ occur in the transverse plane as well as out of the plane—they are not energy conserving and are termed nonadiabatic. The nonadiabatic motions contribute to T_1.

The temperature dependence of T_2 in Region I-A is due to the temperature dependence of τ_V. As the temperature is lowered T_2 becomes shorter until at sufficiently low temperature the particle motions leading to the fluctuating field are principally those of the tunneling excitations.

Region I-B. At the lowest temperatures, the important particle motions are those manifested in the tunneling excitations. In this region, $T < 1.5$ K at $V = 20.0$ cm³/mole, T_2 is given by Eq. (B2.1). We have, using the Gaussian approximation,

$$T_2^{-1} \mid_{\text{I-B}} = \tfrac{2}{3}(\tfrac{1}{2}\pi)^{1/2}(M_2/\omega_T)$$

$$\times \{\tfrac{3}{2} + \tfrac{5}{2} \exp[-\tfrac{1}{2}(\omega_0/\omega_T)^2] + \exp[-2(\omega_0/\omega_T)^2]\},$$

$$(4.13)$$

where ω_0 is the Larmor frequency, M_2 is the Van Vleck second moment, and ω_T is related to J as discussed above. The physical content of this result is the same as that above. Thus see the discussion below Eqs. (4.5, 4.6, and 4.11).

We note that there is a (10/3) effect in both Region I-A and I-B. The physics of the (10/3) effect is independent of the particle motion leading to $H_d(\omega_0)$ and $H_d(0)_z$.

The Nonadiabatic Frequency Shift

Conjugate to the (10/3) effect in the linewidth, T_2, is a small shift in the center of the resonance line, the nonadiabatic frequency shift (Kubo and Tomita, 1954). A detailed discussion of this shift is found in Appendix B. The maximum frequency shift away from ω_0 occurs when the motional frequency, due to tunneling or vacancy waves, is the same as the precession frequency, ω_0. Then the Fourier components of the non-adiabatic part of the dipolar interaction, $H_d(\omega_0)\perp$, have a maximum coupling to the Zeeman resonance at $\omega=\omega_0$. Using the Gaussian approximation to the correlation function, leads to a shift in the resonance frequency in Region I-B that is given by

$$+\delta\omega = \left[\frac{M_2}{3\omega_T}\left(\exp-\frac{\omega_0{}^2}{2\omega_T{}^2}\right)\phi\left(\frac{\omega_0}{\omega_T}\right)\right]$$
$$+2\left[\exp\left(-\frac{2\omega_0{}^2}{\omega_T{}^2}\right)\phi\left(\frac{2\omega_0}{\omega_T}\right)\right], \quad (4.14)$$

where

$$\phi\left(\frac{\omega_0}{\omega_T}\right) = \int_0^{\omega_0/\omega_T} \exp\left(\tfrac{1}{2}X^2\right) dX.$$

The maximum amplitude of $\delta\omega$ occurs when $\omega_0=\omega_T$; for $\omega_0=\omega_T$ the magnitude of $\delta\omega$ is approximately $1/T_2$. In the high- and low-field limits we have $(\omega_0/\omega_T)\gg 1$ or $(\omega_0/\omega_T)\ll 1$, $\delta\omega\rightarrow 0$. (Use of the Lorentzian approximation to the correlation function leads to a frequency shift of about the same magnitude as the Gaussian approximation but with a slightly different frequency dependence.)

4.4 T_2 Experiments, Results

Figure 22 shows the variation of T_2 with inverse temperature measured by Reich (1963) for a number of different molar volumes in both the bcc phase and the hcp phase. We see immediately a manifestation of the volume dependence of the parameters which characterize the particle motion excitations, ϕ, $\omega_3(V, 3)$, and J, and in turn determine the behavior of T_2. In Region I-A, we note that T_2 decreases rapidly as $1/T$ increases. A given value of T_2 occurs at higher temperatures as the molar volume decreases. These features are a consequence of the increase in ϕ with decreasing
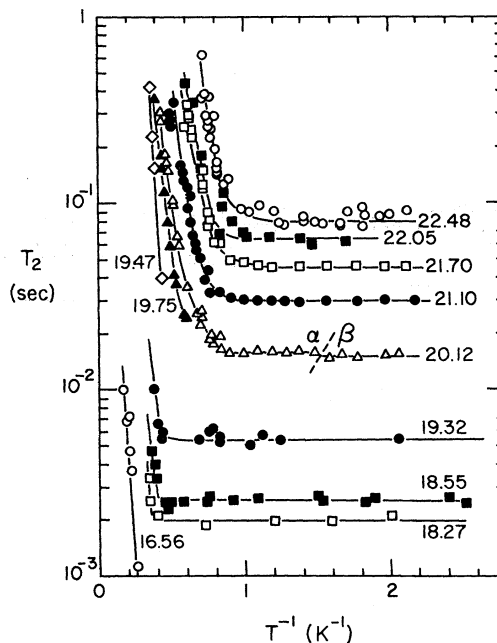

FIG. 22. Data of T_2 vs T^{-1} for various molar volumes. The figure shows the data for T_2 obtained by Reich (1963), ($V \geq$ 20.12 cm³/mole) and by Garwin and Landesman (1964) ($V \leq$ 19.32 cm³/mole). Additional measurements at larger molar volumes have been made by Richardson, Hunt, and Meyer (1965). The limiting low-temperature value is proportional to the exchange frequency J which can be seen to increase rapidly with volume. It is apparent from the high-temperature part of the curves, governed by the vacancy motion, that the activation energy of the vacancies decreases with volume.

molar volume. In Region I-B, T_2 is temperature independent. The details of the data shown in Fig. 22 have been successfully analyzed using Eqs. (4.10) and (4.13) to determine the parameters, ϕ, $\omega_3(V, 3)$, and J. The results so obtained are in good agreement with the values found from determination of these parameters from T_1 and diffusion measurements. Table I summarizes the region in volume and temperature which has been investigated in T_2 experiments.

Figure 23 shows the reduced plot of $[T_2(\omega_0=0)/T_2(\omega_0)]$ vs (ω_0/ω_T) for data in both the hcp and bcc phases (Richardson, 1965). As in the case of T_1 measurements, it is found that the Gaussian approximation to the correlation function yields a good fit to the data in the hcp phase. In the bcc phase, a more satisfactory fit is found by using a Lorentzian function (Richards, 1970). The general features of the (10/3) effect can also be readily seen; the value of T_2 in the high-field limit is about a factor of 3 greater than those in low fields. At the larger molar volumes, the T_2 values are systematically about 30% less than the T_1 values, even though the limit $(\omega_0/\omega_T)\ll 1$ is well established. In this limit, T_1 and T_2 should be equal. The source of this discrepancy is thought to be due to the spin diffusion in the in-
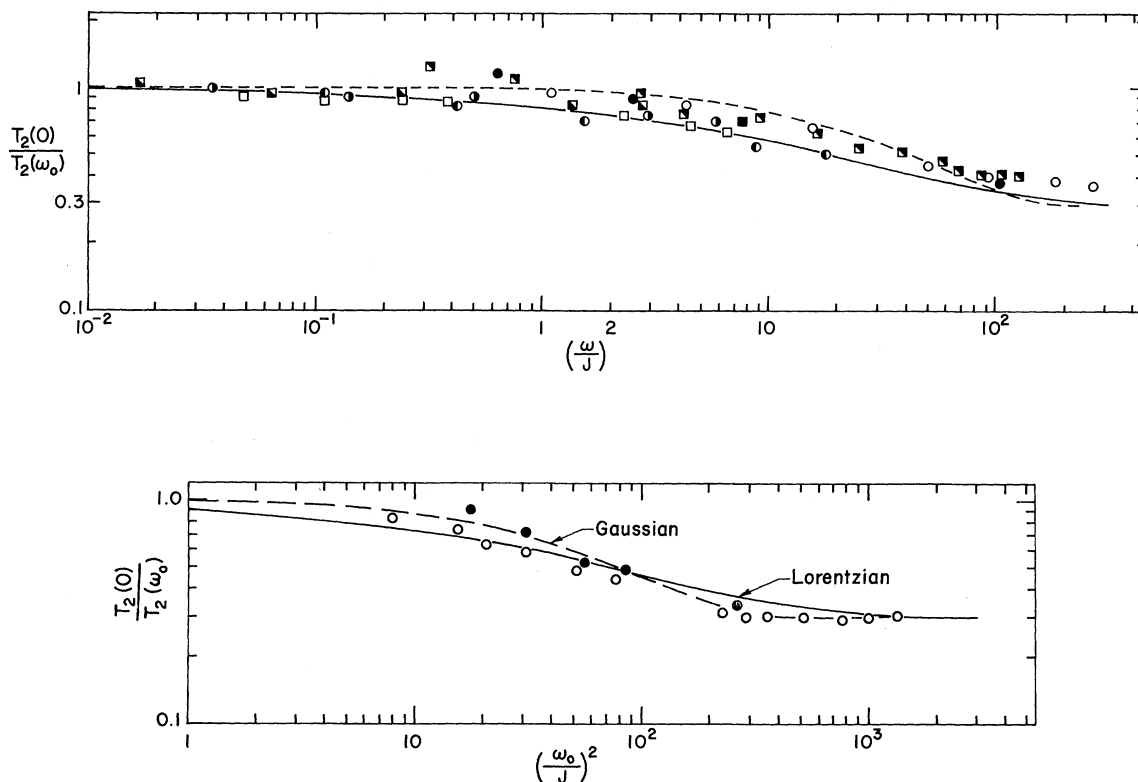
FIG. 23. (a) Reduced plot of T_2^{-1} for bcc ^{3}He. The points in the plot are the "reduced" values of T_2^{-1} for the data listed by Richardson, Hunt, and Meyer (1965) for the bcc phase. The same basic rules as those used in the construction of Fig. 20(a) are applied here. Values of J for each molar volume are obtained from the thermostatic measurements in bcc ^{3}He. The coefficient k in the expression $T_2(0) = T_1(0) = k(J/2\pi)V^2$ has the same value as that used in the plot for the reduced $T_1^{-1}|_{ZT}$ data, $k=30\times10^{-12}$. The lines represent the function

$$\frac{T_2(0)}{T_2(\omega_0)} = \frac{[J_1(0)+5/3 J_1(\omega_0)+2/3 J_1(2\omega_0)]}{10/3 J_1(0)}$$

with the solid line representing the values obtained using the spectral function of the Lorentzian approximation $J_1(\omega_0)/J_1(0) = \exp-(\omega_0/\omega_T)$, and the dashed line representing that of the spectral function of the Gaussian approximation $J_1(\omega_0)/J(0) = \exp-\frac{1}{2}(\omega_0/\omega_T)^2$. For the Gaussian approximation, the theoretical relation between ω_T and J is used, $\omega_T = (M_4/M_2)^{1/2}=4.76J$. For the Lorentzian approximation, the relation $\omega_T=4.16J$ is used rather than $\omega_T=4.76J/\sqrt{2}$, the theoretical value, for the same reasons as those discussed in the application of the $T_1^{-1}|_{ZT}$ data to a reduced plot [Fig. 20(a)]. The points for each different volume are shown with a different symbol to illustrate that, as in the case of the $T_1^{-1}|_{ZT}$ data, an adjustment of the parameter J of the points for a given volume may be made to give better coincidence with the functional form of $J_1(\omega_0)$ resulting from the Lorentzian approximation than that of the Gaussian approximation. Consistent fitting of the data to the Lorentzian relation, Eq. (4.9), produces values of J which are about a factor of 2 larger than those measured in the thermostatic experiments. In the figure, the data points for $V = 24.1$ cm^3/mole and $V = 24.6$ cm^3/mole have been omitted because they are measured in the limit $\omega_0/J\ll1$, where there is no ω_0 dependence of T_2, and because they are systematically 40% less than T_1 in the same limit and would therefore be misleading when presented in the figure. (b) Reduced Plot of T_2^{-1} for hcp ^{3}He. The points in the plot are a presentation of the reduced $(T_2)^{-1}$ data for the hcp phase of ^{3}He taken from the Table I in Richardson, Landesman, Hunt, and Meyer (1966). The same rules are used to plot the points here as those used, in the construction of Figure 20(b). There being no reliable thermostatic measurements of J for pure hcp ^{3}He, $T_2(0)$ is taken at $3/10 T_2'$ where T_2' is the value of T_2 measured in the high-field limit $\omega_0/J\gg1$. J is then calculated using the relation, $J/2\pi= (3/10) T_2'/(kV^2)$ where $k=43.1\times10^{-12}$ is the value derived from the Gaussian approximation. The open circles are the points listed for $V = 19.50$ cm^3/mole (which are incorrectly plotted in Fig. 1 of Richardson, Landesman, Hunt, and Meyer (1965), unfortunately exaggerating the fit of the data to the exact Gaussian relation). The closed circles are the data points for $V = 19.55$ cm^3/mole, for which T_2' is obtained by extrapolation of the theoretical relation for the Gaussian based spectral function $J_1(\omega_0)$ through the data points. The curves labeled Gaussian, the dashed line, and Lorentzian, the solid line, are plotted from Eq. (B1.11) using the same correspondences between ω_T and J as those used in Fig. 20(b). For the Gaussian line, $\omega_T=[M_4/M_2]^{1/2}=6.48$ J, and for the Lorentzian line, $\omega_T=6.48J/\sqrt{2}\pi$. The extra factor $1/\pi$ in the Lorentzian form occurs in order to make a consistent comparison between the limiting theoretical approximations and the data without recalculating the value of J. The open circles can easily be adjusted to fit the Gaussian curve by varying J by approximately 20%. They can also be adjusted to fit the Lorentzian relation but then the value of J used to do this would give a very large discrepancy for the T_1 data of the same specimen using the Lorentz relation. We therefore conclude that for hcp ^{3}He, the Gaussian relation provides the better approximate form for the correlation function. This relation will be used in subsequent calculations of the values of J for hcp ^{3}He.

homogeneous applied magnetic field since it occurs only for $T_1 \sim T_2 > 100$ msec and when D_z is largest.

The Nonadiabatic Frequency Shift—Experimental

The shift in the center position of the resonance line which occurs when $\omega_0 \approx \omega_T$ has been observed by Homer and Richards (1969a). The experimental technique involved forming a sample in the hcp phase ($V = 19.3$ cm^3, $\omega_T/2\pi = 0.82$ MHz) for which the value of ω_T would produce a maximum shift in a *c.w.* NMR spectrometer tuned at 0.82 MHz. The frequency of the maximum in the absorption signal in fixed external field H_0 was measured. Then the pressure on the solid was reduced to form a sample having a value of ω_T that would produce a negligible shift, and the frequency of the maximum in the absorption curve was measured again and observed to shift by 11 cycles. The resulting difference in the frequencies of the maxima was a direct measure of the shift.

The magnitude of the shift is in good agreement with the prediction of Eq. (4.14). The observation of the frequency shift and the details of the 10/3 effect serve to verify the correctness of the structure of models for nuclear relaxation. ^{3}He forms a system in which these effects are basically easier to measure and interpret since the characteristic motional frequency of the sample, ω_T and τ_v^{-1}, may be easily varied (through melting) while the sample is *in situ*.

4.5 Diffusion, Theory

The result of a typical magnetization diffusion experiment on pure ^{3}He is shown in Fig. 24. As with the T_2 experiment, the data is ordered by T^{-1} into two regions, I-A and I-B. In Region I-A, the diffusion of spin is due to the presence of vacancy waves in the system; in Region I-B, the vacancy waves have been frozen out and the diffusion of spin is due to the tunneling process. In Table I we have listed the magnetization diffusion experiments that have been done on pure ^{3}He.

Region I-A. In Region I-A the diffusion of the spins in the externally applied field gradient is due to the presence of a substantial number of vacancies in the system. The diffusion constant for ^{3}He motion has been derived in Appendix C and is given by

$$D_Z(V, 3) \approx A_Z(V, 3)\Delta^2 \tau_v^{-1} = A_Z(V, 3)\Delta^2 z\omega_3(V, 3)x_V,$$

$$\text{(4.15)}$$

where $A_Z(V, 3)$ is a constant of order 1, x_V is the vacancy concentration, $\omega_3(V, 3)$ is the frequency with which a ^{3}He atom tunnels into a vacancy, and z is the number of near neighbors. We write this diffusion constant in the form

$$D_Z(V, 3) = D_Z(V, 3, x=1)x_v, \quad \text{(4.16)}$$

where $D_Z(V, 3, 1) \propto \Delta^2 z\omega_3(V, 3)$ is only mildly volume dependent.
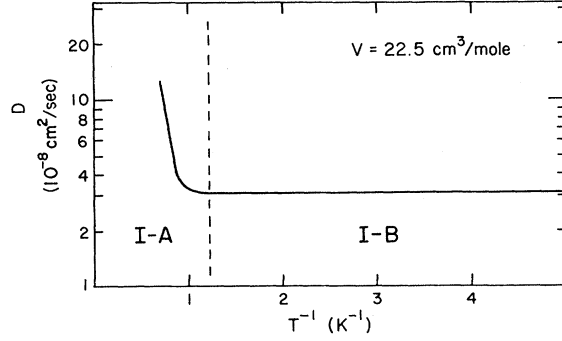

FIG. 24. D_Z vs T^{-1}. The figure shows the typical variation of Zeeman diffusion coefficient with temperature. At high temperatures the measured spin diffusion rate is dominated by the ^{3}He atoms drifting through the wake left by the vacancies tunneling through the lattice. The rate is given by $D_Z(V, 3) = A_Z(V, 3)\Delta^2 z\omega_3(V, 3)x_V$, where $A_Z(V, 3)$ is a constant of order 1, Δ^2 is the lattice parameter, z is the number of neighbors, $\omega_3(V, 3)$ is the tunneling frequency of a vacancy in ^{3}He, and x_V is the vacancy population. At sufficiently low temperatures, the ^{3}He tunneling dominates the observed diffusion rate, and one obtains a temperature-indipendent diffusion rate $D_Z(3, 3) = A_Z(3, 3)\Delta^2 J$, where A_Z is a constant of order 1, and J is the ^{3}He tunneling frequency.

Region I-B. As the temperature is lowered, the vacancies are frozen out, and the tunneling motion of pairs of ^{3}He particles leads to their diffusion in the field gradient. The diffusion constant for this case is derived in Appendix C and is given by

$$D_Z(3, 3) = A_Z(33)\Delta^2 J, \quad \text{(4.17)}$$

where $A_Z(33)$ is a constant of order one, and J is the tunneling frequency. The diffusion constant $D_Z(V, 3)$ is equal to the diffusion constant $D_Z(33)$ at $z\omega_3(V, 3)x_V = J$ for $V = 20.0$ cm^3/mole at $T = 1.5$ K. Note: this is the same condition and temperature as that involved in the transition from Region I-A to Region I-B in a T_2 experiment.

4.6 Diffusion Experiments, Results

Reich (1963) has measured D_z for various molar volumes in Region I-A; his results are shown in Fig. 25. The strong temperature dependence of D_Z at high temperatures may be readily analyzed to yield the characteristic temperature for the excitation of a vacancy wave, ϕ, and the tunneling frequency for vacancies, $\omega_3(V, 3)$. The variation in D_Z with volume in this region is a consequence of the changes in ϕ with volume. The results of the analysis of D_z data are summarized in the final portion of this section where they are compared with the results obtained by other experimental techniques.

In Region I-B, the diffusion coefficient is temperature independent and determined by the ^{3}He tunneling frequency, J. From Eq. (4.17) we expect $D_Z \propto J$. In Fig. 26 the values of D_Z obtained by Thompson, Hunt, and Meyer (1964) are plotted against $(J/2\pi)$. It is clear
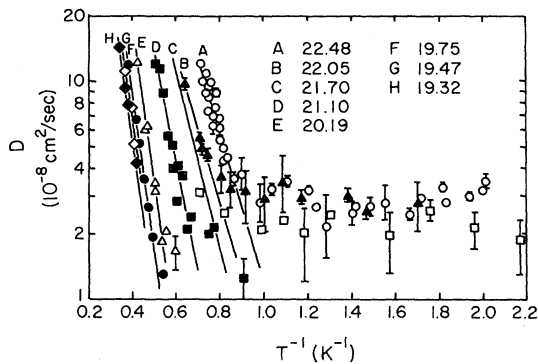
FIG. 25. D_Z vs T^{-1} for various molar volumes. The figure shows the data of Reich (1963) for the diffusion coefficient D_Z versus inverse temperature. The labeling of the data points corresponds to the varous molar volumes at which the measurements were made. At high temperatures the diffusion rate is determined by the vacancy diffusion; the straight lines may be used to calculate the parameters ϕ, the vacancy activation energy, and $\omega_3(V, 3)$, the vacancy tunneling frequency. At lower temperatures the observed diffusion rate is governed by the ^{3}He tunneling and is temperature independent. [After Reich (1963).]

from this plot that D_Z is proportional to J. The solid line in the figure through the data fits the relation $D_Z = (4.4\pm0.4)\times(J/2\pi)\Delta^2$. The value of the coefficient A in Eq. (4.17) has been calculated by Redfield and Yu (1968, 1969) to be 4.12, in excellent agreement with the experiment.

The energy diffusion coefficient, D_E, which is a measure of the rate of energy transfer through the sample has been measured by Hunt and Thompson (1968) in a novel pulse experiment. Their experiment in outline is as follows:

(1) Local spin heating is achieved over a narrow slab of a sample placed in a large magnetic field gradient by "burning a hole" in the inhomogeneously broadened magnetic resonance line.

(2) The recovery of the line shape, with the hole burned in it, to the preburning shape is achieved through diffusion of the magnetic energy through the specimen.

(3) The experiment is performed at T^{-1} corresponding to Region II-B, i.e., at low temperature where the Zeeman system, tunneling excitations, and mass fluctuation waves come to a common equilibrium.

(4) The recovery rate is measured by observing the rate at which the "hole" is broadened as in Fig. 27.

Experimentally Hunt and Thompson looked at the time evolution of the Fourier transform of the hole by observing the free induction decay following the application of a small rf pulse (4°) tuned at a slightly different precession frequency. The time evolution of the beat pattern of the 4° pulses is measured to determine D_E. The whole experiment must be performed in

times short compared with T_1, so it is done with the specimen cooled to Region II. In this region, the strongly coupled excitation systems diffuse together with a single diffusion constant given by

$$D_E = (C_Z D_Z + C_T D_T + C_{MF} D_{MF})/(C_Z + C_T + C_{MF}).$$

$$(4.18)$$

From analysis of the free induction decay, D_E is obtained. Then using Eq. (4.8) and D_Z as measured in a conventional diffusion experiment, D_T can be found. The value of D_T obtained by Hunt and Thompson is $(9.4\pm2.0)(J/2\pi)a^2$. [Redfield and Yu (1968, 1969) have calculated the value $4(J/2\pi)a^2$.)] The experimental situation with regard to diffusion experiments at low temperature needs clarification (Giffard, 1971).

4.7 Properties of the Excitations in Pure ^{3}He

Here we summarize the properties of the excitations in pure solid ^{3}He which have been measured in the NMR experiments we have discussed above and compare the results of NMR measurements of the properties of the excitations with measurements using other techniques.

We begin by observing that the excitations in pure solid ^{3}He can be described by four parameters: the phonons θ_D; vacancy waves ϕ and $\omega_3(V, 3)$; and the tunneling excitations J. NMR experiments on pure ^{3}He do not see the phonons although these excitations are involved in the energy flow chain. Measurements of θ_D come directly from thermostatic measurements, C_V, $(dP/dT)|_V$, etc. The other three parameters, ϕ,
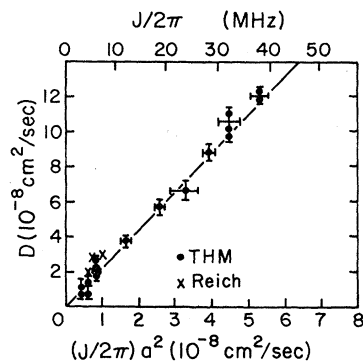

FIG. 26. The diffusion constant D_Z in the bcc phase. The figure shows the limiting low temperature values of D_Z measured by Thompson, Hunt, and Meyer (1967), shown with circles and error bars, and by Reich (1963), shown with crosses. The data points are shown as a function of the quantity $(J/2\pi)$ $a^2\times10^{-8}$ cm^2 sec^{-1} to emphasize that D_Z is determined by the tunneling motion of the ^{3}He atoms. The value of J in the figure should be divided by a factor 2 to conform with the definition of the tunneling energy used in this work. The straight line fits the equation $D_Z = (4.4\pm0.4)\times(J'/2/2\pi)\Delta^2$ cm^2/sec^{-1}, where J' is the value of J used by Thompson, Hunt, and Meyer (1967), and Δ is the lattice constant. The calculation by Redfield and Yu (1968, 1969) predicts $D_Z = 4.12$ $(J/2\pi)\Delta^2$ cm^3/sec for the bcc lattice. [After Thompson, Hunt, and Meyer (1967)].
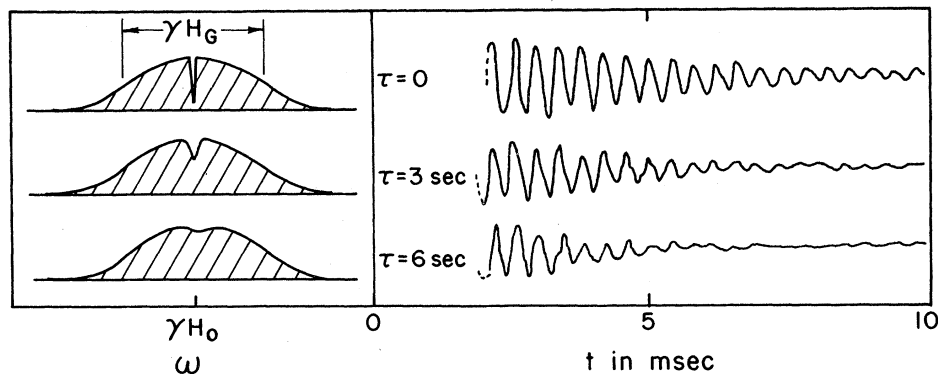
FIG. 27. Measurement of the rate of spin energy diffusion. The figure shows measurements of the time evolution of the recovery of the spin system to thermal equilibrium after a "hole burning" experiment. (See Fig. 6.) The sketches at the left represent the schematic time evolution of the Gaussian hole in the inhomogeneously broadened resonance line. The spin system recovers to thermal equilibrium through spatial diffusion of the energy in the spin system with the diffusion constant $D_E = (k_Z D_Z + k_T D_T)/(k_Z + k_T)$. The specimen is locally heated by application of a saturating 2-mG rf field, h_1, for about 3 sec producing the "hole" in the line at $\tau = 0$. The recovery of the system is monitored by observing the Gaussian free precession signals following small rf pulses ($4°$) applied at various times τ after the saturating field is turned off. The nuclear signal following the $4°$ pulse is the Fourier transform of the line shape; it consists of two components, a very short-lived component due to the entire side resonance line, and a long-lived component due to the narrow "hole". The sketches at the right of the figure represent the long component of the free precession signals after $4°$ pulses applied every 3 seconds. The beat pattern occurs because the frequency of the $4°$ pulse is detuned by a small amount $\delta\omega$ from that of the saturating signal. The $4°$ probe pulse at $\omega_0 + \delta\omega$ thus beats with the hole signal at frequency ω_0. The envelope of the beat pattern is given by $G(t, \tau) = \exp[-\frac{1}{2}(\sigma_0^2 + 2\gamma G^2 D\tau)t^2]$, where σ_0 is the rms width of the hole at $\tau = 0$, G is the field gradient, and t is the time elapsed after the $4°$ pulse. The traces shown are for a solid in which $J/2\pi = 7$ MHz, and at $T \sim 0.1$K. The top trace ($\tau = 0$) corresponds to $\sigma_0 = 2.3 \times 10^2$ rad/sec. [After Hunt and Thompson (1968).]

$\omega_3(V, 3)$, and J, are most easily studied in NMR experiments. The magnitude of these parameters determined in measurements of T_1, T_2, and the diffusion constants D_Z and D_E are all internally consistent and in reasonable

agreement with their values determined from thermostatic measurements. The experimental sources of the parameters we have derived from NMR measurements are listed in Table II.

TABLE II. Experiments used to determine basic parameters: J, θ, and $\omega_3(V, 3)$.[a]

Parameter	See Figure	Data Used
J	31 and 32	Panczyk and Adams (1969); Hatton and Giffard (1967); Bernier and Landesman (1969); Richards, Hatton and Giffard (1965); Richardson, Hunt, and Meyer (1965); Garwin and Landesman (1964); Reich (1963)
θ_D	28	Sample and Swenson (1967); Edwards and Pandorf (1965, 1966, 1968)
ϕ	29 and 50	Reich (1963); Richardson, Hunt, and Meyer (1965); Sample and Swenson (1967); Giffard and Hatton (1967); Miyoshi, Greenberg, Cotts, and Richardson (1970)
$\omega_V(3, 3)$	30	Reich (1963); Richardson, Hunt, and Meyer (1965); Giffard and Hatton (1967)

[a] For each of the parameters, J, θ_D, ϕ, and $\omega_3(V, 3)$ we have tabulated the references to the experiments from which the data is drawn.

Phonons, θ_D

Four recent specific heat measurements, those of Sample and Swenson (1967), and Edwards and Pandorf (1965, 1966, 1968) provide the most reliable data on the Debye temperature. In Fig. 28 we plot θ_D vs molar volume for bcc and hcp ^{3}He. We use the values of θ_D from these plots to characterize the phonon spectrum.

Vacancy Waves, ϕ and $\omega_3(V, 3)$

In the discussion of NMR experiments in pure ^{3}He in Sec. 4, we have seen that the behavior of T_1, T_2, and D_z at high temperatures is due to the vacancy wave excitations. In Region II-A (to be discussed in Sec. 6), the behavior of T_1 is due to the coupling of the vacancy wave excitations to the tunneling excitations. Thus there are within the body of NMR data four independent experiments which are sensitive to the characteristics of the vacancy wave excitations. The vacancy wave excitations have the dispersion relation given in Eq. (3.10); they are characterized by the excitation temperature ϕ and the tunneling frequency $\omega_3(V, 3)$. In Fig. 29 we have plotted ϕ vs molar volume; we have used (1) the diffusion constant measurements of
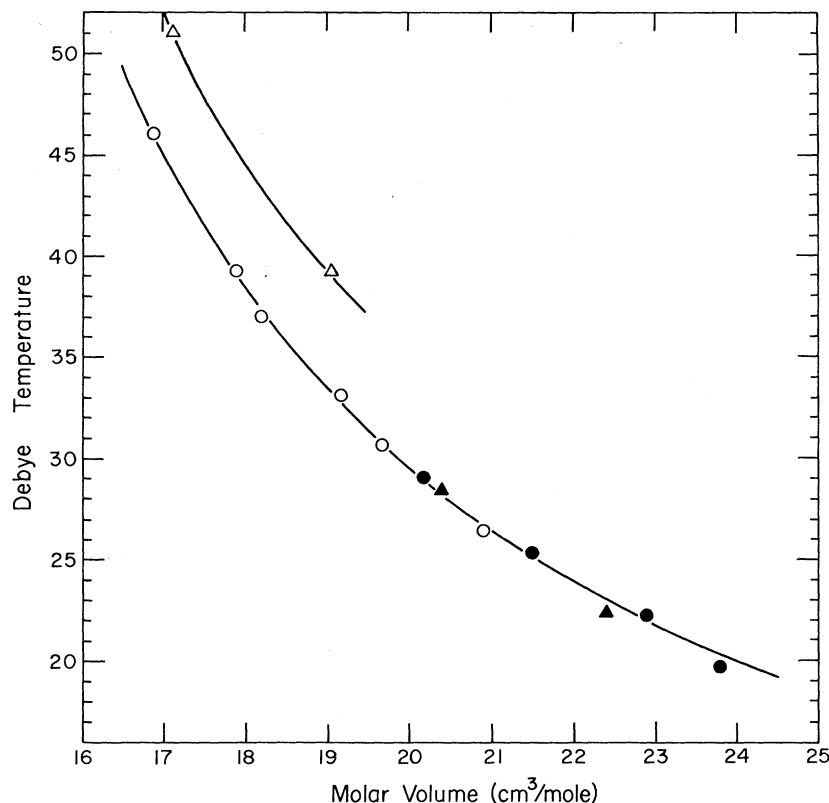
FIG. 28. Debye Temperature. The data are from the following specific heat measurements: △, hcp ³He: Sample and Swenson (1967); ○, hcp ³He: Edwards and Pandorf (1965); ●, bcc ³He: Sample and Swenson (1967); ▲, Edwards and Pandorf (1968). In calculating the properties of the phonons we use the numbers from the smooth curve through the data.

Reich in Region I-A, Fig. 25 to determine ϕ at 18.0 cm³/mole$\leq V \leq$23 cm³/mole using Eq. (4.15); (2) the T_1 measurements of Richardson, Hunt, and Meyer (1965), Fig. 19, in Region I-A to determine ϕ at V=20.4 cm³/mole using Eq. (4.1), and (3) the T_1 measurements of Giffard and Hatton (1967) in Region II-A to determine ϕ at V=20.0 cm³/mole. We have also plotted the values of ϕ from analysis of the specific heat data of Sample and Swenson of Fig. 29. First we note the good agreement between the three independent NMR determinations of ϕ and the good agreement between the NMR values of ϕ and those from the specific heat data. The comparison of different experimental determinations of ϕ is limited because only the diffusion measurements of Reich have been carried out over a wide range of molar volumes. However, at V=20.0 cm³/mole where each of the experiments yields a value of ϕ, there is good agreement. On Fig. 29 we have also plotted the values of ϕ from the theoretical calculations of Hetherington (1968).

The same data which have been analyzed above to yield values of ϕ also yields values of $\omega_3(V, 3)$. In Fig. 30 we have plotted $\omega_3(V, 3)$ vs V: we have used (1) the diffusion data of Reich in Region I-A, Fig. 25, and Eq. (4.15), (2) the T_1 data of Reich at V=20.1 cm³/mole at the temperature of the T_1 minimum (curve E in

Fig. 18), (3) the T_1 data of Richardson, Hunt, and Meyer at V=20.4 cm³/mole at the temperature of the T_1 minimum (Fig. 19) and (4) the T_1 data of Giffard and Hatton (1967) in Region II-A. In Fig. 30, we have also drawn a smooth curve determined from the theoretical calculation of $\omega_3(V, 3)$ outlined at the end of Appendix A.1 and a smooth curve determined from the calculations of Hetherington (1968). We note that the order of magnitude of the four independent experimental determinations of $\omega_3(V, 3)$ is in good agreement with one another and in moderate agreement with the theory of Hetherington.[10] As with ϕ above, the bulk of the independent determinations are near V=20.0 cm³/mole. The volume dependence of $\omega_3(V, 3)$ which is

---

[10] A theory of the vacancy excitation temperature is as difficult as a theory of the ground state in that like the theory of the ground state it involves the cancellation of two large numbers to get a small one. The vacancy excitation temperature (ignoring the bandwidth) is given by

$$\phi = Pv + E_0 - E_d,$$

where Pv is the energy required to make the empty space, E_0 is the energy associated with putting the removed particle on the surface, and E_d is the energy gained by the relaxation of the lattice in the vicinity of the vacancy site. We have $E_0 \approx k_B \theta_D \approx 30$K at V=20.0 cm³/mole. Since ϕ is less than Pv, Fig. 50, we have $|E_d| > |E_0| \approx 30$K. The results of Hetherington are quite reasonable.

given by the data from the diffusion experiment is in reasonable agreement with the volume dependence of the theory of Hetherington. The vacancy tunneling frequencies calculated in Appendix A.1 are slightly smaller than the experimentally determined values. This is not surprising since the calculation in Appendix A.1 did not attempt to account for the distortion of the wavefunction for particles that are near neighbors of a vacancy site. This distortion is very important; it leads to the increase in magnitude of $\omega_3(V, 3)$ and to a decrease in ϕ from the undistorted value to a value comparable with Pv.

We see that the parameters which characterize the vacancy wave excitations are quite well determined by

FIG. 30. Bandwidth vs molar volume. The bandwidth is calculated from the data in the following sources: $\times$, Reich (1963), diffusion; $\bigcirc$, Richardson, Hunt and Meyer (1965), T_1 in the topology $Z-VP$. $\triangle$, Giffard and Hatton (1967), T_1 in the Topology $ZT-VP$. The results of the theory of Hetherington are shown as are the results of the calculation from Appendix A. Both theory and experiment suggest that the vacancy band width is relatively insensitive to volume.

the NMR data.[11] The magnitude of these parameters as determined by the experiments is in good qualitative agreement with theory. To date, only the theory of Hetherington has addressed itself to calculating these parameters from first principles. This is unfortunate because the calculation of ϕ and particularly $\omega_3(V, 3)$ is a sensitive test of the validity of a theory of the ground state and excited state properties of quantum crystals.

The Values of J

The basic zero-point tunneling motion between ^{3}He atoms, characterized by the frequency J, appears as a fundamental parameter of all the nuclear resonance experiments in the temperature Region I-B. There is excellent self-consistency between the values of J deduced in (1) magnetization diffusion measurements,
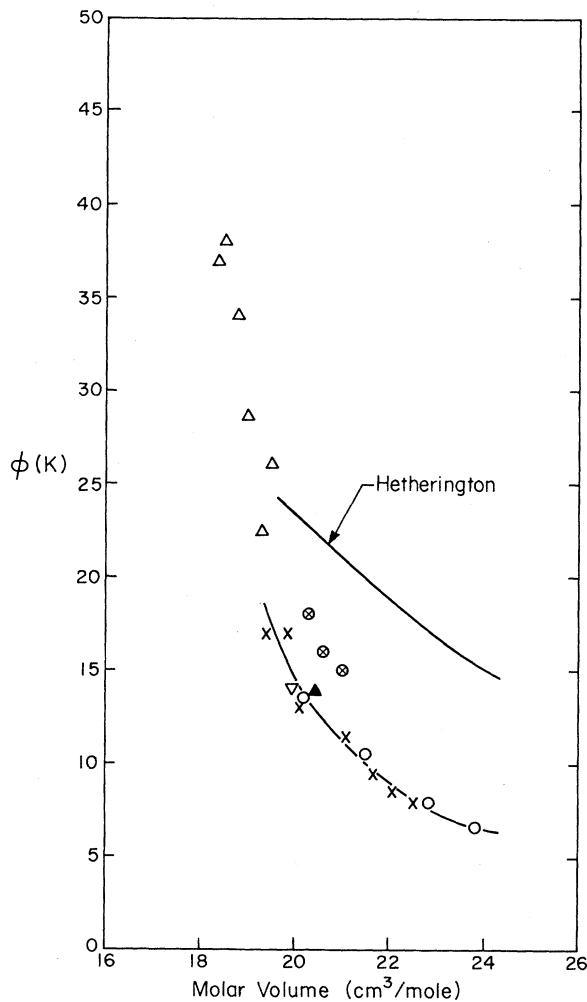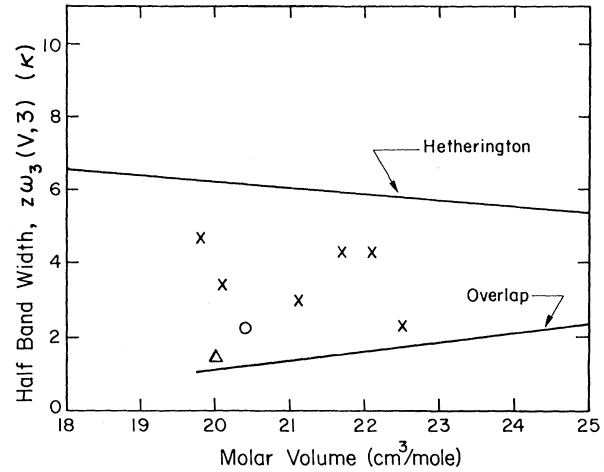

FIG. 29. Vacancy excitation temperature vs molar volume. The excitation temperature is calculated from the data in the following sources: For bcc ^{3}He: $\bigcirc$, Sample and Swenson (1967), specific heat; $\times$, Reich (1963), diffusion; $\triangledown$, Giffard and Hatton (1967), T_1 data in the topology $ZT-VP$; $\blacktriangle$, Richardson, Hunt, and Meyer (1965), T_1 data in the topology $Z-CP$. For hcp ^{3}He: $\triangle$, Reich (1963), diffusion. For hcp ^{3}He–^{4}He; $\otimes$, Miyoshi, Cotts, Greenberg, and Richardson (1970). These data are taken from T_1 and diffusion measurements at 2% ^{3}He in ^{4}He.

---

[11] In the literature there appears a suggestion that the tunneling frequency (or diffusion constant) found from the data of Giffard and Hatton (1967) and Bernier (1970) does not agree with the tunneling frequency determined from the high-frequency data, the diffusion data of Reich, etc. Most of this discrepancy is due to an erroneous factor of 14 in the combination of Eqs. (3) and (4) in Giffard and Hatton. In place of their Eq. (3), write $\eta_D = \tau_D^{-1} = 2(z-1)x_v/\tau_v$. Now the diffusion constant is related to τ_v by

$$6D/\Delta^2 = 2(z-1)x_v/\tau_v.$$

This relation is apparent upon considering relaxation in Region I-A from either of two views, that of diffusion or that of the vacancy tunneling. From the definition of η_D, we have

$$\eta_D = t_D^{-1} = 6D/\Delta^2.$$

Equations (3) and (4) of Hatton and Giffard give $\eta_D = 84D/\Delta^2$. When the correct factor of 14 is used, the vacancy tunneling frequency from high and low temperature data are in good agreement. See Fig. 30.
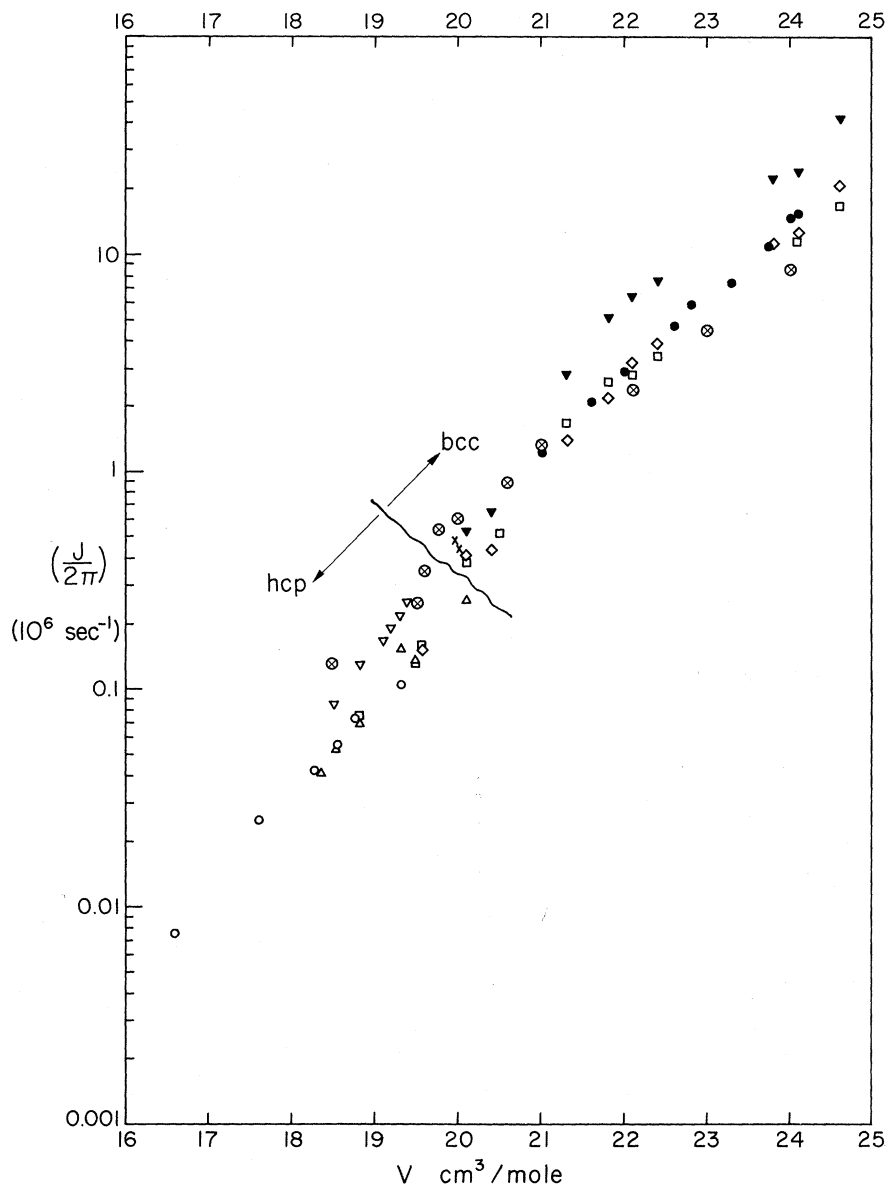
FIG. 31. Experimental Values of J. The figure presents the results of a number of different measurements of the value of J as a function of volume. The types of points fall in two categories: (a) thermostatic measurements and (b) relaxation measurements. The thermostatic measurements derive values of J from thermodynamic quantities calculated with the high-temperature expansion of the partition function for the spin Hamiltonian $\text{Tr}[\exp(\mathcal{3C}/kT)]$ and do not depend upon the details of the approximation used to describe the time evolution of the local dipolar field. There are three kinds of thermostatic measurements which have been made on ^{3}He which yield information about J: Susceptibility measurements, dP/dT measurements, and nuclear relaxation heat capacity measurements. The departure from Curies Law in susceptibility measurements produces information about the sign of J as well as the magnitude. None of the susceptibility results are shown in the figure. Reliable susceptibility measurements have been made by Anderson, Reese, and Wheatley (1961), Pipes and Fairbank (1969), Sites, Osheroff, Richardson, and Lee (1969), and by Kirk, Osgood, and Garber (1969). All of these experiments yield a negative value of J, the magnitude of which is good agreement with other thermostatic measurements. The data of Kirk, Osgood, and Garber (1969) extends to the lowest temperatures $\sim$5mK and covers the widest range of molar volumes. The second class of thermostatic measurement which has been made is the measurement of isochoric pressure change of the solid with temperature. The value of J is determined from the easily derived relation

$$\left(\frac{\partial P}{\partial T}\right)_V = -\left(\frac{\partial \ln |J|}{\partial \ln V}\right)\frac{C_T}{V}$$

where $C_T \simeq 3(\hbar J/k_B t)^2$ for bcc ^{3}He. The measurements have been reported by Panczyk, Scribner, Straty, and Adams (1967), and by Panczyk and Adams (1969) for the bcc phase. The data points of the latter are shown as solid circles in the figure. The third type

of thermostatic measurement is the heat capacity derived from the determination of the topological factors in measurements of the spin lattice equilibrium times at low temperatures (region II) where a long component of the relaxation rate is given by

$$T_1^{-1} = [1 + (k_z/k_T)]^{-1},$$

where $(T^{-1})_{\text{intrinsic}}$ is the frequency independent, and where

$$k_Z/k_T = (\hbar\omega_0)^2/z(\hbar J)^2 = (2/3z)(\omega_0/J)^2$$

z is the number of neighbors, and ω_0 is the Larmor frequency. The time $T_{\text{intrinsic}}$ is the coupling rate of the tunneling system to the lattice. The determination of J from such measurements is made by studying the Larmor frequency dependence of the long relaxation rate. The heat capacity determinations of J by such a technique for pure ^{3}He have been made by Hatton and Giffard (1967) and by Bernier and Landesman (1969), and are shown with the symbol $\otimes$. Both measurements are near 20 cm^3/mole. More extensive measurements as a function of volume have been made by Richards, Hatton, and Giffard (1965) with specimens containing $\sim$200 ppm ^{4}He impurities, and are shown with the symbol $\otimes$. The effect of ^{4}He impurities is to add an additional heat reservoir, due to the mass fluctuation wave bath, in series with the spin-relaxation process so that value of J determined is systematically too large. Also shown in the figure are the values of $(J/2\pi)$ determined from studies of T_{ZT} and T_2. The magnitude of J obtained in such studies depends upon the details of the spectral function. The source of the points in the figure, as well as the spectral function used in the calculation of J is tabulated below:

Experiment	Symbol	Spectral function
Richards, Hatton, and Giffard T_1 (1965) (hcp data only)	$\triangledown$	Gaussian
Richardson, Hunt and Meyer (1965), Richardson, Landesman, Hunt, and Mayer (1966) T_1	$\diamondsuit$	"Self-consistent empirical function"
Richardson, Hunt, and Meyer (1965), T_1 data fitted by Richards (1970)	$\blacktriangledown$	Lorentzian
Garwin and Landesman (1964) T_2 data	$\bigcirc$	Gaussian
Reich (1963) T_2 data hcp phase	$\triangle$	Gaussian
Richardson, Hunt, and Meyer (1965) T_2 data	$\square$	Self consistent empirical function.

Measurements of T_1 and T_2 in the bcc phase have also been made by Reich with substantially good agreement with Richardson, Hunt, and Meyer (1965). The measurements of Richards, Hatton, and Giffard (1965) of T_1 in the bcc phase (not shown in the figure) analysed with the Gaussian correlation function, yield values of J which are in substantial agreement with the values of J obtained in the "heat capacity" experiments shown with symbol $\otimes$. At the larger molar volumes, the values of T_1 are in disagreement with those obtained by Richardson, Hunt, and Meyer, being systematically shorter, perhaps through a difference in the volume determination.

(2) T_2 measurements, (3) measurements of the limiting value of T_1 in low fields, (4) measurements of the Larmor frequency dependence of T_1, and (5) measurements of the nonadiabatic frequency shift. In all of these measurements, however, the exact magnitude of J depends upon the explicit time evolution of the microscopic dipolar field due to the tunneling motion, i.e., upon the validity of the Gaussian or Lorentzian approximations for the correlation function. The value of J determined from a measurement of T_2, for instance, will be larger by a factor $\pi^{1/2}$ if the Lorentzian correlation function is used rather than the Gaussian correlation function. The same factor applies to the calculation of J in almost all of the resonance relaxation experiments. There is one class of nuclear relaxation experiments which does not depend upon the details of the correlation function and still produces information about the magnitude of J. These are T_1 measurements in Region II, in which the topological factors related to the heat capacity of the Zeeman and tunneling energy reservoirs appear as coefficients of the relaxation rates in the form $T_1 = [1 + (k_Z/k_T)]T_{\text{intrinsic}}$. (See Sec. 6 and Appendix A). We have

$$T_1^{-1} = [1 + (k_Z/k_T)]^{-1}T_{\text{intrinsic}}^{-1}$$

$$= \left[1 + \frac{2}{3z}\left(\frac{\omega_0}{J}\right)^2\right]^{-1} T_{\text{intrinsic}}^{-1},$$

where z is the number of nearest neighbors, and where $T_{\text{intrinsic}}$ does not depend upon ω_0. The coefficients k_Z and k_T are derived (see Appendix D) without recourse to an approximation for the correlation function, thus experiments in which T_1 is measured in Region II at different Larmor frequencies yield an independent value of J which can be used to scale the values of J obtained in the other nuclear resonance experiments. This procedure eliminates the possible systematic uncertainties in J that could arise due to any of the errors in approximating the time evolution of the dipolar interaction.

The values of $J/2\pi$ obtained in NMR relaxation experiments are shown in Figs. 31 and 32. We wish to reiterate at this point that the definition of J used in this work differs from that used in most previous papers on NMR in solid helium. We take J to be defined by the Hamiltonian, $\mathcal{H}_T = -2\hbar J \sum'_{RR} \sigma_R \cdot \sigma_{R'}$, Eq. (3.16). This definition is selected to be in agreement with the convention used in most of the reports of thermostatic measurements. In Fig. 32, the values of $J/2\pi$ obtained by Adams and co-workers (Panczyk, 1967, 1969) from elegant low-temperature measurements of the pressure changes in the solid at constant volume, are compared with the values of $J/2\pi$ obtained in the NMR work. The agreement is excellent. Unfortunately, the method does not have sufficient sensitivity to measure the smaller values of $J/2\pi$ for
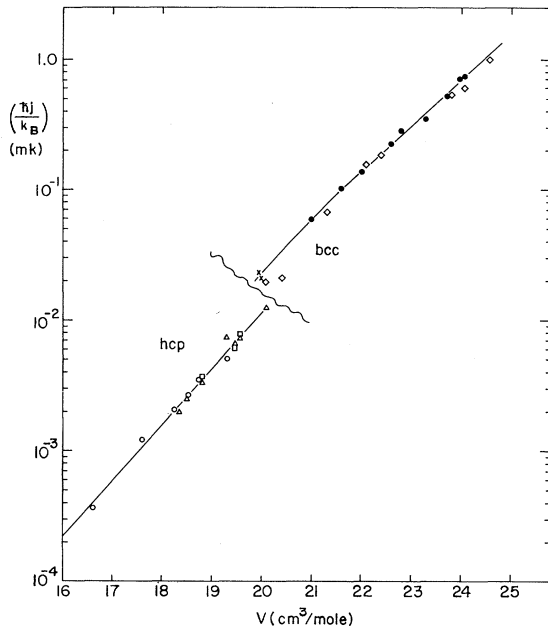
FIG. 32. Values of $(\hbar J/k_B)$. The lines in the figure represent the "smoothed" values of $(\hbar J/k_B)$ in mK used for calculations in this paper. The values are our best guess for the interpretation of all of the experiments to date to obtain the tunneling energy of ^{3}He atoms. The data points upon which the lines are based are shown; the symbols correspond to the same points in Fig. 31. In the bcc phase we have used the thermostatic values of J and the values from the self-consistent correlation function for T_1 fitted to the thermostatic measurements. In the hcp phase, we use the values of J obtained in T_2 measurements. The T_2 data were selected because of the internal consistency and because the Gaussian approximation for the correlation function probably does not lead to a serious error in determining J from T_2 in the hcp phase.

molar volumes less than 21 cm^3 at experimental temperatures greater than 12 mK.

The magnitude and sign of J can be determined in nuclear magnetic susceptibility measurements by fitting the observed size of the nuclear absorption signal at various temperatures to a Curie–Weiss Law of the form $\chi = C/(T-H)$, where C is the Curie Constant, and $H = z\hbar J/4k_B$ is the Weiss Constant. Most of the early experiments measuring the nuclear susceptibility were unreliable for determining either the magnitude or sign of J due to insufficient knowledge about the spin relaxation processes, the effects of ^{4}He impurities, and insufficient resolution of susceptibility at the experimental temperatures employed, typically greater than 50 mK. With the development of new techniques to reach and maintain low temperatures, there have been a number of reliable susceptibility measurements in solid ^{3}He. (See Fig. 31.) All of these experiments deduce values of $J/2\pi$ in agreement with those in Fig. 32. These experiments also give a negative sign to J corresponding to antiparallel spin alignment in the lowest energy state. The consequence of the negative J is that as the solid is cooled to very low temperatures it will undergo an antiferromagnetic spin ordering transition. The transition is expected to occur at a temperature given by

$$T_N = 2.78(\hbar J/k_B), \quad \text{(bcc)},$$

$$T_N = 4.2(\hbar J/k_B), \quad \text{(hcp)}.$$

Thus for the largest possible molar volume and largest value of J, the solid should undergo a Fermi ordering transition at $2mk$ which results from the motional freedom due to the tunneling and the Fermi statistics of the ^{3}He.

In Fig. 32, the values of $J/2\pi$ represent the most accurate available interpretation of all experimental

data to date. Here $J/2\pi$ is probably accurate to within 10% everywhere on the curve. Probably the most spectacular feature of Fig. 32 is the huge change J makes with changes in volume. At 20 cm^3/mole, $\gamma_J = d(\ln J)/d(\ln V) = +20$. The steep change in J with volume is understood theoretically as resulting from the compacting of the wavefunction of an atom in the vicinity of its lattice site as the volume decreases.

5. EXCITATIONS IN DILUTE ^{3}He–^{4}He MIXTURES

5.1 Mass Fluctuation Waves

In pure solid ^{3}He, there are three excitations of interest: the phonons, the vacancy waves, and the tunneling excitations. In solid ^{3}He with small concentrations of ^{4}He, there are these three pure crystal excitations as well as a new excitation associated with the motion of the ^{4}He atom in the ^{3}He medium. In solid ^{4}He with small concentrations of ^{3}He, there are phonons, vacancy waves, and a new excitation associated with the motion of the ^{3}He through the ^{4}He medium. In both dilute limits a new excitation appears, the mass fluctuation wave. We discuss it and its coupling to the pure crystal excitations in this section.

Our discussion of the excitations due to particle motion in the case of pure ^{3}He began with the Hamiltonian, $\mathcal{H}_{PM}$, given by Eq. (3.1). This model Hamiltonian was constructed from the most important matrix elements of the Hamiltonian

$$\mathcal{H} = \sum_{i=1}^{N} T_3(i) + \tfrac{1}{2}\sum_{ij}' v^e(ij), \tag{5.1}$$

where $T_3(i) = p_i^2/2m_3$, and $v^e(ij)$ is an appropriate effective interaction for low-lying harmonic oscillator states. The important matrix elements of $\mathcal{H}$ in Eq. (5.1) are, in addition to the ground-state matrix

elements $\langle \Phi_0 | \mathcal{3C} | \Phi_0 \rangle$, those involving empty lattice sites and doubly occupied lattice sites. In Fig. 33 we represent the ground state

$$\Phi_0 = \prod_{R=1}^{N} \phi_R(x_R), \qquad (5.2)$$

and the excited states schematically. The excited states are denoted by

$$\Psi_{RR'} = b_R^+ b_{R'} \Phi_0.$$

The important matrix elements of $\mathcal{3C}$ are $\langle \Psi_{RR'} | \mathcal{3C} | \Phi_0 \rangle$ which gives rise to the tunneling term, the second term in Eq. (3.1); and $\langle \Psi_{RR'} | \mathcal{3C} | \Psi_{RR'} \rangle$ which gives rise to the hard-core term, the third term in Eq. (3.1). If the particles have spin, and the system is placed in a weak external field, then there are two states per lattice site. The spin variable σ is introduced, and Eq. (3.1) results. We note that the tunneling process preserves spin and that the tunneling matrix element is spin independent.

To construct a model Hamiltonian for the mixture system we consider the matrix elements of

$$\mathcal{3C}_{3,4} = \sum_{i=1}^{N-N_4} T_3(i) + \sum_{i=1}^{N_4} T_4(i) + \tfrac{1}{2} {\sum_{ij}}' v_e(ij), \quad (5.3)$$

where $T_n(i) = p_i^2/2m_n$, and we have assumed the effective interaction to be independent of the nature of the interacting pair, ^{3}He–^{3}He, ^{3}He–^{4}He, or ^{4}He–^{4}He. Suppose we write $T_4(i) = T_3(i) + T_4(i) - T_3(i) = T_3(i) - \tfrac{1}{4} T_3(i)$ and approximate $\mathcal{3C}_{3,4}$ by

$$\mathcal{3C}_{3,4} \approx \mathcal{3C}_3 = \sum_{i=1}^{N} T_3(i) + \tfrac{1}{2} {\sum_{ij}}' v^e(ij). \qquad (5.4)$$

Now as above the important matrix elements of $\mathcal{3C}_3$ involve the states Φ_0 and $\Psi_{RR'}$. In analogy to the spin variable which denotes the possibility of two distinguishable states at each lattice site, we use an index λ to refer to two distinguishable states at each lattice site; these are a ^{3}He ground state or a ^{4}He ground state. Then, we have

$$\mathcal{3C}_{PM} = \sum_{RR',\lambda} t_\lambda(RR') b_{R\lambda}^+ b_{R'\lambda} + \sum_{R,\lambda\lambda'} \phi_0 b_{R\lambda}^+ b_{R\lambda'}^+ b_{R\lambda'} b_{R\lambda},$$
$$(5.5)$$

where unlike the spin case, the matrix element for the tunneling process depends upon the state label. We have

$$t_3(RR') = \int dx \phi_R^{(3)}(x) T_3(x) \phi_{R'}^{(3)}(x) \qquad (5.6)$$

(a) $|\Phi_0\rangle =$ ⊝   ⊝   ⊝   ⊝   ⊝   ⊝

(b) $|\Psi_{RR'}\rangle =$ ⊝   ⊝⊝   ⊝   ⊝   ——   ⊝

and

$$t_4(RR') = \int dx \phi_R^{(4)}(x) T_3(x) \phi_{R'}^{(4)}(x), \qquad (5.7)$$

where $\phi_R^{(3)}$ and $\phi_R^{(4)}$ are single-particle ground-state wave functions for ^{3}He and ^{4}He atoms, respectively. Of course the tunneling process preserves state. We have not included a spin index to label the ^{3}He particles because the ^{4}He particles move through the ^{3}He medium relatively unaffected by its spin configuration.[12]

The tunneling excitations in the ^{3}He–^{4}He dilute solution are given by the Hamiltonian

$$\mathcal{3C}_T = \sum_{RR',\lambda\lambda'} [t_\lambda(RR') t_\lambda(RR')/-\phi_0]$$
$$\times b_{R\lambda}^+ b_{R'\lambda} b_{R'\lambda'}^+ b_{R\lambda'}. \quad (5.8)$$

The terms in this Hamiltonian with $\lambda = \lambda'$ correspond to the tunneling of a particle to a neighboring lattice site and its immediate return. This process reduces the single-particle energy by t^2/ϕ_0 per particle. The terms of interest in Eq. (5.8) are those with $\lambda \neq \lambda'$, we write

$$\mathcal{3C}_T = -2 \sum_{RR'} M(RR')_{34} b_{R4}^+ b_{R'4} b_{R'3}^+ b_{R3}, \qquad (5.9)$$

where $M(RR')_{34} = t_3(RR') t_4(RR')/\phi_0$. Now the operator combination in Eq. (5.9) can be rearranged to give

$$b_{R4}^+ b_{R'4} b_{R'3}^+ b_{R3} = a_R^+ a_{R'}^-, \qquad (5.10)$$

where $a_R^+ = b_{R4}^+ b_{R3}$, and $a_R^- = b_{R3}^+ b_{R4}$. The operator a_R^+ creates a mass fluctuation at R, a_R^- destroys a mass fluctuation at R. The Hamiltonian, $\mathcal{3C}_T$ can be written in the form

$$\mathcal{3C}_T = -2 \sum_{RR'} M(RR')_{34} a_R^+ a_{R'}^-. \qquad (5.11)$$

A single-particle state corresponding to a ^{4}He particle tunneling through the ^{3}He medium is created by

$$a_k^+ = \sum_R \exp(i\mathbf{k}\cdot\mathbf{R}) a_R^+. \qquad (5.12)$$

The equation of motion for a_k^+ is given by

$$i\hbar(d/dt) a_k^+ = [a_k^+, \mathcal{3C}_T] = -2m(k) a_k^+,$$

where

$$m(k) = \sum_{R' \neq (R)} M(RR')_{34} \exp[i\mathbf{k}\cdot(\mathbf{R}-\mathbf{R}')]. \quad (5.13)$$

For a simple cubic crystal we have

$$m(k) = 4M(\Delta)_{34}(\cos k_x \Delta + \cos k_y \Delta + \cos k_z \Delta). \quad (5.14)$$

As $k \to 0$, we have

$$m(k) \sim 2z[t_3(\Delta) t_4(\Delta)/\phi_0][1 - (k^2 \Delta^2/z)]. \quad (5.15)$$

The excitation created by a_k^+ is called a mass fluctuation wave; it has the dispersion relation
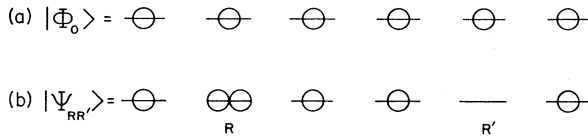
$$\hbar\omega(k) = 2m(k)$$

FIG. 33. Wavefunctions. The important states for calculating the matrix elements that lead to particle motion Hamiltonians are $|\Phi_0\rangle$ and $|\Psi_{RR'}\rangle$. For $|\Phi_0\rangle$, each lattice site is occupied by a single particle. For $|\Psi_{RR'}\rangle$ the lattice site R is doubly occupied while the lattice site R' is vacant.

---

[12] As in the case of the vacancy waves, the mass fluctuation wave in ^{3}He must be dressed with a spin fluctuation cloud. In ^{4}He, the mass fluctuation wave, a ^{3}He atom, is not so dressed. See Footnote 9.
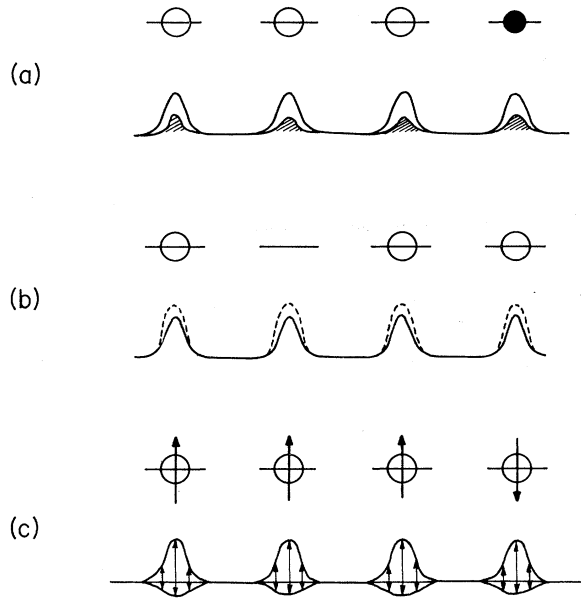
FIG. 34. Densities. (a) When there is a single ^{4}He atom on a linear chain with three ^{3}He atoms, the single-particle density at each lattice site is one; it is the sum of two contributions; $0.75 \mid \phi^{(3)} \mid^2 + 0.25 \mid \phi^{(4)} \mid^2$. We have distorted the wavefunction of the ^{4}He atom to emphasize the change in the single-particle density in the vicinity of a lattice site. (b) When there is a vacancy on a linear chain with three ^{3}He atoms, the single-particle density at each lattice site is 0.75. (c) When there is a spin $\downarrow$ on a linear chain with three spins $\uparrow$ the single-particle density at each lattice site is one; it is the sum of two contributions, $0.75 \mid \phi \mid^2 + 0.25 \mid \phi \mid^2$. Here we have shown the appearence of the single-particle density for the $k \rightarrow 0$ mode on a four atom chain.

and it represents a ^{4}He particle tunneling through the ^{3}He medium. Independent of the details of the crystal structure the bandwidth of the mass fluctuation waves is $4zM(\Delta)_{34}$. This ^{4}He particle in a mass fluctuation wave state is delocalized just like the vacancy that is in a vacancy wave state. Thus there is a finite amplitude of ^{4}He particle at each lattice site. See Fig. 34. For a linear chain with ten lattice sites occupied by nine, ^{3}He atoms and one, ^{4}He atom, there is one particle at each lattice site; i.e.,

$$\langle N_R \rangle = \sum_\lambda b_{R\lambda}{}^+ b_{R\lambda} = N_R{}^{(3)} + N_R{}^{(4)} = 1.$$

But this one particle is 90% ^{3}He, and 10% ^{4}He. To localize a ^{4}He particle in a region of the lattice, one constructs a wave packet by the proper superposition of mass fluctuation waves; e.g.,

$$\Psi_k = \int dk' C(k, k') a_{k'}{}^+,$$

where $C(k, k') \propto \exp[-\lambda^2(k-k')^2]$. For conceptual purposes, the localized wave packets are often more convenient than the individual mass fluctuation waves.

We may estimate the magnitude of the parameter which characterizes $m(k)$, $t_3(\Delta) t_4(\Delta)/\phi_0$ by noting that when Eq. (3.12) is put in pseudo spin form, Eq. (3.16),

we have

$$\hbar J = t_3(\Delta) t_3(\Delta)/\phi_0. \qquad (5.17)$$

Thus if we write $t_4(\Delta) = \lambda t_3(\Delta)$, we have

$$2zM(\Delta)_{34} = \lambda 2zM(\Delta)_{33} = \lambda(2zJ). \qquad (5.18)$$

The bandwidth for the mass fluctuation waves is $\Delta\epsilon_{MF} = 4\lambda z\hbar J$. At $V = 20.0$ cm^3/mole, we have $J = 0.35 \times 10^6$ MHz $= 16$ μK and $\Delta\epsilon_{MF} = 0.5$ mK for $\lambda = 1$. Thus the bandwidth for mass fluctuation waves is rather large. Below, we discuss the mass fluctuation wave lifetime.

We compute the energy associated with this system of excitations by noting that $m(k)$ goes from $-2z\lambda\hbar J$ to $2z\lambda\hbar J$, as k goes from 0 to π/Δ. Thus we approximate $m(k)$ by $m(k) = -2zJ$ for $0 < k < \pi/2\Delta$, and $m(k) = +2zJ$ for $\pi/2\Delta \leq k \leq \pi/\Delta$. In the limit $k_B T \gg \Delta\epsilon_{MF}$, we find that this energy spectrum yields

$$E_{MF} = N\langle \epsilon \rangle - \beta[\langle \epsilon^2 \rangle - \langle \epsilon \rangle^2] + \cdots, \qquad (5.19)$$

where

$$\langle A \rangle = \sum_k A_k / \sum_k 1.$$

Thus the specific heat and energy constant for the mass fluctuation waves are

$$C_{MF}/Nk_B = x_4(7/4)\lambda^2 z^2 (\beta\hbar J)^2 \qquad (5.20)$$

and

$$k_{MF} = -x_4(7/4)\lambda^2 z^2 (\beta\hbar J)^2. \qquad (5.21)$$

Recent work on mass fluctuation waves by Landesman and Bernier (1970), and Balakrishnan and Lange (1970) lead to a specific heat which has a numerical factor different from what we obtain here. The specific heat of $x_4 \cdot z$ pairs of ^{3}He atoms interacting by the Hamiltonian $\mathcal{3C}_T$ is given by (D.7)

$$C_T/Nk_B = (x_4)\tfrac{3}{8}z(\beta\hbar J)^2.$$

For $\lambda = 1$, $C_{MF} \approx 50C_T$; the specific heat of x_4 ^{4}He atoms is about 50 times greater than that of the $x_3 z$ tunneling ^{3}He pairs. Let us understand this result. At concentrations $x_4 < 1000$ ppm, each ^{4}He atom is isolated from the other ^{4}He atoms in the system. It sees all of its neighbors to be ^{3}He atoms and it undergoes a tunneling process involving any one of its neighbors with equal energetic benefit to itself. This situation is analogous to a single inverted spin in a ferromagnetic crystal—all of its neighbors have spin $\uparrow$ —it has spin $\downarrow$. The spin sees the sea of ferromagnetism about it as an inert medium through which it tunnels with a resulting energy reduction. Now contrast this with a spin system at $k_B T \gg \hbar J$, where the z neighboring spins about a given spin have no particular correlation among themselves or with the given spin; the spin sees a noisy undulating sea of paramagnetism. The ^{4}He atom alone in a ^{3}He lattice sees the lattice as a well ordered inert medium. The obvious analog in this case to temperature, which in the spin system takes the ordered spin state into the disordered spin state at $T \approx T_N$, is the concentration.

Here we have discussed the mass fluctuation wave that corresponds to a ⁴He atom propagating in a ³He medium. The propagation of a ³He atom in a ⁴He medium can also be termed a mass fluctuation wave. Both the ⁴He atom in a ³He medium and a ³He atom in a ⁴He medium are fermions (Andreev and Lifshitz, 1969). At experimentally realizable temperatures $T > 1$ mK, the thermal energy is greater or about equal to the bandwidth for the mass fluctuation waves, and at dilute concentrations, $x_4 < 1000$ ppm or $x_3 < 1000$ ppm, the fermi nature of these excitations is of no consequence. For dilute ³He in a ⁴He medium, the mass fluctuation wave is the spin carrying excitation. This system can be regarded as a hot–dilute fermi gas. For dilute ⁴He in a ³He medium, the mass fluctuation wave is a spin disordering perturbation just like the vacancy wave.

Andreev and Lifshitz (1969) have suggested a simple criterion for the existence of impurity excitations (impuritons) and defect excitations (defectons). Here we refine their argument for impuritons slightly and work out the existence criterion for mass fluctuation waves and vacancy waves. A single ⁴He particle in ³He has a smaller zero-point motion than the ³He particles which make up the medium in which the ⁴He sits. We regard the ³He medium as an elastic continuum, and consider the ⁴He particle to be a sphere of volume $v_4 = \Delta^3 (1-\epsilon)^3$, where ϵ is a measure of the distortion of the elastic continuum in the vicinity of the ⁴He. From the calculations of Mullin (1968), Guyer (1968a) and Varma (1969), we have $\epsilon \approx 10^{-2}$; i.e., using a microscopic model of a quantum crystal, one finds that replacing a ³He by a ⁴He leads to a distortion of the lattice in the vicinity of the ⁴He atom. The neighbors of the ⁴He move toward it; they shift their equilibrium positions by about 1%. We transfer this result to a continuum model of the lattice and argue that the ⁴He looks to the continuum like an "undersized" sphere. The continuum shrinks in on the sphere and creates a pressure field in the solid given by

$$\mathbf{p}(r) = p_0 (\Delta/r)^3 \mathbf{e}_r,$$

where $p_0 = -(6/5)\beta\epsilon$, and β is the bulk modulus; $\beta = -V(\partial P/\partial V)_T$. A second "undersized" sphere, 2, at a distance R away from the first "undersized" sphere, 1, interacts with the pressure field with an energy of interaction given by

$$\Delta E = \oint \mathbf{p}_1(r) \cdot \mathbf{u}_2(r) \ ds, \tag{5.24}$$

where the integral is over the surface of sphere 2, $\mathbf{p}_1(r)$ is the pressure on the surface of sphere 2 due to sphere 1, $\mathbf{u}_2(r)$ is the displacement of the surface of sphere 2; Fig. 35. Equation (5.24) represents the work done to contract sphere 2 in the pressure field of sphere 1. Now we have $\mathbf{u}_2(r_2) = \epsilon \Delta \mathbf{e}_r$; thus Eq. (5.24) can be evaluated (Bitter 1931) to yield

$$\Delta E(R) = -(48/5)\pi\epsilon^2\beta\Delta^3[\Delta^3/R(R^2-\Delta^2)]. \tag{5.25}$$

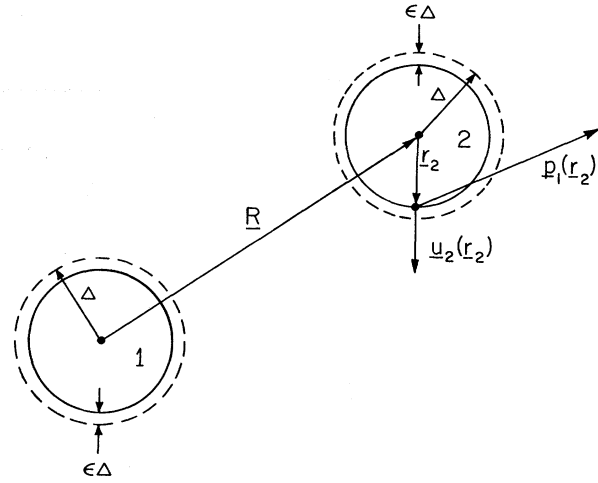For $R = \Delta x^{-1/3}$; i.e., for R equal to the average distance

FIG. 35. Interacting Spheres. An "under" sphere, 1, embedded in an elastic continuum creates a pressure field around itself, $\mathbf{p}_1(r)$. In order to place a second similar sphere, 2, at $\mathbf{R}$ from 1, work must be done to displace the continuum in the presence of the pressure field, $\mathbf{p}_1(r)$, to accommodate the second sphere. The work done to place the second sphere is proportional to $\mathbf{p}_1(\mathbf{r}) \cdot \mathbf{u}_2(\mathbf{r})$.

between ⁴He atoms, we have an energy of interaction given by

$$\Delta E(R = \Delta x^{-1/3}) \approx -(48/5)\pi\epsilon^2\beta\Delta^3 x \tag{5.26}$$

for $x \ll 1$. Now the mass fluctuation wave will be a good excitation if the kinetic energy associated with this state, $z\lambda J$, is larger than the potential energy of attraction between ⁴He neighbors at a distance $\Delta x^{-1/3}$ apart; i.e.,

$$z\lambda J > \Delta E(R = \Delta x^{-1/3}),$$

or

$$x < z\lambda J / 32\epsilon^2\beta\Delta^3. \tag{5.27}$$

At $V = 20.0$ cm³/mole, $\lambda J \approx J = 0.35 \times 10^6$ MHz; $\beta = 500$ atm, $\beta\Delta^3/k_B = 100°$K, $\epsilon \approx 10^{-2}$; we have

$$x < 10^{-3}.$$

Thus we expect mass fluctuation waves to be good excitations up to $x \approx 1000$ ppm.[13] At higher concentrations, the interaction between ⁴He particles is great enough to require that they be treated as a strongly interacting gas. The simple picture of an excitation associated with the independent motion of the ⁴He atoms breaks down. In Sec. 7 where we deal with nondilute mixtures this point is taken up in further detail. We note that Eq. (5.27) for x_c depends very strongly on volume through the factor J.

_____

[13] The existence criterion of Andreev and Lifshitz does not include the factor ϵ^2 and gives much too low a concentration limit.

5.2 Interactions

The mass fluctuation waves couple strongly to the tunneling excitations and the phonons. We now discuss these coupling mechanisms.

Phonon–Mass Fluctuation Interactions. The phonons see a mass fluctuation wave as a dynamic mass fluctuation just as they see the vacancy waves. Thus they couple to the mass fluctuation waves through

$$\mathcal{3C}_{P,\mathrm{MF}} = \tfrac{1}{2} \sum_R \Delta m_R(t) \dot{u}_R^2,$$

where the time evolution of $\Delta m_R(t) = m_R(t) - m_3$ is due to the mass fluctuation excitations in the system. In Appendix A.6 we have worked out the rate of energy transfer from the mass fluctuation excitations to the phonons, viz Eq. (A6.20). Here

$$T_{\mathrm{MFP}}^{-1} = 1500 (\Delta m/m)^2 (k_B T/\hbar) (T/\theta_D)^6$$

where $\Delta m = m_4 - m_3$. This calculation is exactly analogous to that discussed in some detail in Sec. 3 for the vacancy–phonon coupling. Further it is essentially the calculation that would be required to assess the lifetime of the mass fluctuation waves due to their interaction with the phonons. The lifetime of the mass fluctuation waves, approximately T_{MFP}, is much longer than $(\lambda J)^{-1}$ for $T < 2K$.

Tunneling–Mass Fluctuation Interactions. The tunneling excitations are strongly coupled to the mass fluctuations by the same mechanism that couples them to the vacancy waves. The tunneling excitations see the mass fluctuation as a dynamic spin fluctuation through

$$\mathcal{3C}_{\mathrm{TMF}} = -\hbar J \sum_{RR'} \Delta\alpha(RR', t) \boldsymbol{\sigma}_R \cdot \boldsymbol{\sigma}_{R'},$$

where the time evolution of $\Delta\alpha(RR', t)$ is due to the mass fluctuation waves, cf. Eq. (3.43). The rate of change of the energy of the tunneling excitations due to coupling to the mass fluctuation waves through $\mathcal{3C}_{\mathrm{IMF}}$ leads to a decay in the energy of the tunneling system at the rate

$$1/T_{\mathrm{TMF}} = x_4 2(z-1)\lambda J,$$

where $\lambda J = t_3 t_4/\phi_0$; see Appendix (A.5). As in our discussion below Eq. (3.44) this rate is the rate at which a tunneling pair of particles becomes uncorrelated through the motion of a ^{4}He particle changing place with one of the tunneling pair. Both a vacancy and a ^{4}He atom are magnetically inert objects—both disrupt the magnetic regularity that the tunneling excitations look for.

Vacancy–Mass Fluctuation Interaction. The vacancy–mass fluctuation interaction occurs at a rate proportional to the product of x_v and x_4. It is of no importance in the experimentally accessible temperature range.

6. NMR IN DILUTE ^{3}He–^{4}He MIXTURES

6.1 Dilute ^{4}He in ^{3}He Mixtures, Theory

There are four kinds of excitations in dilute mixtures of ^{4}He in ^{3}He that are responsible for the results of NMR experiments, the three pure ^{3}He excitations discussed in Sec. 3 and the mass fluctuation waves. In this section we discuss: (1) the features of NMR experiments that depend upon the existence of the additional excitation, the mass fluctuation wave, (2) the experimental exploration of dilute ^{4}He in ^{3}He mixtures in the region where the mass fluctuation waves are important, and (3) the probable behavior of dilute mixtures of ^{3}He in ^{4}He. This latter system, dilute ^{3}He in ^{4}He, has yet to be studied extensively; however, there are some clues in the NMR experiments on nondilute mixtures at lowest concentrations, $x_3 \approx 0.01$, that suggest that the sort of behavior that we anticipate for dilute ^{3}He in ^{4}He is beginning to be observed (Miyoshi, 1970a).

The results of a typical T_1 experiment on nominally pure ^{3}He were shown in Fig. 12. But as we stressed above pure ^{3}He is an idealization unachievable in the laboratory. In Fig. 36 we show more detail of the kind of results that are achieved in a typical T_1 experiment on ^{3}He containing various dilute concentrations of ^{4}He. We notice that the behavior of T_1 in the high-temperature region, $T > 0.5K$ at $v = 20.0$ cm^3/mole, is essentially independent of ^{4}He concentration, and that the behavior of T_1 at low temperatures, $T < 0.5K$ at $v = 20.0$ cm^3/mole, approaches a limiting behavior as $x_4 \to 0$ which we can regard as pure ^{3}He behavior. It is because the pure ^{3}He behavior at low temperatures can only be assessed by experimentally taking the limit $x_4 \to 0$ that we have left the discussion of pure ^{3}He at low temperatures to this section.

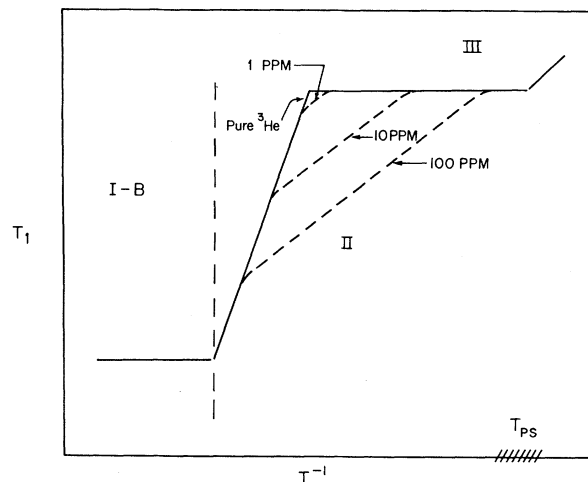The high-temperature behavior of T_1 in dilute mixtures is the same as in "pure" ^{3}He; it is that of Region I

FIG. 36. T_1 vs T^{-1} at low temperature for $x_4 \neq 0$. When small concentrations of ^{4}He are put into ^{3}He, the low temperature behavior of T_1 is seriously altered. (1) A relaxation process that is proportional to x_4 and considerably milder in temperature dependence than $\exp\phi \mid T$ appears. (2) There is temperature and concentration independent plateau at low temperatures, Region III. This is also present in pure ^{3}He. (3) At lowest temperature, there is a further temperature dependence in T_1. There is some sensitivity of T_1 at lowest temperatures to the concentration of ^{4}He.

which we discussed in detail in Sec. 4. At low temperatures, T_1 has two distinct kinds of behavior as a function of T^{-1} which occur in Regions II and III on Fig. 36. We will discuss this behavior in detail.

Before doing so, it will be useful to review the nomenclature developed in Appendix B to describe relaxation processes. The relaxation of the rf energy to the reservoir in Regions II and III is relatively more complicated than in Region I. Throughout Region I, the rf energy was coupled to particle motion excitations that were tightly coupled to the reservoir. Thus throughout Region I, only two systems were involved: the Zeeman system which is heated by the rf field, and the vacancy system or the tunneling system both of which are tightly coupled to a reservoir. The T_1's which described relaxation in Region I are the intrinsic times for the pair of systems involved. The *intrinsic times* are defined for a pair of systems coupled together, as shown in Fig. 52, in Appendix A. They measure the rate at which energy passes between two systems when one of the two systems is completely isolated except for its connection to the other, and the other system remains tightly coupled to a reservoir. In Region II, we find that three or more systems are involved in the relaxation process. Energy is transferred among the systems involved in the relaxation process in series, i.e., $0{\rightarrow}1{\rightarrow}2{\rightarrow}3$ etc. Relaxation through a particular series of three or more systems is referred to as relaxation through a particular topology. See Fig. 52. When we have a relaxation process involving three or more systems, the T_1 measured for this relaxation process involves an intrinsic time and a topological factor in the form

$$T_1^{-1}\,|_{\text{topology}} = (1/T_{\text{intrinsic}}) \times (\text{topological factor}).$$

The topological factor is a function of the energy constants (specific heats) of the systems involved in the relaxation process. The T_1's measured in this circumstance (three or more systems) are referred to as topological times. Let us introduce a notation which depicts the qualitative features of a particular relaxation process. In Region I-B, we have energy flow out of the system by the chain: Zeeman→tunneling→vacancy wave→phonon→reservoir. The weak link in the energy flow chain and the source of the long time is the Zeeman-tunneling coupling. We denote the topology of relaxation by $Z\text{-}TVP$. This is a two system relaxation process; the vacancy waves and phonons are simply the link which keeps the tunneling system tightly coupled to the reservoir. The T_1 which describes relaxation in the topology $Z\text{-}TVP$ is the same as the intrinsic time which describes the relaxation of Zeeman energy to the tunneling excitations. We will find that in Region II-A, the energy flow chain is also Zeeman→tunneling→ vacancy wave→phonon→reservoir. But in Region II-A, the weak link in this chain is the tunneling–vacancy wave coupling. We denote the topology of relaxation by $ZT\text{-}VP$. This is a three-system relaxation process. The T_1 which describes relaxation in the topology ZT-
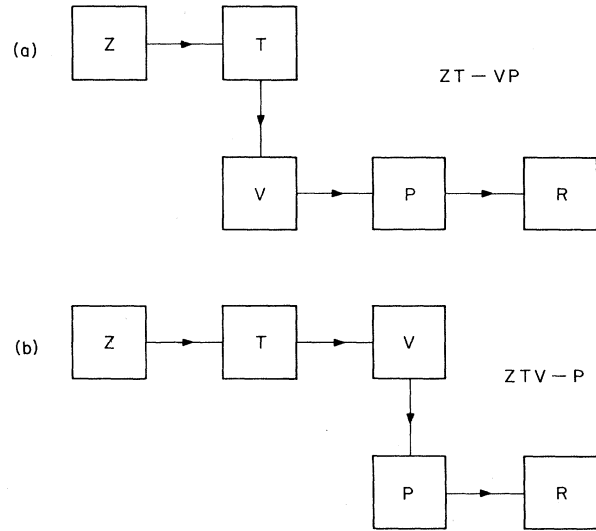

FIG. 37. Topologies: (a) $ZT\text{-}VP$, and (b) $ZTV\text{-}P$.

VP is the intrinsic time which describes the relaxation of tunneling energy to the vacancy wave excitations multiplied by a topological factor involving the energy constant of the Zeeman system and the tunneling system.

The important intrinsic times and topological times are calculated in Appendix A.

Region II. In Region II, the route by which energy put into the Zeeman system gets to the reservoir is "bottlenecked" by one of the particle motion excitations. This is best understood by contrast to Region I. In Region I, energy was transferred from the Zeeman system to the particle motion excitations by the dipolar field. Throughout Region I, the particle motion excitations are strongly coupled to the phonons; thus the particle motion excitations are always at the lattice or reservoir temperature. The onset of Region II occurs when the particle motion excitations become uncoupled from the lattice or reservoir.

In Region II-A, the route of energy relaxation is that in Fig. 37(a), Zeeman→tunneling→vacancy wave→ phonon $ZT{\rightarrow}VP$. At $T>0.5$, the long time in the chain of energy flow is due to the Zeeman-tunneling coupling through $\mathcal{H}_d$. This long time is temperature independent. The times which describe the coupling of systems further along the chain, T_{TV} and T_{VP}, are temperature dependent, so that as the temperature is lowered we expect to see T_1 change its behavior and become temperature dependent. The weak link in the energy flow chain, $Z{\rightarrow}T{\rightarrow}V{\rightarrow}P$, is the tunneling to vacancy wave link. As the temperature is lowered the number of vacancies goes to zero as $\exp(-\beta\phi)$, the Zeeman and tunneling systems come to a mutual equilibrium at a temperature above the lattice temperature, and the coupled systems slowly lose their excess energy to the vacancy waves which remain tightly coupled to the phonons. The topology of this process, $ZT\text{-}VP$, is

shown in Fig. 37(a). A comparison of the long time in the two rival topologies shown in Fig. 37(a),(b) is made in Appendix A7. There we show that at $v=20.0$ cm³/mole topology $ZT\text{-}VP$ is faster than topology $ZTV\text{-}P$.

The situation we have described here is quite simple and if it always held true the low-temperature T_1 data would be very easy to understand. But in experimentally achievable pure solid ³He samples, there are small concentrations of ⁴He. These impurities are not static. Because of their tunneling motion through the ³He medium, they constitute a system of excitations that can rival the vacancy waves for de-excitation of the tunneling system. The ⁴He impurities as mass fluctuation waves couple to the tunneling system just as do the vacancy waves. Both the vacancy waves and the mass fluctuation waves are magnetically inert and can interfere with the tunneling of a ³He pair. The concentration of ⁴He impurities in the purest samples is $x_4 \approx 1$ ppm. At $T \approx 0.5$ K, the number of vacancies present at $v=20.0$ cm³/mole is $N_v \approx 10^{-12}$. Although there are far fewer vacancies present, the vacancy waves are much more mobile than the ⁴He mass fluctuation waves. The mass fluctuation waves rival the vacancy waves in coupling to the tunneling energy when

$$x_4\omega_4(3,3) \approx x_v\omega_v(3,3);$$

at $v=20.0$ cm³/mole, $\omega_4(3,3) \approx J=0.4$ MHz, $\omega_V(3,3) \approx 10^4$ MHz, thus we have equality at $x_V \approx 10^{-4}x_4$. For $x_4=10^{-6}$, this is at $T=0.6$K. At more substantial concentrations of ⁴He, 100 ppm or 1000 ppm, the mass fluctuation waves completely dominate the vacancy waves at temperature as low as 0.6K. Now the energy flow route $Z \rightarrow T \rightarrow MF$ will be a useful alternative to the vacancy route, $Z \rightarrow T \rightarrow V$, only if the mass fluctuation waves can get rid of the energy they acquire fast enough. Recall that the mass fluctuation waves interact with the phonons in the same way as the vacancy waves. Both excitations are seen by the phonons as dynamic mass fluctuations. Thus we must compare the two energy flow topologies shown in Fig. 38, $ZT\text{-}MFP$ and $ZTMF\text{-}P$. As we show in Appendix A7, the long time is associated with the topology $ZTMF\text{-}P$; the weak link in $Z \rightarrow T \rightarrow MF \rightarrow P$ is the link between the mass fluctuation waves and the phonons. Of course the link between the tunneling system and the mass fluctuation waves is temperature independent, whereas the mass fluctuation wave–phonon link is temperature dependent. Thus at lowest temperatures, in the absence of any other new relaxation mechanisms, the mass fluctuation wave–phonon link must be the weakest.

In Region II of the T_1 vs T^{-1} plot, we will see a rivalry between the vacancy waves and the mass fluctuation waves for relaxation of the system. The two topologies that rival one another are those shown in Fig. 38. In both of these topologies, the energy relaxation process involves more than two systems, so the relaxation rate depends upon an intrinsic rate and a topological factor. From Appendix A7 we have a topological factor $k_T/(k_T+k_Z)$ for the topologies $ZT\text{-}VP$ and $ZT\text{-}MFP$ shown in Figs. 37(a) and 38(a). Also from Appendix A7 we have a topological factor $k_{MF}/(k_T+k_Z+k_{MF})$ for the topology $ZTMF\text{-}P$ shown in Fig. 38(b). Since $k_{MF} \propto x_4$, and x_4 is small, we may approximate this by

$$k_{MF}/(k_Z+k_T).$$

Thus for both topologies in Region II, we expect to find a dependence of T_1^{-1} upon the Larmor frequency, through the topological factor, of the form $(T_1)^{-1} \propto (k_Z+k_T)^{-1}$. The observation of this Larmor frequency dependence is one of the experimental tests which establishes the structure of the relaxation topologies in Region II. As the concentration of ⁴He impurities is increased toward the limit for dilute mixtures, $x_4 \approx 1000$ ppm, the energy constant k_{MF} in the denominator of the topological factor may become comparable to k_Z+k_T. Then, it is possible to study the frequency or concentration dependence of T_1 and extract k_{MF}.

Region III. In Regions I and II, the routes by which energy is transported from the Zeeman system to the reservoir involve a transfer of energy among the excitations in the solid pointwise in the bulk of the solid. This behavior is to be contrasted with that in Region III. where the energy put into the Zeeman system by the rf field leaves the solid by diffusion of the particle motion excitations to the boundaries of the solid. In our discussion of both Regions I and II, we took it as a matter of faith that once the energy being transferred among the excitations got to the phonons it was immediately transferred to the reservoir. Let us first discuss this point. All of the mechanisms which coupled the particle motion excitations to the reservoir involved
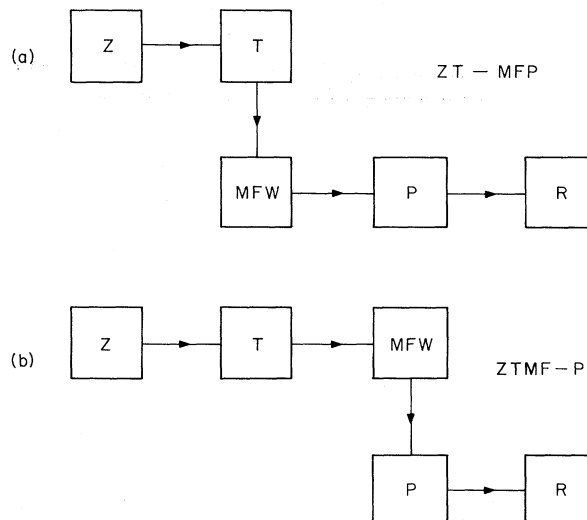

FIG. 38. Topologies: (a) $ZT\text{-}MFP$, and, (b) $ZTMF\text{-}P$.

two phonons. Thus the phonons which finally receive the rf energy have energies determined by the ambient temperature. These phonons carry the energy they receive to the boundaries of the system by a diffusion process which is characterized by the thermal conductivity mean free path.

$$\lambda_K = 3K/C_P c, \tag{6.1}$$

where K is the steady state thermal conductivity, C_P is the specific heat of a phonon gas, and c is the velocity of sound; i.e. $D_P \sim c\lambda_K$. The thermal conductivity mean free path is limited at low temperature by the size of the sample, $\lambda_K \approx l$. There exists adequate thermal conductivity data on solid helium to determine the time required for phonon energy to diffuse a distance on the order of the size of a typical sample chamber, 1 cm. [See Hogan, Guyer, and Fairbank, (1969) and the literature referenced therein.] Instead of using this data, it is easiest to recall that temperature pulse experiments on solid helium indicate that phonon energy will diffuse a distance of about 1 cm on a time scale that varies from 10 μsec at low temperatures, $T < 1$K, to 1 msec at high temperatures, $T \approx 2$K (Ackerman, 1968). The diffusion of phonon energy across a sample chamber of typical dimension 1 cm, and its exit from the sample chamber on reaching the boundary, is complicated somewhat at lowest temperatures because of the Kapitza resistance (Pollack, 1969). Yet there is no reason to believe that times greater than about 1 msec are required for phonons to leave a 1 cm sample chamber even at the lowest temperatures (Mueller, 1970). The typical T_1 seen at low temperatures is substantially greater than 1 sec. Thus once the phonons receive the energy from the particle motion excitations they carry it to the reservoir on a time scale that is fast compared to the long time in the energy flow chain.

As the temperature is lowered, the weak link in the energy flow chain is the mass fluctuation wave–phonon link. The energy has a hard time getting to the phonons. Thus in Region III, we see the energy leave the system by the diffusion of the particle motion excitations to the boundaries of the sample.

6.2 Experiments on Dilute ^{3}He–^{4}He Mixtures, Results

T_1 *in Region II*. Most of the early T_1 experiments on solid ^{3}He have explored some part of Region II and Region III (Reich, 1963; Richards, 1965; Richardson, 1965). However, as pointed out above, these experiments were done with unknown amounts of ^{4}He impurities. Hence, it is difficult to use the results of these early experiments in this region in other than a qualitative way. Recently there have been a series of experiments by several groups that have carefully explored the effects of ^{4}He impurities in NMR experiments at low temperatures. The pioneering experiments of this
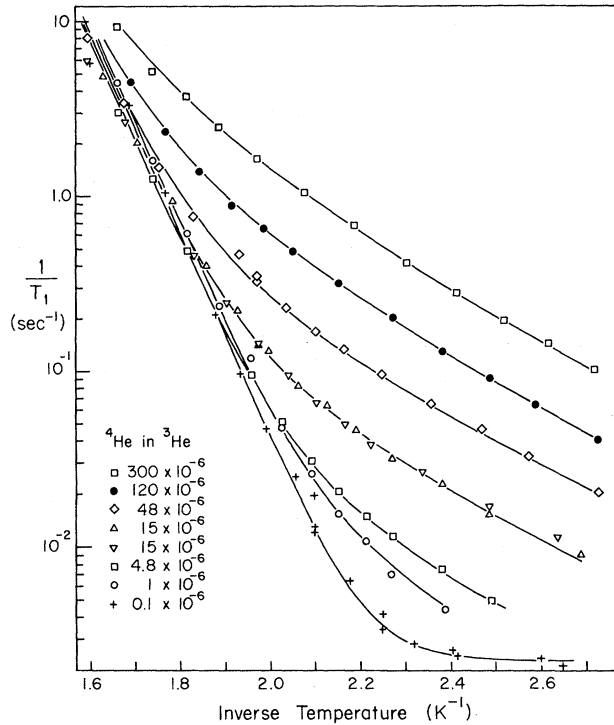

FIG. 39. T_1 Data in Region II-B; (concentration dependence). The data from the thesis of Giffard (1968), T_1^{-1} vs T^{-1} are shown. The topological factor $k_T/(k_Z + k_T)$ has been removed. The behavior characteristic of ZT-VP is seen in the data at 10^{-1} ppm. Even a small concentration of impurities, $x_4 \approx 15$ ppm drastically alters T_1^{-1} vs T^{-1}. From the data at higher concentrations, the dependence $T_1^{-1} \propto x_4$ is easily verified.

series, those of Giffard and Hatton (1967) and Giffard (1968) are most illuminating; the experiments of Bernier and Landesman (1969), Bernier (1970) and Reich and Yu (1969) are corroborative and complementary to these experiments. In Fig. 39, we show the results of the T_1 experiments of Hatton and Giffard on bcc ^{3}He at $v = 20.0$ cm^3/mole at impurity concentrations from $x_4 < 1$ ppm to $x_4 = 300$ ppm; the plot is log T_1 vs $1/T$. Over the temperature and concentration range explored, the relaxation rate contains a topological factor, $k_T(k_Z + k_T)$. The data shown in Fig. 39 has had the topological factor divided out. We first note that as the concentration of ^{4}He impurities approaches zero, the intrinsic T_1 approaches a limiting curve which is a straight line on the log T_1 vs T^{-1} plot. The limiting T_1 curve will fit the analytic expression

$$T_1^{-1} = 1.9 \times 10^{10} \exp - (13.4/T), \tag{6.2}$$

and corresponds to relaxation of the system through the topology shown in Fig. 37a, ZT-VP. The expected intrinsic relaxation time for this topology is related to the vacancy excitation temperature and the vacancy tunneling frequency by

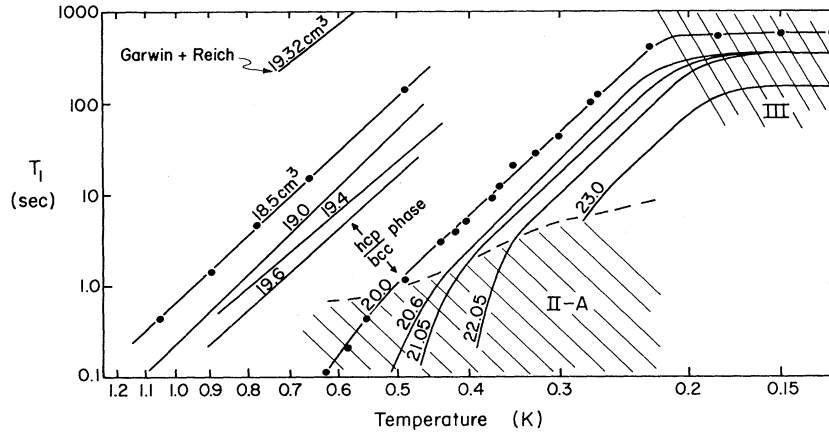$$T_1^{-1} = 2(z-1)\omega_V(3, 3) \exp (-\beta\phi).$$

FIG. 40. T_1 Data in Region II-B; (Volume Dependence). The data of Richards, Hatton, and Giffard (1965), T_1 vs T, are shown. The topological factor $k_T|(k_z+k_T)$ has been removed; the data are on samples containing less than 500 ppm ⁴He. The Region II-A has been shaded. The remainder of the data corresponds to II-B and III; data in Region III has also been shaded. For the hcp phase region II-A does not occur; see Fig. 13. The T_1 data in Region II-B is mildly volume dependent and has the temperature dependence corresponding to $ZTMF-P$.

Thus the limiting curve provides a good measure of ϕ and $\omega_V(3, 3)$. We have $\phi=13.4$, and $\omega_V(3, 3)=1.4\times10^9$; these values of the vacancy excitation temperature and the tunneling frequency were plotted on Figs. 29 and 30 above. They are in reasonable agreement with the values of these quantities obtained from NMR measurements in Region I, and with specific heat data. We note that at $T^{-1}>2.25\text{K}^{-1}$, the limiting T_1 curve becomes temperature independent; 0.44K is the temperature for the transition from Region II to Region III at $x\leq1$ ppm. At concentrations as low as 15 ppm, the transition from Region II to Region III occurs below the experimentally realized temperatures at approximately 0.25K.

As small concentrations of impurities are added to solid ³He, the behavior of T_1 as a function of temperature departs from the exponential behavior characteristic of the tunneling–vacancy wave topology, $ZT-VP$. If we define

$$(1/T') = (1/T_{\text{expt}}) - (1/T_{TV}), \qquad (6.4)$$

where T_{TV}^{-1} is given by Eq. (6.3), and T_{expt}^{-1} is the measured intrinsic relaxation rate plotted in Fig. 39. We find that $(T')^{-1}$ is proportional to the ⁴He concentration, and proportional to a high power of the temperature, T^7 or T^8. This is precisely the behavior we expect for the topology $ZTMF-P$ in which the Zeeman, tunneling, and mass fluctuation systems come to mutual equilibrium and lose their energy to the phonons by a two-phonon process with the mass fluctuation waves. The experiments of Giffard and Hatton and Giffard constitute a direct experimental observation of phonons scattering from mass fluctuation waves. From Appendix A6 we have

$$1/T_{MFP}= 1500(\Delta m/m)^2(k_BT/\hbar)(T/\theta)^6. \quad (6.5)$$

From Eq. (6.5) we see that T_{MFP} depends relatively mildly on volume; it goes as θ_D^{+6}. Now we look at the low-temperature T_1 data of Richards, Hatton, and Giffard (1965) which is shown in Fig. 40. We recognize

that this data, which is on samples made at nine molar volumes, and containing ⁴He impurity concentrations of about 500 ppm, is primarily on phonons scattered from mass fluctuation waves. Thus we may use it to test the volume dependence of T_1 as given by Eq. (6.5). From Fig. 28 we have

$$[\theta_D(20.0)\theta_D(23.0)]^6= (29.5/21.8)^6\approx6;$$

this is to be compared with the variation of the T_1 with volume, at $T=0.3$K, by a factor of 10. Looking at the data on the hcp phase, we have $[\theta_D(18.5)/\theta_D(19.6)]^6= (42.5/36.6)^6\approx2.5$; this is to compared with the variation of T_1 with volume, at $T=0.7$ K, by a factor of about 7. Within the uncertainties introduced by the unknown concentration of ⁴He impurities in the various samples, the volume dependence of T_1 in Region II is consistent with expectations.

In the data of Richards, Hatton, and Giffard (1965) displayed in Fig. 40, we also note that at the higher temperatures in the bcc phase, e.g. at $T>0.35$ at $v=20.5$ cm³/mole, T_1 becomes a much faster function of temperature and there is no evidence for similar behavior in the data in the hcp phase. Both of these facts are a consequence of the volume (or pressure) dependence of the vacancy excitation temperature. In the bcc phase, the excitation temperature for vacancies is low enough that the topology $ZT-VP$ is observed, whereas, in the hcp phase, the vacancy excitation temperatures are so large that there are not enough vacancies present to see this topology.

The data of Giffard and Hatton, and Giffard were at $x_4\leq300$ ppm. Thus the concentration of ⁴He impurities was too small to permit a determination of the specific heat of the mass fluctuation wave system from a study of the topological factor in $T_1^{-1}|_{MFP}$. Bernier and Landesman (1969) and Bernier (1970) have reported data on bcc ³He at $v=20.1$ and 21.0 cm³/mole in Region II at concentrations up to 2800 ppm. The T_1 and T_2 data in these experiments in Region II is in quantitative and qualitative agreement with that in the experiments

of Giffard and Hatton, and Giffard. By going to higher concentrations of ^{4}He impurities, Bernier and Landesman, and Reich and Yu (1969) are able to study the specific heat of the mass fluctuation waves. The basic idea behind these experiments is that the times which characterize the decays observed in a T_1 experiment depend upon an intrinsic time and a topological factor. Thus a study of T_1 as a function of frequency (Reich, 1969) yields information about the topological factor and k_{MF}. A study of T_1 as a function of concentration at fixed frequency and temperature also yields k_{MF}. For example, if the system is at T_0 and the topology of relaxation is the topology $ZTMF-P$, then we have

$$T_1^{-1}\,|_{MFP} = (T_{MFP})^{-1}[k_{MF}/(k_Z+k_T+k_{MF})]. \quad (6.6)$$

Now data on $T_1\,|_{MFP}$ as a function of ω_0^2 yields k_T+k_{MF}, independent of a quantitative microscopic theory of the interaction which leads to relaxation, as the intercept of $T_1\,|_{MFP}$ with zero on the ω_0^2 axis. At this intercept we find $k_Z(\omega_0) = k_T+k_{MF}$; if k_T is known, then k_{MF} can be found. Bernier and Landesman, and Bernier have used a different technique with a similar physical basis to study $k_{MF}/(k_Z+k_T+k_{MF})$ at $v=20.1$ cm^3/mole in Region II-B at $x_4 \leq 2800$ ppm; they find

$$k_{MF} = 825 x_4 k_T. \quad (6.7)$$

At $v=21.0$ cm^3/mole in Region II-B at $x_4 \leq 2800$ ppm, Bernier and Landesman saw *no* convincing evidence for $k_{MF} \neq 0$. The T_1 and T_2 data at $v=21.0$ cm^3/mole were in good agreement with the expectations from similar data at 20.0 cm^3/mole (Bernier, 1970). We may understand the first of these results, Eq. (6.7), by recalling that

$$k_{MF} = 50 x_4 k_T [\omega_4(3, 3)/J]^2, \quad (6.8)$$

Eq. (5.22). Thus for $\omega_4(3, 3) \approx 4J$, the mass fluctuation wave specific heat is equal to its experimentally observed value. If a ^{3}He-^{4}He pair tunnel at about four times the rate at which a ^{3}He pair tunnels, then, the specific heat due to the mass fluctuation waves is in agreement with experiment. A tunneling rate for a ^{3}He-^{4}He pair that is four times that of a ^{3}He-^{3}He pair is somewhat unexpected but not impossible. Alternative explanations of the data of Bernier and Landesman and others (Richards, 1965; Reich, 1969) in terms of the concept of "exchange enhancement" has required that a ^{3}He pair in the vicinity of a ^{4}He atom (assumed stationary) tunnel 30 times faster than they do in bulk helium. It is difficult to support this requirement theoretically (Glyde, 1969). "Exchange enhancement" provides no explanation of the T_1 data (Guyer, 1969).

A study of the frequency dependence of the topological factor in Region II at low concentrations provides an independent measurement of k_T and J. This approach has been used by Richards, Hatton, and Giffard (1965), Richardson, Hunt, and Meyer (1965), and Reich and Yu (1969) to determine J. We have discussed this

application of frequency analysis of T_1 above. It provides a very useful and independent measurement of the specific heat of a particle motion excitation system.

T_1 in Region III. Region III, at $T^{-1} > 2.3$ at $x_4 = 1$ ppm, and $v=20.0$ cm^3/mole, was first observed in the experiments by Richards, Hatton, and Giffard (1965). In Region III, Richards, Hatton, and Giffard found that the long-time behavior of the time evolution of M_z toward equilibrium was nonexponential, and that the T_1 which was chosen to characterize this nonexponential recovery was temperature independent. Subsequently, Hunt, Richardson, Thompson, Guyer, and Meyer (1967) showed that T_1 was sample chamber size dependent, and that at very low temperatures, $T < 0.1$K, a temperature dependence set in with T_1 increasing mildly with further reduction in temperature. Finally, Giffard (1968) has done a careful study of this region as a function of controlled concentrations of ^{4}He impurities. He finds no strong or systematic dependence of T_1 in the temperature-independent region on concentration, and that the further increase in T_1 at low temperatures in a mixture with a particular ^{4}He concentration occurs at a temperature near T_{PS}, the phase separation temperature for that concentration. A typical result from the experiments of Giffard is shown in Fig. 41. On that figure the low-temperature data is divided into two regions labeled III-A, the temperature-independent region, and III-B.

Regions III-A, B. In Region III-A, the energy put into the system by the rf field gets to the reservoir or an excitation system tightly coupled to the reservoir by spatial diffusion of the particle motion excitations. The experimental evidence for this is the observation of non-exponential behavior of the long-time recovery of $M_Z(t)$ to $M_Z(0)$ in the three experiments mentioned above, the observation of short-time behavior,

$$M_Z(t) \sim 1/t^{1/2},$$

which is suggestive of a one-dimensional random walk (Giffard, 1968), and the observation of a sample chamber size dependence. The time scale for this diffusion process is about 1000 sec. On this time scale the Zeeman system, the tunneling system, and the mass fluctuation wave system have been in equilibrium a long time. Thus the diffusion in space of any one of these excitations carries the other excitations with it. In Appendix C, we show that the diffusion constant for energy in this circumstance is given by

$$D_E = (k_Z D_Z + k_T D_T + k_{MF} D_{MF})/(k_Z+k_T+k_{MF}), \quad (6.9)$$

where D_Z, D_T, and D_{MF} are the diffusion constants for the Zeeman energy (magnetization), the tunneling energy, and the mass fluctuation energy, respectively. This formula is a manifestation of the strong coupling among the diffusing excitations. If any one of the excita-
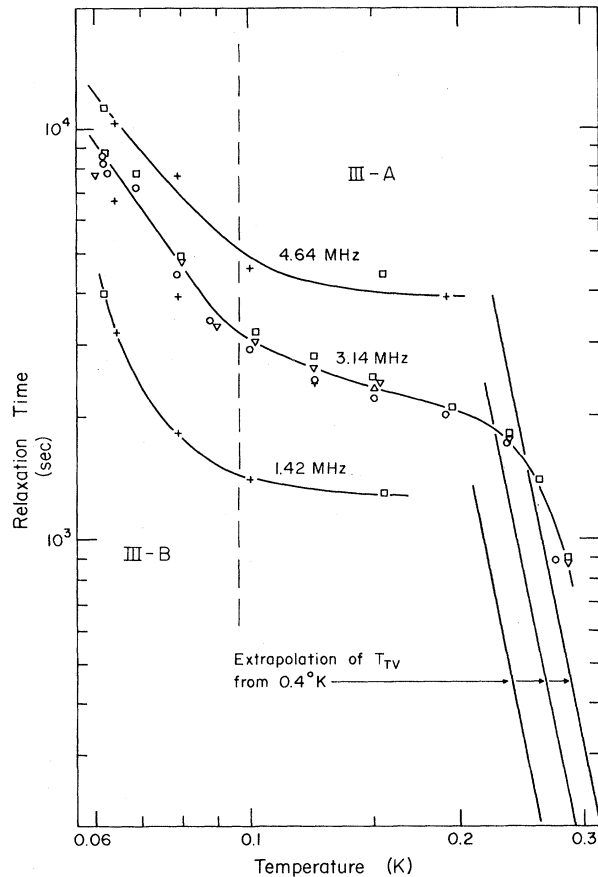
FIG. 41. Low-Temperature Plateau. Typical data from the thesis of Giffard (1968) (Giffard, 1971) are shown. On the right, the extrapolation to low temperatures of the T_1 data of region II-B is shown. Recall that the time dependence of $M_z(t)$ in Region III is qualitatively different from the exponential time dependence in Regions I and II. Thus the mismatch between the extrapolation of Region II-B data and the Region III data. T_1 is frequency dependent in Region III but only approximately in the way called for by the topological factor in D_E, Eq. (6.10). At temperatures in the vicinity of 0.1 K the plateau behavior goes over to a mildly temperature-dependent behavior.

tions has a large (specific heat) × (diffusion constant), its motion will dominate the diffusion of the energy. From Appendix C where we discuss the diffusion constant of each excitation, we have $D_Z = D_Z(3, 3) = A_Z(3,3)\Delta^2 J$, $D_T = D_T(3,3) = A_T(3,3)\Delta^2 J = \alpha A_Z(3,3)\Delta^2 J$, where α is a constant of order 1, and $D_{MF} \approx D_4(3, 3) = A_4(3,3)A^2\omega_4(3,3)$. Since, $k_{MF} \propto x_4$, and $x_4 \lesssim 300$ ppm, we have

$$D_E \approx D_Z(1 + \alpha k_T/k_Z)(1 + k_T/k_Z)^{-1}. \qquad (6.10)$$

The characteristic time for energy to diffuse a distance l with diffusion constant D_E is

$$t_D \sim l^2/D_E = (l^2/D_Z)(1 + k_T/k_Z)(1 + \alpha k_T/k_Z)^{-1}. \qquad (6.11)$$

Giffard, Hatton, and Truscott (1971) have found a

frequency dependence in T_1 throughout Regions III-A and III-B which is not consistent with $T_1 \propto t_D \propto (1/D_E)$ and any choice of $1 \leq \alpha \leq 2$. A recent theoretical calculation by Redfield and Yu (1968, 1969) has given $\alpha = 1$; this result predicts $D_Z \approx D_T$, or that there is no frequency dependence in T_1. As mentioned above, the direct measurement of D_Z and D_T by Hunt and Thompson (1968) gave $D_T \approx 2D_Z$, or $\alpha \approx 2$. This discrepancy between theory and experiment is unsettled. We take $t_D \approx T_1 \approx 10^3$ sec at $v = 20.0$ cm^3/mole and find $l \approx 0.003$ cm. This is a relatively short distance. It is not characteristic of the size of the sample chamber; it may be characteristic of the typical distance between structural defects. The energy delivered to the structural defect is converted at the defect into an excitation that can cross the sample chamber, with a typical dimension 1 cm, in a time much less than 1000 sec. It seems likely that the energy conversion process at the defect converts the energy in the particle motion excitations into phonons. This conversion process very probably involves the ^{4}He impurities. It is possible to construct plausible models for what is going on in the vicinity of the defects, however, there isn't adequate experimental data against which to test these models.

Giffard (1968) has constructed a model for the energy conversion process to phonons which also explains the temperature dependence that leads to Region III-B in terms of the phase separation process. In Giffard's model, the transition from the behavior of Region III-A to that of Region III-B occurs at $T = T_{PS}$. The analysis Giffard made of his data verified this point. However, Giffard calculated the phase separation temperature using the critical temperature, $T_C = 0.35$K, from the experiment of Edwards, McWilliams, and Daunt (1962) at 35 atm. Adams and Panczyk (1968) have found $dT_C/dP = -1.7$ mK/atm. Using a critical temperature appropriate to pressures of about 100 atm, $T_C \approx 0.23$ K, we find that T_{PS} for a mixture of 100 ppm is about 50 mK. Thus the phase separation temperature for the mixtures investigated by Giffard is substantially below the temperature range available in his experiment. We believe there is no compelling reason to associate the behavior observed in Region III-B with the phenomena of phase separation.

6.3 Dilute ^{3}He in ^{4}He Mixtures, Theory

There are as yet no experiments on systems with small concentrations of ^{3}He in ^{4}He. The excitations in these systems are:

(1) the mass fluctuation waves which represent the motion of a ^{3}He atom through the ^{4}He medium; the mass fluctuation waves carry a nuclear moment and are fermions; their magnetization is the Zeeman system,

(2) vacancy waves characterized by an excitation temperature of about 15K at $P \approx 30$ atm, and

(3) a phonon gas characteristic of nearly pure ^{4}He.
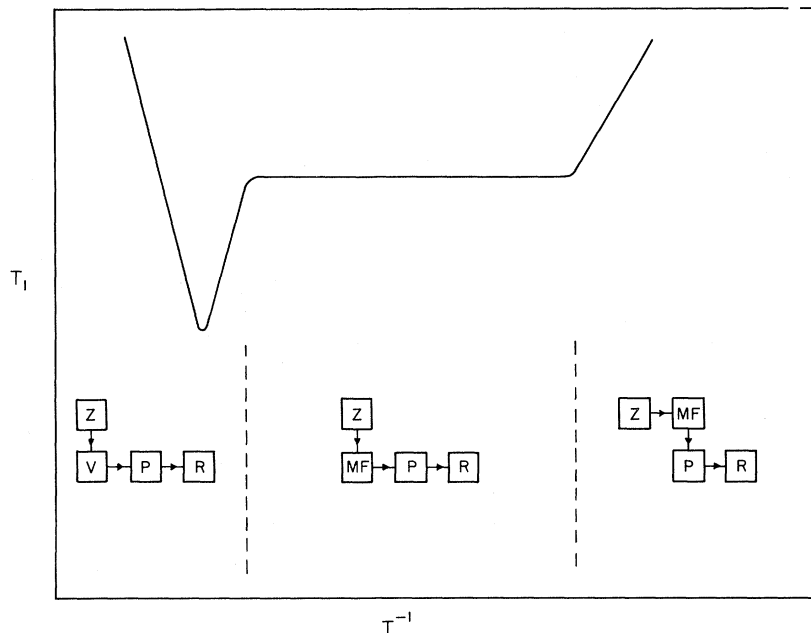
The interactions among these excitations are:

(1) Zeeman–vacancy wave; through the agency of $\mathcal{H}_d$;

(2) Zeeman–mass fluctuation wave; through the agency of $\mathcal{H}_d$. (This is the analog of the Zeeman–tunneling interaction in nearly pure ^{3}He);

(3) Masss fluctuation wave–phonon; and

(4) Mass fluctuation wave–vacancy; this is the analog of the tunneling–vacancy wave interaction in nearly pure ^{3}He.

Let us sketch the major features we would expect for this system. The Zeeman system and mass fluctuation waves are coupled by $\mathcal{H}_d$. For a magnetically dilute system, we have

$$T_1^{-1} \approx M_2 x_3 \tau_3 \{ [1/(1+\omega_0^2 \tau_3^2)] + [4/(1+4\omega_0^2 \tau_3^2)] \},$$
$$(6.12)$$

where $\tau_3^{-1} = \omega_3(V, 4) + \omega_3(4, 4)$, $\omega_3(4, 4)$ is the tunneling rate for a ^{3}He atom through ^{4}He, $\omega_3(V, 4)$ is the tunneling rate for a ^{3}He atom into a vacant neighboring lattice site, and

$$T_2^{-1} \approx M_2 x_3 \tau_3 \{ 1 + \tfrac{5}{3}[1/(1+\omega_0^2 \tau_3^2)]$$
$$+ \tfrac{2}{3}[1/(1+4\omega_0^2 \tau_3^2)] \}. \quad (6.13)$$

Equations (6.12, 6.13) embody both the Zeeman–vacancy and the Zeeman–mass fluctuation wave interaction. Both of these interactions convert the Zeeman energy to particle motion energy. The energy in the particle motions, the vacancy waves, and the mass fluctuation waves couples strongly to the phonons. The

result for T_{MFP} is exactly the same as that discussed above for the nearly pure ^{3}He case, except for the factor of concentration. We have

$$1/T_{MFP} \approx (\Delta m/m)^2 (k_B T/\hbar)(T/\theta)^6. \quad (6.14)$$

The factor of concentration is absent because the particle motion system which receives the energy from the Zeeman system is exactly the same size as the mass fluctuation system. Compare this case with that of nearly pure ^{3}He where the particle motion system is the tunneling system, and the mass fluctuation system is smaller by x_4.

In Fig. 42 we show what we believe would be the results of a typical T_1 experiment on dilute ^{3}He in ^{4}He.

7. NONDILUTE ^{3}He–^{4}He MIXTURES

7.1 Introduction

In this section we will discuss: (1) the excitations that exist in solid helium specimens with greater than 1000 ppm ^{4}He, (2) the results of experiments performed on these systems, and (3) the analysis of these experiments to provide information about the excitations in solid mixtures.

Solid mixtures have the same basic excitations as those in pure ^{3}He and in dilute mixtures; i.e., phonons, vacancy waves, and tunneling excitations. The primary theoretical problem is that of understanding how the dilution of the ^{3}He component of the system will affect the characterization of the excitations and their motion through the crystal. Consider an intermediate mixture, $x \simeq 0.5$. Almost all of the ^{3}He atoms will have at least
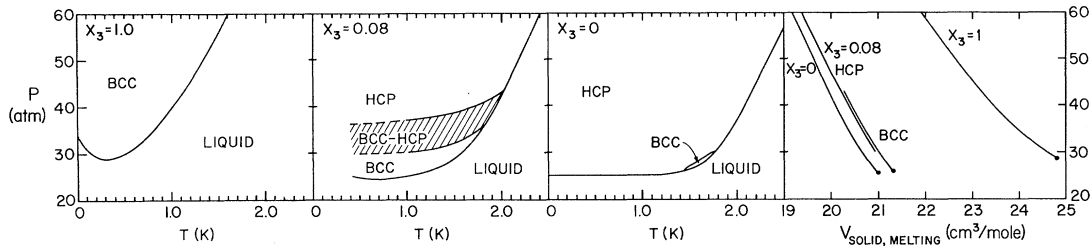
FIG. 43. Phase diagrams for mixtures. The figure shows the $P-T$ diagrams for pure ^{3}He $(x_3=1.0)$, pure ^{4}He$(x_3=0)$, and 8% mixture, and the $P-V$ diagram for all three. The ^{3}He diagram has been intensely studied (Mills, Gilly, and Sydoriak, 1961; Scribner, Panczyk, and Adams, 1969, and references therein) because of the information obtained about both the Fermi liquid and solid spin entropies. The minimum pressure for formation of solid ^{3}He occurs at $T=0.32$ K, and $p=28.9$ atm. In the case of ^{4}He (Schuch and Mills, 1962; and references therein) a minimum pressure of 25 atm is required for the formation of the solid. The melting properties of solid mixtures have been recently reviewed by Tedrow and Lee (1970). The diagram for the 8% mixture is from the work of Miyoshi, Cotts, Greenberg, and Richardson (1970). According to the Gibbs phase rule, the presence of a isotopic mixture permits the extra degree of freedom that allows the mixed hcp–bcc phase shown in $P-T$ space for $x=0.08$. The molar volume of a mixture is essentially given by the linear combination of the two partial components $[V(x_3, P) \simeq x_3 V(x_3=1, P)+(1-x_3) V(x_3=0, P).]$ (Mullin, 1968).

one ^{3}He atom as a nearest neighbor, and most atoms will have several ^{3}He neighbors; therefore, at low temperatures, the mutual tunneling of ^{3}He atoms will be an important mechanism for relaxation of the magnetization. (We expect the equivalent of Region I-B in pure ^{3}He to show up in mixtures.) At higher temperatures, we expect the analog of Region I-A in pure ^{3}He, i.e., if there are enough vacancies present we expect a region in which vacancy wave motion is important. Careful NMR studies of the mixtures will provide information about the parameters which characterize the vacancy wave excitations and the tunneling excitations.

In order to understand the changes that occur in the solid mixtures as pure ^{3}He is diluted further and further, we must first understand how the phase diagrams of the mixtures, $P-V-T$, vary with concentration. We compare various mixtures at the same molar volume; pure ^{3}He at 20.5 cm^3/mole occurs at 100 atm, whereas 8% ^{3}He in ^{4}He at 20.5 cm^2/mole occurs at $P\approx30$ atm. Figure 43 shows the melting curve of pure ^{3}He, pure ^{4}He, and the mixture $x_3=0.08$. We see that as the mixture goes from $x_3=1$ (pure ^{3}He) to $x_3=0$ (pure ^{4}He):

(1) the region of the $P-T$ plane occupied by the bcc phase decreases,

(2) the pressure required to form a solid mixture at a fixed volume decreases,

(3) the intermediate mixtures, $0<x<1$, have an hcp–bcc mixed phase region, and

(4) at sufficiently low temperature, the mixtures undergo an isotopic phase separation.

We will not discuss the physics of the phase diagrams in Fig. 43 in any detail. But we want the general feature of the phase diagram to be available for use in our interpretation of the experiments.

In that which follows, we tailor the expressions derived above to describe relaxation in pure ^{3}He to suit the present case, and then discuss the expreimental results for T_1, T_2, and D_Z measurements. We then summarize

the new information obtained about the excitations in mixtures at the end of the discussion.

7.2 T_1 Relaxation, Theory

In Fig. 44 we show the results of a typical T_1 experiment on a dilute ^{3}He-^{4}He mixture; $v=20.6$ cm^3/mole, $x_3=0.02$. As in the case of pure ^{3}He, the behavior of T_1 is ordered by T^{-1} into several regions.

Region I-A. In Region I-A, the relaxation process is that of vacancy wave motion. The effect of dilution is primarily to reduce the size of the average dipolar field seen at the site of each spin. We expect that, all other things being equal, T_1 will increase with dilution as a result of the weaker coupling of a spin to its environment via $\mathcal{3C}_d$. Let us examine the expressions derived to describe relaxation of the Zeeman system due to the presence of vacancy waves. From Sec. 4, we have Eq. (4.1)

$$T_1^{-1}=(2M_2/3)\{[\tau_V/(1+\omega_0^2\tau_V^2)]+[4\tau_V/(1+4\omega_0^2\tau_V^2)]\}.$$

$$(7.1)$$

We modify this equation to make it appropriate to nondilute mixtures. (1) Ignore for the moment any concentration dependence in τ_V^{-1}, the rate of ^{3}He tunneling into a vacant lattice site. (2) Perform the lattice sum called for in the second moment only, over the lattice sites occupied by ^{3}He atoms; the second moment for mixtures becomes

$$M_2(V, x)=x_3 M_2(V, x_4=0).$$

$$(7.2)$$

We therefore carry over the formalism derived for pure ^{3}He and the attendant interpretation of experiments; we make two modifications of the formalism, $M_2 x_3$ is to replace M_2 and τ_V is replaced by $\bar{\tau}_V$,

$$\bar{\tau}_V^{-1}=zx_V\omega_3(V, M),$$

$$(7.3)$$

where $\omega_3(V, M)$ is the rate of tunneling of a ^{3}He particle in a mixture, denoted by M, into a vacant

neighboring lattice site. This change in the microscopic frequency, $\omega_3(V, 3) \rightarrow \omega_3(V, M)$, and the mixture dependence of $x_V = x_V(M)$ are the only changes in τ_V.

Region I-B. In Region I-B, the behavior observed for T_1 is that characterizing relaxation of the Zeeman system to the tunneling system. In this region, vacancy waves and/or phonons couple the tunneling excitations to the lattice. In the spirit of the discussion above of dilution in Region I-A, we attempt to carry over the formalism developed for pure ^{3}He. We observe that the fourth moment involved in the time evolution of $\mathfrak{IC}_d$ contains double summation [Eq. (A2.11)] over the

FIG. 44. T_1 for Mixtures. The variation of T_1 with inverse temperature for the mixture $x_3 = 0.02$ is compared with that of pure ^{3}He at the same molar volume, $V = 20.6$ cm^3/mole, and precession frequency, $\omega_0/2\pi = 3.5$ MHz. The curve for the 2% mixture comes from the data of Miyoshi, Cotts, Greenberg, and Richardson (1968), and that for ^{3}He is based upon interpolation of the T_1 measurements of Reich (1963). We note that in Region I-A, ($T^{-1} < 0.7$) the vacancy contribution to the relaxation process is decreasing exponentially with temperature in both cases and with about the same slope. However the dilute mixture is in the hcp phase, whereas the pure specimen is in the bcc phase. In the case of pure ^{3}He, the activation energy for the vacancies in the hcp phase is about 50% greater than that of the bcc phase so that we conclude that the activation energy for vacancies decreases as the specimen is diluted at constant volume in the same crystallographic phase. The pure ^{3}He specimen displays no minimum in T_1 because ω_T is greater than the precession frequency ω_0. The minimum in T_1 occurs for the dilute mixture because the effective correlation frequency due to the tunneling has been decreased by the dilution process $\omega_T(x_3) \simeq (x_3)^{1/2}\omega_T(x_3 = 1)$.

lattice sites occupied by He^3 spins so that

$$M_4(V, x) = x_3{}^2 M_4(V, x = 0).$$

Carrying over the definition of ω_T from Appendix A.2, we have

$$\omega_T(x) = [M_4(x)/M_2(x)]^{1/2}$$
$$= [x_3{}^2 M_4(x = 0)/x_3 M_2(x = 0)]^{1/2} \quad (7.4)$$

or

$$\omega_T(x_3) = (x_3)^{1/2}\omega_T(x_3 = 1).$$

With this effective correlation frequency and the same modification of M_2 as we had above, $M_2(x_3) = x_3 M_2$, we find

$$T_1{}^{-1} = \frac{2}{3}(\frac{1}{2}\pi)^{1/2} \cdot \frac{M_2(x = 0)}{(x_3)^{1/2}\omega_T(x = 0)}$$

$$\times \left\{ \exp\left[-\left(\frac{\omega_0{}^2}{2x_3\omega_T{}^2} \right) \right] + 4 \exp\left[-\left(\frac{2\omega_0{}^2}{x_3\omega_T{}^2} \right) \right] \right\} \quad (7.5)$$

(using the Gaussian approximation).

We anticipate that some modification of these results will occur in the dilute limit, $x_3 \rightarrow 0$, for then very few ^{3}He atoms have ^{3}He neighbors, and we expect the tunneling motion of single ^{3}He particles through the ^{4}He matrix characterized by $\omega_3(4, 4)$ to govern the relaxation. As $x_3 \rightarrow 0$, the rate of relaxation of the Zeeman system is given by Eq. (6.12), where we let $\tau_V \rightarrow \infty$,

$$T_1{}^{-1} = \frac{2}{3}(x_3) M_2(x_4 = 0)$$

$$\times \{ [\tau_3/(1 + \omega^2 \tau_3{}^2)] + [4\tau_3/(1 + 4\omega_0{}^2 \tau_3{}^2)] \}, \quad (7.6)$$

where $\tau_3{}^{-1} = z\omega_3(4, 4)$. Thus we expect that as x_3 goes from nondilute concentrations, $0.95 > x_3 > 0.05$, toward dilute concentrations the source of the motions which will contribute to T_1 will go from ^{3}He–^{3}He tunneling, Eq. (7.5), toward ^{3}He–^{4}He tunneling, Eq. (7.6). Of course in the extremely dilute limit $x_3 < 1000$ ppm, we may also regard the ^{3}He atoms as mass fluctuation waves. But even before this limit is achieved we expect to see evidence in T_1 for the ^{3}He–^{4}He tunneling motion.

Region II. In the limit of nondilute mixtures where mass fluctuation waves do not propagate, the relaxation of energy dumped into the tunneling system occurs through coupling to the vacancy waves and/or the phonons. The treatment of relaxation in this region would be qualitatively similar to our treatment of Region II in Sec. 4. Behavior characteristic of Region II has yet to be observed in the preliminary experiments on the nondilute mixtures. Hence, we will not discuss Region II behavior for the nondilute mixtures in detail.

7.3 T_1 Experiments, Results

Figure 45 shows the variation of T_1 with inverse temperature for mixtures with $x_3 = 0.08$ and 0.02, $V = 21$ cm^3/mole, and $\omega_0 = 3.5$ MHz. The solid line is the behavior which would be observed for pure ^{3}He under the
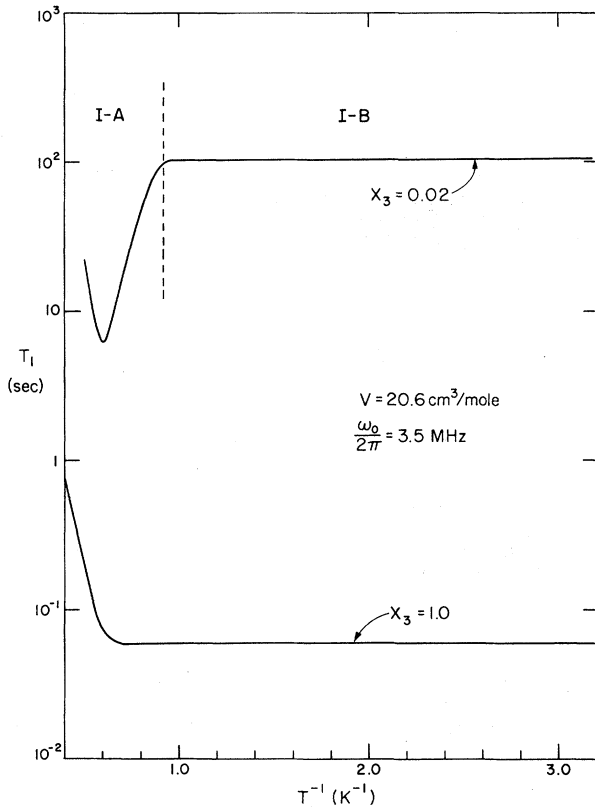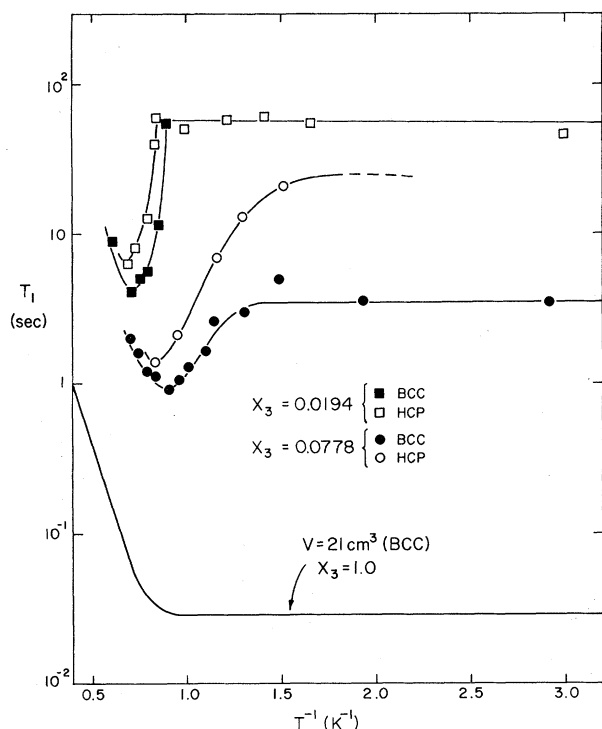
FIG. 45. T_1 for Mixtures at various concentrations. The figure shows T_1 measurements by Miyoshi, Cotts, Greenberg, and Richardson (1970) for the mixtures $x_3 = 0.0194$ and 0.0778 at $V = 21$ cm³/mole compared with the relaxation rate for pure ³He at the same precession frequency, 3.5 MHz. The open circles and open squares correspond to measurements of the relaxation rate for the hcp phase, and the solid circles and squares are measurements in the bcc phase. For this molar volume there are rather wide temperature ranges over which the bcc and hcp phase exist simultaneously. The relaxation rates observed in the mixed phase region have two components; a rapid one due to the contribution of the hcp phase which has the higher activation energy for vacancies, and a slower component from the fraction of the specimen in the bcc phase. The relative amplitude of the two components varies continuously with temperature as the mixed phase region is crossed. For $x_3 = 0.0778$, the specimen ultimately becomes completely a bcc solid at low temperatures for this molar volume, and for $x_3 = 0.0194$ the specimen becomes a hcp solid at low temperatures. The minimum in T_1 occurs at higher temperatures for the hcp component than for the bcc component, as expected. The plateau value of T_1 in region I-B increases rapidly with decreasing ³He concentration as a result of the weakening of the local dipolar field through the dilution process.

same conditions. Only Region I is seen in the data. For this particular sample, two relaxation rates are measured; i.e., $M_Z(t)$ decays back to $M_Z(0)$ as the sum of two components with different characteristic times. This occurs because the molar volume we have selected lies in the mixed phase region of Fig. 43. At the high-temperature end of the diagram, most of the sample is in the bcc phase, with a relatively low value of ϕ; as the temperature is lowered a large fraction of the $x_3 = 0.02$ sample occurs in the hcp phase and ultimately all of the specimen is hcp with a relatively high value of ϕ. Thus there is a steep decrease in τ_V, $\tau_V \propto \exp[-\beta\phi(M)]$. By $\phi(M)$, we mean the excitation temperature for a va-

cancy in a mixture designated by M. The qualitative description of the behavior of T_1 due to the presence of vacancy waves observed here is exactly the same as the qualitative description of T_1 in pure ³He in Region I-A. Information about τ_V and ϕ extracted from measurements of T_1, D, and T_2 in mixtures is summarized in the concluding section of this discussion.

In Region I-B, we observe a temperature-independent plateau given by the relaxation rate T_{ZT}^{-1}. We plot the T_1 data as a function of ω_0 from Region I-B in the same way we plotted this kind of data for pure ³He. See Fig. 20. Figure 46 shows a plot of $[T_1(\omega_0=0)/T_1(\omega_0)]$ versus $(\omega_0^2/x_3\omega_T^2)$ for all points measured in both phases and for concentrations $x_3 = 0.32$, 0.08, and 0.02. The parameters $T_1(\omega_0=0) = Kx^{1/2}[J(V)/V^2]$ and ω_T are calculated using the value of J for the same molar volume for pure He³ and Eqs. (A2.18 and A2.19). There are no adjustable parameters used in constructing the plot in Fig. 46. The fit of the mixture data to the spectral function of pure ³He is excellent. We take this as strong evidence that the value of J is unaffected by dilution. This interpretation is useful for the understanding of the problem of ³He doped with small quantities of ⁴He. Early attempts to explain the effects of
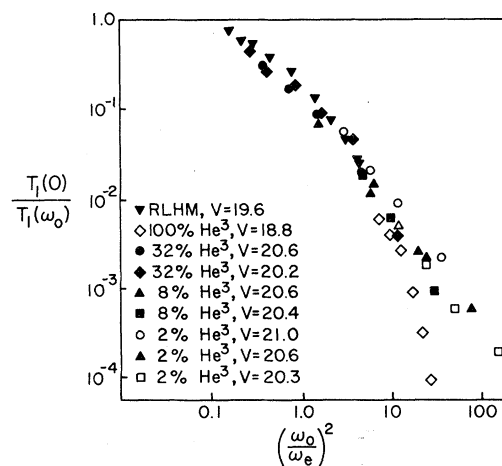

FIG. 46. Reduced plot of T_1 for mixtures. The figure shows a plot of $[T_1(0)/T_1(\omega_0)]$ versus $(\omega_0/\omega_e)^2$, obtained in the measurements by Miyoshi, Cotts, Greenberg, and Richardson (1970). The values of $T_1(\omega_0)$ are those measured at various molar volumes, ³He concentration, and Larmor frequencies in thermal region I-B. The quantity ω_e is the effective correlation frequency of the diluted pairs of spins $\omega_e = (x_3)^{1/2}\omega_T(x_3=1)$ and $T_1(0)$ is the zero-field limit of the relaxation rate given by Eq. 7.5 in the text $T_1(0) = Kx^{1/2}[J(V)/V^2]$. In plotting the points in the figure, the values of J used for each volume were obtained from these measured in pure ³He, Fig. 32. There are thus no adjustable parameters in making the plot shown. Since the data for mixtures fit upon the data of pure ³He in this plot, we conclude that the tunneling frequency between ³He pairs with a fixed molar volume is unaffected by the variation in the background medium from a predominantly ³He lattice to a predominantly ⁴He lattice. At the larger values of the Larmor frequency, the data points for the most dilute specimens, $x_3 = 0.02$, depart from the data obtained in richer mixtures. This is possibly evidence for the tunneling motion of ³He atoms with ⁴He neighbors, since T_1 varies as ω_0^2 [rather than as $\exp(\text{constant } x\omega_0^2)$].

⁴He doped in ³He in Region II used arguments that the average neighbor distance of pairs of ³He atoms around the site of a ⁴He atom decreased, thereby making large changes in the average value of J for such pairs. The result being discussed here on nondilute mixtures implies that J remains essentially constant for gross dilution. We therefore conclude that it probably does not change significantly for very dilute ⁴He in ³He.

We note that in Fig. 46 the data from the 2% mixture deviate from the universal relaxation curve in the limit of large values of ω_0/ω_T. Because $\omega_T^2 \propto x_3$, the data points for the $x_3 = 0.02$ mixture are at large values of ω_0^2/ω_T^2. We suspect that these deviations are evidence of the influence of ³He tunneling with the ⁴He. Let us suggest a model that incorporates this idea. We argue that as the very dilute limit is approached, 1000 ppm $<$ $x_3 < 0.05$, a ³He atom at lattice site R sees two kinds of ³He neighbors: (1) neighbors which are single isolated ³He atoms, and (2) neighbors that are members of clusters of ³He atoms of two or more. The isolated ³He atoms move with the characteristic frequency $\omega_3(4, 4)$ and contribute a dipolar field at R which fluctuates with frequency $\omega_3(4, 4)$. The clusters of ³He atoms move with a characteristic frequency ω_c, which is a complicated average of J and $\omega_3(4, 4)$, and contribute a dipolar field at R which fluctuates with frequency ω_c. Of course there is a continual transfer of particles between these two groups by virtue of the very tunneling processes that give rise to the fluctuations in each group but, if the rate at which particles are transferred between the two groups is small compared to the rate of fluctuation of the field due to each group, then the groups can be regarded as independent, and the contributions of the groups to the dipolar field at lattice site R are independent. We can estimate a concentration at which this independence of motion occurs. The cross section of a ³He atom for forming a pair is approximately $z\Delta^2$; thus the mean free path for pair formation is $\lambda_p = \Delta/zx_3$. The rate at which a single ³He forms pairs is

$$\omega_p = \Delta\omega_3(4, 4)/\lambda_p = zx_3\omega_3(4, 4).$$

We require that the rate at which pairs are formed by singles be small compared to the rate at which the dipolar field due to the single fluctuates, i.e., $\omega_p \ll \omega_3(4, 4)$ or $x_3z \ll 1$. This criterion suggests that at $x_3 \to 1\%$, the picture of groups of ³He atoms having substantially independent motions has some validity.

Let us adopt this picture. We regard the ³He atoms moving in the neighborhood of lattice site R as being made up of two independent components. Each component of the field particles contributes an independent dipolar field at R with a characteristic time dependence. Then, the relaxation of the spin at R will be dominated by whichever fluctuating field has the strongest Fourier component at ω_0. The spectral function for the ³He–⁴He tunneling goes approximately as

$$(2x_3/3)M_2[\tau_3/(1+\omega_0^2\tau_3^2)]$$

and the resulting rate for relaxation in the high frequency limit, $\omega_0\tau_3 \gg 1$, is

$$T_1^{-1}(3-4) \simeq (10/3)(x_3M_2/\omega_0^2\tau_3). \qquad (7.7)$$

On the other hand the relaxation rate due to He³ pair exchange is

$$T_1^{-1}(3-3) \simeq (\tfrac{1}{2}\pi)^{1/2}\tfrac{2}{3}x_3^{1/2}(M_2/\omega_T)$$
$$\times[\exp(-\omega_0^2/2x_3\omega_T^2)] \qquad (7.8)$$

in the equivalent limit $(x_3)^{-1}(\omega_0/\omega_T)^2 \gg 1$. The experimentally observed relaxation rate will depend upon the relative strength of the two independent fields so that

$$T_1^{-1}|_{\exp} = [c/T_1(3-4)] + [(1-c)/T_1(3-3)], \qquad (7.9)$$

where c is the concentration factor describing the number of isolated spins. The character of the high-frequency dependence of the spectral function due to 3–4 tunneling is much milder than that of 3–3 tunneling, ω_0^{-2} rather than $\exp[-(\omega_0^2/2x_3\omega_T^2)]$, so that eventually as ω_0 increases the (3–4) rate dominates the relaxation process. The motion of the isolated singles dominates the relaxation process. The data shown in Fig. 46 for 2% ³He in the hcp phase has an ω_0^2 dependence for T_1 in high fields. The same data fits the Gaussian correlation function model of exchange in low fields. Both of these results are in qualitative agreement with the discussion here.

Region II. The characteristic properties of Region II have been observed in only one published experiment on mixtures, that of Garwin and Reich (1964a) at $V = 19.3$ cm³ and $x_4 = 0.01$. The relaxation time varies as T^{-7} and is possibly the direct phonon coupling with the ³He tunneling bath. The ⁴He concentration is sufficiently large that the mass fluctuation waves do not propagate so they can't transfer the energy from the tunneling system to the phonons. In the same paper, the authors report a very interesting heat capacity measurement. A sequence of 90° pulses is applied at intervals long compared with T_{ZT} but quite short compared with T_1. (Each 90° pulse dumps a calibrated amount of heat into the energy reservoir.) The magnitude of the signal following each pulse is proportional to the temperature of the Zeeman system which is in equilibrium with the tunneling bath but not the lattice. The heat capacity obtained in the analysis of this experiment was 350 times the heat capacity of the ³He tunneling reservoir. This result is perhaps the most puzzling of any of the NMR experiments performed in solid helium. A possible explanation is that the heat capacity observed in the experiment is that due to isotopic phase separation. Edwards, McWilliams, and Daunt (1962) have measured the specific heat of mixtures and find an excess heat capacity above the phase separation temperature, i.e., a precursor to the phase separation which is sufficiently large to account for the observed anomalous specific heat. However, it is not clear how the spin system communicates its energy
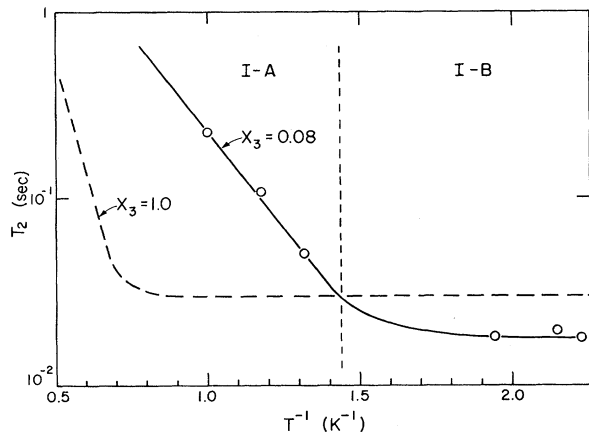
FIG. 47. T_2 for mixtures. The figure shows the values of T_2 in the bcc phase measured at $V=21$ cm³/mole for a mixture in which $x_3=0.08$ [Miyoshi, Cotts, Greenberg, and Richardson (1970)]. The data are compared with those obtained by Reich (1963) at $V=21.1$ cm³/mole for $x_3=1.0$. The two important features that arise from the comparison are that: (1) in Region I-A, $(T^{-1}<1.5\mathrm{K}^{-1})$ where the vacancy motion governs the spin equilibrium time, the characteristic energy for vacancy activation is much lower than that of pure ³He and (2) the temperature-independent value of T_2 for the 8% mixture in Region IB is $(T^{-1}>1.5$ K$^{-1})$ lower than the value of T_2 for pure ³He. The latter result is not predicted from simple considerations of the effects of dilution upon the tunneling motion of the pure ³He solid. If the important motion for the relaxation were the tunneling between ³He pairs, T_2 would be expected to increase as $x_3^{-1/2}$.

to such a heat reservoir without heating the lattice first.

7.4 T_2 and Diffusion Experiments

In Fig. 47, we show the results of a typical T_2 measurement on nondilute ³He–⁴He mixtures. As in the case of pure ³He, the behavior of T_2 is ordered by T^{-1} into two regions.

Region I-A. In Region I-A, both D_Z and T_2 behave essentially as they do in pure ³He. As was the case of T_1, we expect that the primary effect of dilution is to decrease the local dipolar field from M_2 to x_3M_2, thus making T_2 longer than it would be with the same vacancy wave motion in pure ³He solid. We modify Eq. (4.10) to take into account that only x_3N lattice sites are occupied by ³He atoms in making the second moment calculation. We obtain

$$T_2^{-1}= \frac{2x_3M_2(x_3=1)}{3\omega_0} \left(\frac{3}{2}\eta+ \frac{5}{2}\frac{\eta}{1+\eta^2} + \frac{\eta}{1+4\eta^2}\right),$$

$$(7.10)$$

where η is $\omega_0\tau_V$.

The diffusion coefficient that is measured in mixtures does not reflect the spin dilution since, in this region, the motion of the spins is due entirely to the presence of vacancy waves in the system. The expression for pure He³ vacancy diffusion $D_Z(V, 3) \propto \Delta^2\omega_V(3, 3)$ becomes $D_Z=\Delta^2\omega_V(3, 4)$, where $\omega_V(3, 4)\approx\omega_V(3, 3)$.

In Region I-B, the tunneling motion dominates both T_2 and the diffusion process so that they become temperature independent.

Figure 48 shows the values of T_2 vs T^{-1} for $V=21.0$ cm³/mole and $x_3=0.08$. As in the case of the T_1 for this
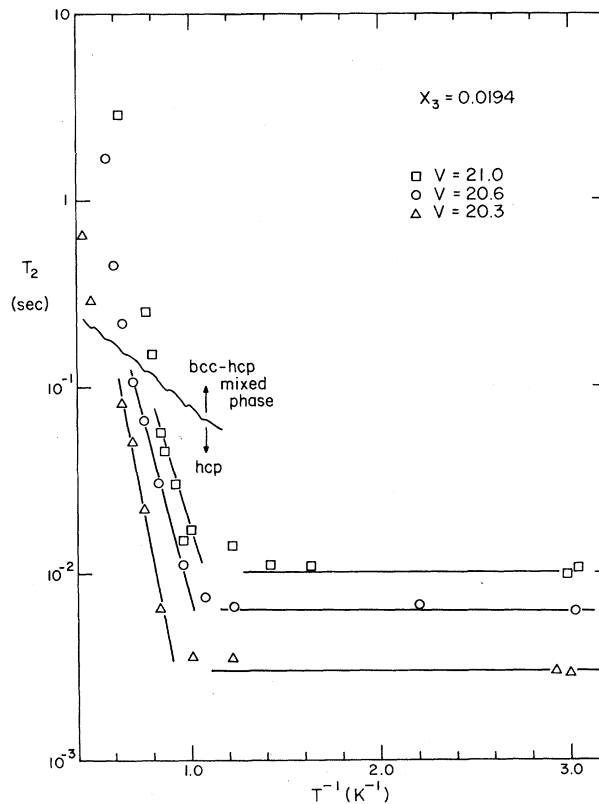

FIG. 48. T_2 at various molar volumes for a dilute mixture. The figure compares the values of T_2 obtained by Miyoshi, Cotts, Greenberg, and Richardson (1970) for the dilute mixture $x_3=0.0194$ at various molar volumes. In Region I-A, $T^{-1}<1.2$, the activation energy for the vacancy wave motion is seen to increase with molar volume as in pure ³He. For this particular concentration, the solid passes through the bcc–hcp mixed phase region into the pure hcp phase for volumes shown at temperatures in Region I-A. At lower temperatures, Region I-B, where the tunneling motion is responsible for the relaxation process, T_2 becomes independent of temperature. The variation of T_2 with volume in this region is quite large for this concentration. In pure ³He, T_2 increases from 15 msec to 30 msec when the volume is increased from 20.1 to 21.1 cm³/mole (see Fig. 22). In this specimen the value of T_2 increases by more than a factor of 3 when the volume is increased only from 20.3 to 21.0 cm³ so that the rate of change of T_2 with volume is twice as great for the dilute mixture $x_3=0.0194$ as for pure ³He. In the static or rigid lattice limit, where there is no tunneling motion, T_2 is of order 500 μsec for $x_3=0.02$ and $V=20$. In the rigid-lattice limit, T_2 varies with volume as V^2 so that T_2 would only increase by about 6% in going from 20.3 to 21 cm³/mole. The observed values of T_2 then, are too large and show far too much change with volume to be accounted for solely by the dipole motion of the rigid lattice.

A plausible explanation is that the observed relaxation is due to contributions from two independent field fluctuations so that the observed value of T_2 is the mixture relaxation rate of a small number, a, of isolated spins and the relaxation rate of $(1-a)$ spins which see the effects of the ³He tunneling motion.

$$T_2^{-1}|_{\mathrm{expt}}= (c/T_2)|_{\mathrm{static}}+[(1-c)/T_2]|_{\mathrm{motion}}.$$

concentration and volume, the relaxation process in Region I is characterized by two exponentials in the recovery time due to the existence of a mixed bcc–hcp phase solid. T_2 for both phases decreases rapidly with $1/T$ due to the depletion of vacancy waves. Measurements of T_2 and D_Z for mixtures in Region I-A have been analyzed (Miyoshi, 1970) to yield the parameters ϕ and τ_V for the mixture. The values for these parameters are summarized in the concluding part of this section.

As the temperature is lowered to reach Region I-B, the values of T_2 and D_Z become temperature independent. (D_Z has not been measured in this region because it is characteristically much too short.) The magnitude of T_2 is governed by the tunneling motion in the solid. Figure 49 shows the values of T_2 measured as a function of x for various molar volumes. The solid lines are the values of T_2 for the same molar volumes expected from consideration of the dilution of ^{3}He pair tunneling; the T_2 equivalent of Eq. (7.5). In the high-field limit we find

$$T_2^{-1} = \tfrac{10}{3}(\tfrac{1}{2}\pi)^{1/2}[M_2(x)/\omega_T(x)],$$

or

$$T_2^{-1} = \tfrac{10}{3}(\tfrac{1}{2}\pi)^{1/2}x_3^{1/2}[M_2(x_3=1)/\omega_T(x_3=1)]. \quad (7.11)$$

Thus, in the data shown in Fig. 49 we expect $T_2 \sim x_3^{-1/2}$. But T_2 does not increase as x_3 gets smaller.

We argue that this data gives evidence for the existence of a frozen-in component of the dipolar field. By this we mean that in the nondilute mixtures, there are particle clusters in which the potential energy at a pair of lattice sites is such that the interchange of the particles localized near these lattice sites is not energetically advantageous. The interchange may lead to an inequivalent energy for the system which is greater than the energy before interchange. Thus the motion must involve unlike pairs. The motion of the ^{3}He–^{4}He pair will be frozen out by energy considerations. Although it is difficult to quantify this concept, its consequence is that there is a contribution to H_d at R which is due to essentially static ^{3}He atoms. These static ^{3}He atoms give an independent dipolar field at R that contributes to T_2. We write

$$T_2^{-1}\big|_{\text{expt}} = aT_2^{-1}\big|_{\text{static}} + (1-a)T_2^{-1}\big|_{\text{motion}},$$

where $T_2^{-1}\big|_{\text{motion}}$ is given by Eq. (7.11), and a is a measure of the static component of the local dipolar field. We may use the data shown in Fig. 49 to obtain an estimate of a. Certainly $T_2\big|_{\text{static}}$ is not less than the natural dipolar linewidth,

$$[T_2(x_3)]^{-1}\big|_{\text{natural}} \sim \omega_d(x_3) \approx \omega_d(x_3)^{1/2}.$$

Now from Abragam we have $T_2\big|_{\text{natural}} \approx 10$ μsec. Thus we have

$$[T_2(x_3)]^{-1}\big|_{\text{natural}} \approx 10^5(x_3)^{1/2}.$$

For the data at $x_3 = 0.08$, $V = 20.2$ cm^3/mole we have $T_2\big|_{\text{motion}} \approx 20$ msec and $T_2\big|_{\text{expt}} \approx 2$ msec. Thus, we
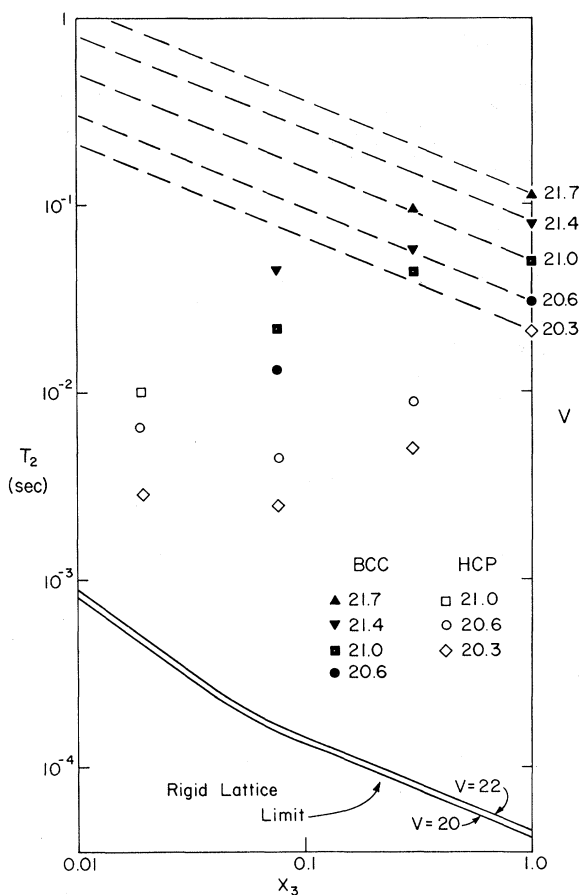

Fig. 49. The concentration dependence of T_2. The figure shows the values of T_2 in Region I-B for the mixtures measured by Miyoshi, Cotts, Greenberg, and Richardson (1970) at various molar volumes. T_2 decreases with concentration rather than increasing as might be expected from considerations of dilution on the ^{3}He–^{3}He tunneling motion shown with the dashed lines. The measured values of T_2 at the minimum dilution measured, $x_3 = 0.0194$, remain greater than that predicted for the rigid lattice (shown with solid lines), and display a strong variation with change in volume.

calculate $a(3\times10^4) + (1-a)50 = 500$ or $a \lesssim 0.02$. For plausible values of a it is possible to understand the results of the T_2 experiment.

Our description of the T_1 and T_2 data on nondilute mixtures is not very satisfactory. To understand the T_1 data, we introduced a local dipolar field due to the motion of isolated ^{3}He atoms. To understand the T_2 data, we have introduced a local dipolar field due to frozen in ^{3}He atoms. The need for this "*ad hoc*" approach to the nondilute mixtures in Region I-B provides compelling evidence of the need for a good first principles theory. When we have such a theory we will know how to extract $\omega_3(4,4)$, J, etc., quantities of great interest, from the experiments.

7.5 Properties of Excitations in ^{3}He–^{4}He Mixtures

In this section we summarize the properties of the excitations in solid ^{3}He–^{4}He mixtures which have been

measured in the NMR experiments described in Secs. 4 and 7. The properties of the excitations in pure ^{3}He are discussed at the end of Sec. 4. In principle, the class of experiments discussed in Secs. 6 and 7 provides a wealth of information about the excitations in mixtures. In practice, the new information that is reasonably well established is limited.

Tunneling Frequency. The experiment of Miyoshi, Cotts, Greenberg, and Richardson (1970) indicates that at fixed molar volume J is essentially independent of concentration. This result is made plausible by the results of theories of ^{3}He–^{4}He mixtures (Glyde, 1968) specific heat data (Sample and Swenson, 1967).

Mass Fluctuation Waves, $\omega_4(3, 3)$ *and* $\omega_3(4, 4)$. The experiments of Giffard and Hatton (1967), Giffard (1968), Bernier and Landesman (1969), Bernier (1970), and Reich and Yu (1969) suggest that $v = 20.0$ cm^3/mole $\omega_4(3, 3) \approx 4J$. Data on these excitations remains limited. There have been no experiments on mass fluctuation waves in $x_3 \to 0$ mixtures. Such experiments would measure $\omega_3(4, 4)$. There is some evidence for effects due to $\omega_3(4, 4)$ in the data of Miyoshi, Cotts, Greenberg, and Richardson (1970). The usefulness of that data is presently limited by the inadequacy of the theory on nondilute mixtures.

Vacancy Waves; $\phi(M)$ *and* $\omega_V(3, M)$. It is gratifying that the nondilute mixture experiments have provided a substantial amount of new data on the nature of vacancy excitations in quantum crystals. From the experiment of Miyoshi, Cotts, Greenberg, and Richardson (1970), we are able to determine the vacancy excitation temperature and vacancy tunneling frequency for ^{3}He–^{4}He mixtures approaching $x_3 \to 0$. In Fig. 50, we show the excitation temperature for vacancy waves as a function of pressure for pure ^{3}He (see Fig. 29) and ^{3}He–^{4}He mixtures with $x_3 = 0.32$, 0.08 and 0.02. We have plotted the data against pressure in order to illustrate a simple point. The energy required to create a vacancy in bcc ^{3}He is very nearly Pv. This energy is just the energy required to create the empty lattice site that is the vacancy. Let us look first at the bcc data on ϕ. At $P \approx 30$ atm, $x_3 = 1$, $\phi \approx 5$ K we estimate that the energy required to create a vacancy in bcc ^{4}He is about 5 K. The vacancy waves are a substantial contributor to the thermostatic properties of the bcc phase even in ^{4}He. Unfortunately bcc ^{4}He exists only in a small P–T sliver of the phase diagram so that thermostatic verification of this result is virtually impossible. For $P \approx 25$ atm and $x_3 \approx 0.02$, the solid mixture is in the hcp phase. The excitation temperature for vacancies in hcp ^{4}He is about 12 K–15 K. Should the vacancy waves contribute noticeably to the thermostatic properties of hcp ^{4}He? From the data of Edwards and Pandorf (1965) on hcp ^{4}He at 25 atm, we have $\theta_D^{(4)}(T_m) = 23$ K and for which $\phi^{(4)} = 15$ K. This is to be compared with bcc ^{3}He at 20 cm^3/mole, $P \approx 105$ atm, for which Edwards and Pandorf find $\theta_D^3(T_m) = 24$ K, and for which $\phi^{(3)} = 14.5$ K. Thus we expect the vacancy excitations in

static properties comparable to that which they make for bcc ^{3}He at $P = 105$ atm. At melting in hcp ^{4}He at 25 atm, the ratio of the vacancy and phonon contributions to the specific heat is about 1%. Thus the vacancy wave excitations don't seriously affect the thermostatic properties of hcp ^{4}He. At melting in bcc ^{3}He at 105 atm, the vacancy wave excitations make up 50% of the specific heat. Actually the values of ϕ derived by Sample and Swenson for bcc ^{3}He come from an analysis in which all excess specific heat beyond $(T/\theta_D^\circ)^3$ is assumed to be due to vacancies. This certainly isn't true, since $\theta_D(T) < \theta_D^\circ$ at $T > 1$ K. Thus the ϕ calculated by Sample and Swenson must account for too much of the excess specific heat. The ϕ of Sample and Swenson should be less than the NMR values.

The values of the tunneling frequency for a ^{3}He particle into a neighboring lattice site in solid ^{4}He, $\omega_V(3, 4)$ is essentially equal to $\omega_V(3, 3)$. This observation follows from the fact that Miyoshi, Cotts, Greenberg, and Richardson (1970) found D_0 in mixtures, $D = D_0 x_V$, to be in good agreement with the results of Reich in pure ^{3}He. Thus we conclude that $\omega_V(3, 3) \approx \omega_V(3, 4)$; the vacancy bandwidth is the same size in both ^{3}He and ^{4}He crystals.

It is appropriate here to make some comments on two recent suggestions about a superfluid state in solid ^{4}He. Chester (1970) has suggested that the possibility of such a state is not inconsistent with the known properties of the solid ^{4}He ground-state wavefunction. Further he has suggested that the ground-state wavefunction for the superfluid solid state should have ground-hcp ^{4}He at 25 atm to make a contribution to the thermo-
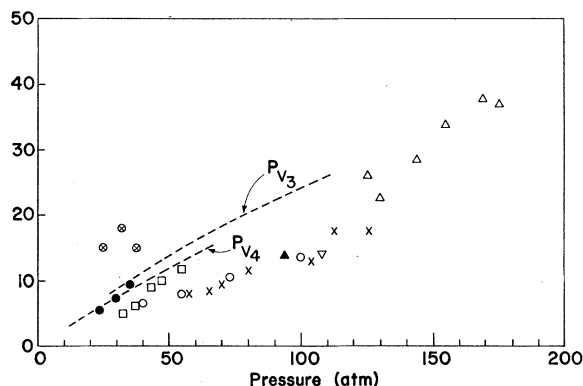

FIG. 50. Vacancy excitation temperature vs pressure. The excitation temperature is calculated using the data from the following sources: For hcp ^{3}He: △, Reich (1963), diffusion; For bcc ^{3}He: ✕, Reich (1963), diffusion; ▲, Richardson, Hunt and Meyer (1965), T_1; ▽, Giffard and Hatton (1967), T_1; ○, Sample and Swenson (1967), specific heat. For bcc ^{3}He–^{4}He mixtures: □, Miyoshi, Cotts, Greenberg, and Richardson (1970), T_1 and diffusion, ($x_3 = 0.32$); ●, Miyoshi, Cotts, Greenberg and Richardson (1970), T_1 and diffusion ($x_3 = 0.08$). For hcp ^{3}He–^{4}He mixtures: ⊗, Miyoshi, Cotts, Greenberg, and Richardson (1970), T_1 and diffusion ($x_3 = 0.02$). For bcc ^{3}He and bcc ^{3}He, the vacancy excitation temperature is less than PV. For hcp ^{3}He and hcp ^{4}He, the vacancy excitation temperature is about PV. There should be lots of vacancies in bcc ^{4}He.
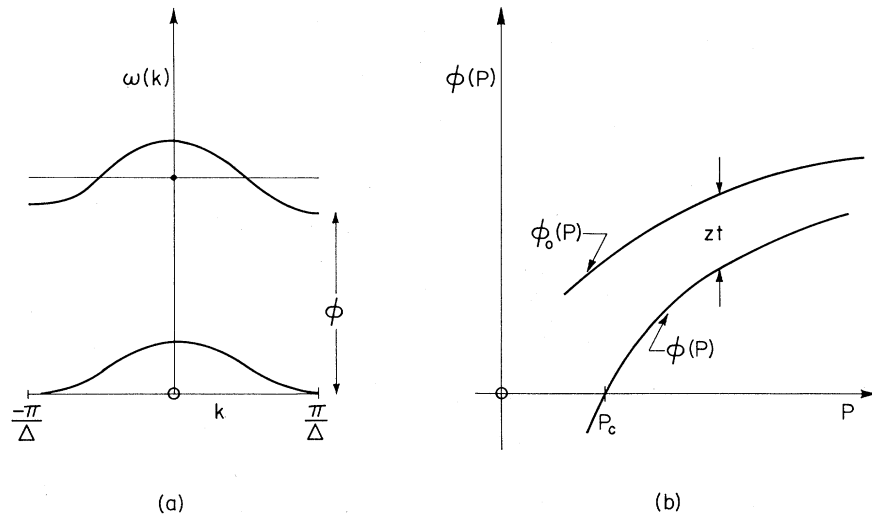
FIG. 51. Ground-state vacancies. Chester (1970) has suggested that in addition to thermally excited vacancies there are ground-state vacancies, i.e., two bands of vacancy excitations. The thermally excited band is depleted as $T{\to}0$, the ground-state band is not. Andreev and Lifshitz have suggested that $\phi(P) = \phi_0 - zt{\to}0$ at some pressure; i.e., the thermally excited vacancy band becomes a ground-state vacancy band at P_c.

(a)

(b)

state vacancies. We take this latter statement to mean that the single-particle density peaks at $N+n_v$ equivalent points in space, the lattice sites, but that in the vicinity of each lattice site we have less than one particle, $\langle n_R \rangle = N/(N+n_v)$. The excitation spectrum for the solid would have two vacancy wave bands as shown in Fig. 51a. The ground-state vacancies, whose number is n_v, move through the crystal just as do the thermally activated vacancies. At $T=0$ K, there are only ground-state vacancies in the system. Andreev and Lifshitz (1969) have made a similar proposal. Andreev and Lifshitz have suggested that the lower edge of the vacancy band approaches 0 at some pressure. See Fig. 51b. At pressure P_c the ground-state vacancies can occur. The NMR experiments we have discussed permit us to consider the likelihood that there are ground state vacancies. Since ground-state vacancy waves must move through the solid in the same way as thermally activated vacancies, they must contribute to a T_1 measurement in the same way as thermally activated vacancies. It is harder to form thermally activated vacancies in solid ^{4}He than in solid ^{3}He; it is harder to form thermally activated vacancies in hcp ^{3}He than in bcc ^{3}He. Thus in the absence of pathological behavior on the part of ^{4}He, we may use bcc ^{3}He as a test of the above hypothesis. We believe there are no ground-state vacancies in bcc ^{3}He. The data of Giffard and Hatton, and Giffard discussed in Sec. 4 shows relaxation due to thermally activated vacancies at concentrations of 10^{-14}. Therefore the number of ground-state vacancies in solid ^{3}He at $V=20.0$ cm^3/mole is less than $10^{-14}N$; $n_v/N < 10^{-14}$.

The theory of thermally activated vacancy excitation should also show the possibility of ground-state vacancies if they exist. The possibility of these excitations is ruled out by any plausible calculations with the theory (Mullin, 1971).

8. CONCLUDING REMARKS

Because of the large zero-point motion of the particles in a quantum crystal, there are particle motion excitations in these systems: (a) tunneling excitations, (b) vacancy wave excitations, and (c) mass fluctuation waves. We have described these excitations and the physics they give rise to that is observable in NMR experiments. We have also described the results of NMR experiments and the information that is obtainable from them about the particle motion excitations.

Our description of the particle motion excitations has stressed the interplay of theory and experiment. A qualitative idea of the nature of the excitation leads to the expectation of certain phenomena to be observed, perhaps by NMR. The observation of the expected phenomena in turn leads to a quantitative understanding of the excitation. From the observation of unexpected phenomena, one can glean new and interesting aspects of physics. The progress that has been made in understanding the excitations in quantum crystals has followed closely this pattern of mutual feedback between theory and experiment. We are hopeful that future work in this field will follow this same pattern and that it will be as profitable as what has gone before.

9. ACKNOWLEDGMENTS

APPENDIX A: RELAXATION TIMES

A.0. Introduction to T_1

In this Appendix we calculate the rate for the relaxation of energy between the various systems of excita-

tions that are present in the quantum crystals. These calculations amount to an exercise in the application of a basic computational scheme due to Abragam (1961) that is reviewed below. The application of this computational scheme to Zeeman–vacancy relaxation was apparent following the observation by Goodkind and Fairbank (1959) of the high-temperature behavior of T_1. The experiments of Reich (1963) and Garwin and Landesman (1964) in which the Zeeman–tunneling relaxation was observed were interpreted by Garwin and Landesman and Hartman (1964) using the computational scheme of Abragam. At the same time, Garwin and Landesman introduced the multiple bath picture of the relaxation process that has been so fruitfully applied to solid ^{3}He. Garwin and Landesman, and P. M. Richards (1965) have described the tunneling–vacancy wave relaxation process. The relaxation rates calculated below have not previously been described in the literature.

Consider a solid which is inhabited by two kinds of excitations, designated 1 and 2, which are weakly interacting with one another. By weakly interacting we mean that the 1-system and 2-system come to thermal equilibrium within themselves on a time scale short compared to the rate at which energy is transferred from the 1 system of excitations (1-system) to the 2 system of excitations (2-system). We write the Hamiltonian for the solid as

$$\mathcal{3C} = \mathcal{3C}_1 + \mathcal{3C}_2 + \mathcal{3C}_{12} = \mathcal{3C}_0 + \mathcal{3C}_{12}, \qquad (A0.1)$$

where $\mathcal{3C}_0 = \mathcal{3C}_1 + \mathcal{3C}_2$, $\mathcal{3C}_1$ and $\mathcal{3C}_2$ are the Hamiltonian for the 1-system and 2-system respectively, and $\mathcal{3C}_{12}$ is the interaction between 1 and 2. The form of Eq. (A0.1) contains the crux of the physical arguments we want to make about the system. We assume that the excitations in the 1-system are in thermal equilibrium among themselves and move independently of the excitations in the 2-system (which are also in thermal equilibrium) except for $\mathcal{3C}_{12}$. That is we have

$$[\mathcal{3C}_1, \mathcal{3C}_2] = 0 \qquad (A0.2)$$

but $[\mathcal{3C}_1, \mathcal{3C}_{12}] \neq 0$ and $[\mathcal{3C}_2, \mathcal{3C}_{12}] \neq 0$. We will choose $\mathcal{3C}_{12}$ to be a plausible analytic representation of the interaction of the 1-system with the 2-system.

The rate at which energy is lost from the 1-system to the 2-system due to $\mathcal{3C}_{12}$ is calculated as follows:

1. Compute $d\langle \mathcal{3C}_1 \rangle / dt$,

$$d\langle \mathcal{3C}_1 \rangle / dt = d \, \mathrm{Tr} \, \mathcal{3C}_1 \sigma / dt = \mathrm{Tr} \, \mathcal{3C}_1 \dot{\sigma}, \qquad (A0.3)$$

where σ is the density matrix for the system.

2. Use the interaction representation to do the calculation of the density matrix Then, we have

$$d\langle \mathcal{3C}_1 \rangle / dt = \mathrm{Tr} \, \mathcal{3C}_1 \dot{\sigma}^*, \qquad (A0.4)$$

where $\dot{\sigma}^* = \exp(i\mathcal{3C}_0 t) \dot{\sigma} \exp(-i\mathcal{3C}_0 t)$, and in general we write $O^*(t) = \exp(i\mathcal{3C}_0 t) O \exp(-i\mathcal{3C}_0 t)$. In the interaction representation, the equation of motion for

$\sigma^*(t)$ is:

$$i\hbar \dot{\sigma}^*(t) = [\mathcal{3C}_{12}^*(t), \sigma^*(t)]. \qquad (A0.5)$$

The solution to this equation by iteration to second order in $\hbar^{-1}$ is

$$\sigma^*(t) = \sigma^*(0) - \frac{i}{\hbar} \int_0^t [\mathcal{3C}_{12}^*(t'), \sigma^*(0)] \, dt'$$

$$+ \left(\frac{i}{\hbar}\right)^2 \int_0^t dt' \int_0^t dt'' [\mathcal{3C}_{12}^*(t), [\mathcal{3C}_{12}^*(t''), \sigma^*(0)]].$$

$$(A0.6)$$

From this equation we find $\dot{\sigma}^*(t)$ to be

$$\dot{\sigma}^*(t) = -\frac{i}{\hbar} [\mathcal{3C}_{12}^*(t), \sigma^*(0)] + \left(\frac{i}{\hbar}\right)^2$$

$$\times \int_0^t dt' [\mathcal{3C}_{12}^*(t), [\mathcal{3C}_{12}^*(t'), \sigma^*(0)]]. \qquad (A0.7)$$

3. Now we specialize Eq. (A0.7) because of the noise character of $\mathcal{3C}_{12}^*(t)$: (a) $\mathcal{3C}_{12}^*(t)$ is regarded as a noise source. Therefore we want to calculate $d\langle \mathcal{3C}_1 \rangle / dt$ for an ensemble of $\mathcal{3C}_{12}$'s or equivalently we want to use a $\dot{\sigma}^*(t)$ in Eq. (A0.4) which is obtained by ensemble averaging Eq. (A0.7). We denote $\dot{\sigma}^*(t)$ appropriately ensemble averaged by $\langle \dot{\sigma}^*(t) \rangle_{Av}$. In general, quantities that are ensemble averaged over $\mathcal{3C}_{12}$ are denoted by brackets, $\langle \ \rangle_{Av}$. (b) Assume $\sigma(0)$ and $\mathcal{3C}_{12}^*(t)$ are uncorrelated. (c) Replace $\sigma^*(0)$ under the time integral in Eq. (A0.7) by $\sigma^*(t)$. (d) Put the upper limit in the time integral in Eq. (A0.7) at $+\infty$. Carrying out (a)–(d) we obtain

$$\frac{d}{dt} (\langle \mathcal{3C}_1 \rangle) = \left(\frac{i}{\hbar}\right)^2$$

$$\times \int_0^\infty dt' \, \mathrm{Tr} \, \mathcal{3C}_1 \langle [\mathcal{3C}_{12}^*(t), [\mathcal{3C}_{12}^*(t'), \sigma^*(t)]] \rangle_{Av}.$$

$$(A0.8)$$

4. We assume that the 1-system and the 2-system are in thermal equilibrium throughout the relaxation process (as the 1-system loses energy to the 2-system), and that the density matrix has the form

$$\sigma^*(t) = \exp[-\beta_1(t)]\mathcal{3C}_1 \exp-(\beta_2 \mathcal{3C}_2), \qquad (A0.9)$$

where $\beta_1(t)^{-1} = k_B T_1(t)$, and β_2, the inverse temperature of the 2-system, has a fixed value because the 2-system is attached to an external reservoir at inverse temperature β_2. The 1-system relaxes from a higher temperature to the temperature of the 2-system. The 2 system is in equilibrium with a reservoir. As $\beta_1(t)$ approaches β_2 we have

$$\sigma^*(t) = \exp-[\beta_1(t) - \beta_2]\mathcal{3C}_1 \exp-\beta_2\mathcal{3C}_0$$

$$\approx [1 - \beta_1(t) - \beta_2]\sigma_0(\beta_2), \qquad (A0.10)$$

where $\sigma_0(\beta_2) = \exp(-\beta_2\mathcal{3C}_0)$ is the equilibrium density matrix for H_0 at inverse temperature β_2. Using Eq.

(A0.10) in Eq. (A0.8) leads to

$$d\langle\mathfrak{IC}_1\rangle/dt = -[\beta_1(t)-\beta_2]\left(\frac{i}{\hbar}\right)^2$$

$$\times \int_0^\infty dt'' \langle \mathfrak{IC}_1[\mathfrak{IC}_{12}*(t), [\mathfrak{IC}_{12}*(t''), \mathfrak{IC}_1(t)]]\rangle \quad (A0.11)$$

where $\langle\cdots\rangle = \mathrm{Tr} \exp(-\beta\mathfrak{IC}_0)\cdots$.

We may obtain an alternative expression for $d\langle\mathfrak{IC}_1\rangle/dt$ by using Eqs. (A0.9) and (A0.10) directly, i.e.,

$$\frac{d}{dt}\langle\mathfrak{IC}_1\rangle = \frac{d}{dt}\frac{\mathrm{Tr}\,\mathfrak{IC}_1\sigma*(t)}{\mathrm{Tr}\,\sigma*(t)} = -(d/dt)\beta_1(t)\langle\Delta\mathfrak{IC}_1{}^2\rangle,$$

$$(A0.12)$$

where

$$\langle\Delta\mathfrak{IC}_1{}^2\rangle = \langle(\mathfrak{IC}_1-\langle\mathfrak{IC}_1\rangle)^2\rangle.$$

5. The quantity T_{12} is defined by the equation

$$\dot{\beta}_1(t) = -T_{12}{}^{-1}[\beta_1(t)-\beta_2]. \quad (A0.13)$$

This time, T_{12}, is called the *intrinsic* time. It is the characteristic time for decay of energy from the 1-system to the 2-system when: (1) these two systems are an isolated pair, and (2) the 2-system remains always at the equilibrium temperature, Fig. 52. Now recall that the specific heat of the 1-system is given by

$$C_1 = \frac{d}{dT}\langle\mathfrak{IC}_1\rangle = +\frac{d\beta}{dT}\frac{dE_1}{d\beta} = -\frac{d\beta}{dT}\langle\Delta\mathfrak{IC}_1{}^2\rangle = \frac{d\beta}{dT}k_1,$$

$$(A0.14)$$

where we have defined the *energy constant* k_1 by

$$k_1 = dE_1/d\beta.$$

The combination of Eqs. (A0.11)–(A0.13) and the definition of k_1 leads to

$$T_{12}{}^{-1} = (\hbar^2 k_1)^{-1}$$

$$\times \int_0^\infty dt \langle\mathfrak{IC}_1(0)[\mathfrak{IC}_{12}*(0), [\mathfrak{IC}_{12}*(t), \mathfrak{IC}_1(0)]]\rangle, \quad (A0.15)$$

where we have used the fact that the expectation value in the integral depends upon the relative time only, to simplify the integrand. Equation (A0.15) may be brought to the form

$$T_{12}{}^{-1} = \frac{1}{\hbar^2}k_1{}^{-1}\int_0^\infty dt \langle[\mathfrak{IC}_1(0), \mathfrak{IC}_{12}*(0)][\mathfrak{IC}_1(0), \mathfrak{IC}_{12}*(t)]\rangle$$

or

$$T_{12}{}^{-1} = \frac{1}{\hbar^2}k_1{}^{-1}\int_0^\infty d\tau \langle p_{12}(t)p_{12}(t+\tau)\rangle, \quad (A0.16)$$

where $p_{12}(t) = [\mathfrak{IC}_1(0), \mathfrak{IC}_{12}*(t)]$. This is the fundamental formula for the intrinsic time. See also Eq. (A0.22) below.

Let us specialize Eq. (A0.16) by writing the perturbation $\mathfrak{IC}_{12}$ in the form

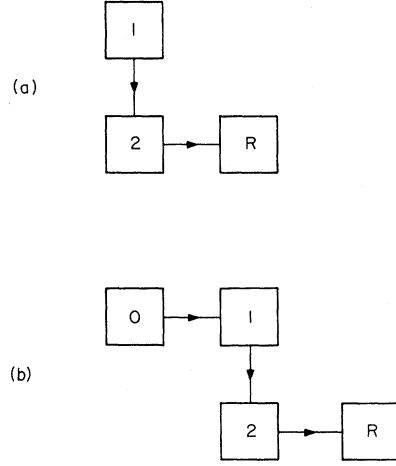$$\mathfrak{IC}_{12} = h_1 h_2, \quad (A0.17)$$

Fig. 52. Topologies. (a) The topology for the calculation of the intrinsic time. (b) The topology for the calculation of the topological time.

where h_1 depends upon the coordinates of the 1-system only, and h_2 depends upon the coordinates of the 2-system only. We write $\mathfrak{IC}_{12}*(t) = h_1*(t)|_1 h_2*(t)|_2$, where by $h_1*(t)|_1$ we mean h_1 time evolved according to $\mathfrak{IC}_1$. Now we write the expectation value in Eq. (A0.16) in the form

$$\langle p_{12}(t)p_{12}(t+\tau)\rangle = \langle p_1(t)p_1(t+\tau)\rangle_1\langle h_2(t)|_2 h_2(t+\tau)|_2\rangle_2$$

$$\equiv G_1(t)F_2(t), \quad (A0.18)$$

where

$$p_1(t) = [\mathfrak{IC}_1(t), h_1(t)]$$

and

$$\langle\cdots\rangle_n = \mathrm{Tr} \exp(-\beta\mathfrak{IC}_n)\cdots.$$

The function $\langle p_{12}(t)p_{12}(t+\tau)\rangle$ is called the correlation function. Its separate pieces, $G_1(t)$ and $F_2(t)$ are also correlation functions. The perturbation to the 1-system due to the 2-system is through $\mathfrak{IC}_2$ driving the term h_2 in $\mathfrak{IC}_{12}$. Let us carry out Fourier analysis of the motion of G_1,

$$G_1(t) = \int d\omega e^{+i\omega t}G_1(\omega) = \langle p_1(t)p_1(t+\tau)\rangle_1$$

or

$$G_1(\omega) = (2\pi)^{-1}\int dt e^{-i\omega t}G_1(t). \quad (A0.19)$$

Then we find

$$T_{12}{}^{-1} = \frac{1}{\hbar^2}k_1{}^{-1}\int_0^\infty dt f_2(t)\int d\omega e^{i\omega t}G_1(\omega)$$

$$= (\hbar^2 k_1)^{-1}\int d\omega G_1(\omega)F_2(-\omega),$$

where

$$F_2(\omega) = \int_0^\infty dt F_2(t)e^{-i\omega t}. \quad (A0.20)$$

Thus the product of the power spectrum of h_2 and p_1

yields the relaxation rate. The function

$$\int d\omega G_1(\omega) F_2(-\omega)/\hbar^2 k_1$$

is called the spectral function. Its separate pieces $G_1(\omega)$ and $F_2(\omega)$ are also spectral functions.

Suppose that we have calculated T_{12} and we want to know T_{21}, the rate at which energy is transferred from 2 to 1. Using energy conservation for the coupled systems we must have

$$d(\langle \mathfrak{IC}_1 \rangle + \langle \mathfrak{IC}_2 \rangle)/dt = 0.$$

Now $\langle \mathfrak{IC}_1 \rangle$ is given by $\langle \mathfrak{IC}_1 \rangle = \text{Tr } \mathfrak{IC}_1 \exp(-\beta \mathfrak{IC}_1)$ so that

$$d\langle \mathfrak{IC}_1 \rangle/dt = (d\langle \mathfrak{IC}_1 \rangle/d\beta)\dot{\beta}_1 = k_1 \dot{\beta}_1,$$

and

$$d\langle \mathfrak{IC}_2 \rangle/dt = (d\langle \mathfrak{IC}_2 \rangle/d\beta)\dot{\beta}_2 = k_2 \dot{\beta}_2.$$

Thus energy conservation implies $\dot{\beta}_1 = -(k_2/k_1)\dot{\beta}_2$. We define T_{21} by the equation of motion for β_2

$$\dot{\beta}_2 = -T_{21}^{-1}(\beta_2 - \beta_1) \qquad (A0.21)$$

and using Eq. (A0.13) we have

$$-T_{12}^{-1}(\beta_1 - \beta_2) = (k_2/k_1)(T_{21})^{-1}(\beta_2 - \beta_1)$$

or

$$T_{21}^{-1} = T_{12}^{-1}(k_1/k_2). \qquad (A0.22)$$

This result is in agreement with the intuitive notion of energy flow. For $k_1 \gg k_2$, a relatively small change in β_1 implies a large energy flux to the 2-system and a relatively large change in β_2, or $T_{21}^{-1} \gg T_{12}^{-1}$.

In the remainder of this Appendix we illustrate the application of these general results to various systems of coupled excitations. There are four excitations, phonons, vacancy waves, tunneling excitations, and mass fluctuation waves, with which we deal. Thus there are $(4 \cdot 3)/2! = 6$ basic interactions among these excitations. See Table III.

A.1 Zeeman-Vacancy Wave Relaxation

We will discuss in some detail the relaxation of the Zeeman system to the vacancy system as an illustration of the basic ideas which are developed in a general way above. We take the Hamiltonian describing the coupled Zeeman–vacancy system to be

$$\mathfrak{IC} = \mathfrak{IC}_Z + \mathfrak{IC}_V + \mathfrak{IC}_{ZV}. \qquad (A1.1)$$

Here the Zeeman system is taken to be described by

$$\mathfrak{IC}_Z = -\mathbf{H}_0 \cdot \sum_i \boldsymbol{\mu}_i. \qquad (A1.2)$$

The vacancy system is described by

$$\mathfrak{IC}_V = \sum_\mathbf{k} \epsilon_V(\mathbf{k}) C_V^+(\mathbf{k}) C_V(\mathbf{k}), \qquad (A1.3)$$

where $C_V^+(\mathbf{k})$ is defined in Eq. (3.7) of the text. The motion of a vacancy wave through the lattice does not directly perturb the Zeeman system. The Zeeman–

vacancy interaction comes about because of the modulation of the dipole–dipole interaction between the nuclear magnetic moments by the vacancy motion. Thus $\mathfrak{IC}_{ZV}$ is given by the dipolar Hamiltonian

$$\mathfrak{IC}_{ZV} = \mathfrak{IC}_d = \sum_{q=-2}^{+2} \sum_{i<j} B_{ij}{}^q S_{ij}{}^q, \qquad (A1.4)$$

where the B's are a function of the relative position of particles i and j, and the S's are a function of the spins of particles i and j. The dipolar Hamiltonian, $\mathfrak{IC}_d$, is discussed in great detail by Abragam (1961) and Slichter (1963).

The correspondence of this problem with the general problem discussed above is made by associating $\mathfrak{IC}_1$ with $\mathfrak{IC}_Z$, $\mathfrak{IC}_2$ with $\mathfrak{IC}_V$, and H_{12} with $\mathfrak{IC}_d$. We consider the relaxation of the Zeeman system to the vacancy system. Then, the basic equation, Eq. (A0.15), involves the time evolution of $\mathfrak{IC}_{12}^*(t)$

$$\mathfrak{IC}_{12}^*(t) = \mathfrak{IC}_{ZV}^*(t)$$
$$= \sum_{q=-2}^{+2} \sum_{i<j} \exp(i\mathfrak{IC}_0 t) B_{ij}{}^q S_{ij}{}^q \exp(-i\mathfrak{IC}_0 t).$$
$$(A1.5)$$

It is *assumed* that in $\mathfrak{IC}_0 = \mathfrak{IC}_Z + \mathfrak{IC}_V$, the $\mathfrak{IC}_Z$ piece time evolves the spin part of $\mathfrak{IC}_{ZV}$, and the $\mathfrak{IC}_V$ piece time evolves the position part of $\mathfrak{IC}_{ZV}$, i.e., the B's. We have

$$\exp(i\mathfrak{IC}_0 t) B(0) S(0) \exp(-i\mathfrak{IC}_0 t)$$
$$= \exp(i\mathfrak{IC}_V t) B(0) \exp(-i\mathfrak{IC}_V t)$$
$$\times \exp(i\mathfrak{IC}_Z t) S(0) \exp(-i\mathfrak{IC}_Z t)$$
$$= B(t)|_V S(t)|_Z \qquad (A1.6)$$

and

$$\mathfrak{IC}_{ZV}(t) = \sum_{q=-2}^{+2} \sum_{i<j} B_{ij}{}^q(t)|_V S_{ij}{}^q(t)|_Z$$
$$= \sum_{q=-2}^{+2} \sum_{i<j} B_{ij}{}^q(t)|_V S_{ij}{}^q(0) \exp(-iq\omega_0 t), \qquad (A1.7)$$

since $S_{ij}{}^q(t)|_Z = S_{ij}{}^q(0) \exp(-iq\omega_0 t)$. So the correlation function called for in Eq. (A0.15) is given by

$$\langle p_{12}(t) p_{12}(t+\tau) \rangle = \sum_{qq'} \sum_{i<j} \exp(-iq\omega_0 \tau)$$
$$\times \exp[-i(q+q')\omega_0 t]$$
$$\times \langle B_{ij}{}^q(t) B_{ij}{}^{q'}(t+\tau) [\mathfrak{IC}_Z, S_{ij}{}^q(0)][\mathfrak{IC}_Z, S_{ij}{}^{q'}(0)] \rangle.$$
$$(A1.8)$$

We proceed further by using the following steps:

(a) The correlation between $p(t)$ abd $p(t+\tau)$ is taken between a given pair of spins at t, and the same pair at $t+\tau$.

(b) The B^q's are spherical harmonics so that only the term $q = -q'$ contributes in $\sum_{qq'}$.

TABLE III. Interaction matrix.[a]

	Phonon	Vacancy wave	Tunneling	Mass fluctuation wave
Phonon	D_p			
Vacancy wave	(A-4): phonon scattering from the mass fluctuation and lattice distortion	D_v		
Tunneling	(A-3): phonon modulation of the vacancy wave tunneling process interferes with the regularity of the spin arrangement		$D(3,3)$	
Mass fluctuation wave	(A-6): phonon scattering from the mass fluctuation and lattice distortion		(A-5): mass fluctuation wave interferes with the regularity of the spin arrangement	$D_{MF}(4)$

[a] There are four excitations and $4 \times 3/2! = 6$ interactions among them. The intrinsic rates for transfer of energy among the four systems of excitations by the six interactions are calculated in Appendix A. The part of the Appendix dealing with each interaction is noted. The diagonal components of the interaction matrix are the self-interactions that would appear in the self-diffusion constants; in the case of the phonons the self-interaction is seen in the thermal conductivity.

(c) The commutator of S^q with H_Z has the simple form

$$[S_{ij}^q, \mathfrak{IC}_Z] = -q\hbar\omega_0 S_{ij}^q. \quad (A1.9)$$

From (a)–(c) it follows that

$$T_{ZV}^{-1} = \frac{1}{\hbar^2} k_Z^{-1} \sum_{q=-2}^{+2} q^2 (\hbar\omega_0)^2 \sum_{i<j} \langle S_{ij}^q(0) S_{ij}^{-q}(0) \rangle_Z$$

$$\times \int_0^\infty dt \langle B_{ij}^q(0) B_{ij}^{-q}(t) \rangle_V \quad (A1.10)$$

It is conventional to write this result in the form

$$T_{ZV}^{-1} = J_1(\omega_0)_V + J_2(\omega_0)_V, \quad (A1.11)$$

where

$$J_q(\omega_0)_V = \int_0^\infty G_q(t)_V \exp(-iq\omega_0 t)\, dt, \quad (A1.12)$$

$$G_1(t)_V = \sum_{i<j} [(\omega_0)^2/k_Z] \langle B_{ij}^1(0) B_{ij}^{-1}(t) \rangle_V$$

$$\times \langle S_{ij}^1(0) S_{ij}^{-1}(0) \rangle_Z, \quad (A1.13)$$

and

$$G_2(t)_V = 4 \sum_{i<j} [(\omega_0)^2/k_Z] \langle B_{ij}^2(0) B_{ij}^{-2}(t) \rangle_V$$

$$\times \langle S_{ij}^2(0) S_{ij}^{-2}(0) \rangle_Z. \quad (A1.14)$$

We *assume* that the B correlation function has a simple time dependence

$$\langle B_{ij}^q(0) B_{ij}^{-q}(t) \rangle_V = \langle B_{ij}^q(0) B_{ij}^{-q}(0) \rangle_V \exp(-t/\tau_V), \quad (A1.15)$$

where τ_V is a characteristic time related to the vacancy motion in the solid which we will discuss in detail below. After a straightforward but considerable computational effort we can show that for a powder

$$G_1(t) = \tfrac{1}{3} M_2 \exp(-t/\tau_V), \quad (A1.16)$$

and

$$G_2(t) = \tfrac{4}{3} M_2 \exp(-t/\tau_V), \quad (A1.17)$$

where

$$M_2 = \sum_{i<j} [(\omega_0)^2/k_Z] |B_{ij}^0(0)|^2 S_{ij}^1(0) S_{ij}^{-1}(0) \quad (A1.18)$$

is the well-known Van Vleck second moment of the dipolar field. The second moment is given by

$$M_2 = (9/20)\gamma^4 \hbar^2 \sum_{i \neq (j)} [1/|\mathbf{R}_i - \mathbf{R}_j|^6]. \quad (A1.19)$$

Using Eqs. (A1.12–19), we may write Eq. (A1.11) in in the simple form

$$T_{ZV}^{-1} = \tfrac{2}{3} M_2 \{ [\tau_V/(1+\omega_0^2\tau_V^2)] + [4\tau_V/(1+4\omega_0^2\tau_V^2)] \}. \quad (A1.20)$$

This equation provides an explicit example of the basic ideas discussed in the text (Sec. 4). If we have the qualitative dependence of τ_V on the temperature,

$$\lim_{T \to +\infty} \tau_V \to 0, \quad \text{and} \quad \lim_{T \to 0} \tau_V \to +\infty,$$

then

$$\lim_{T \to +\infty} T_{ZV}^{-1} \sim (10/3) M_2 \tau_V \sim 0,$$

and

$$\lim_{T \to 0} T_{ZV}^{-1} \sim (4/3) M_2 (\omega_0^2 \tau_V)^{-1} \sim 0.$$

At both extremes of $\omega_0 \tau_V$, the relaxation time goes to $+\infty$. A minimum occurs in T_1 at $\omega_0 \tau_V = 0.62$, i.e., when the basic microscopic frequency, τ_V^{-1}, is comparable with the "looking" frequency of the spins.

The tunneling rate for vacancy waves. The rate for tunneling of a ^{3}He particle into a neighboring vacancy site is given by

$$\tau_V^{-1} = x_V z \omega_3(V, 3). \quad (A1.21)$$

TABLE IV. Parameters used in the calculation of T_1 at $V = 20.0$ cm³/mole at all temperatures.[a]

v_0 cm³/mole	Δ Å	α^2 [b] (Å)⁻²	$z\omega_V(3,3)$ half-bandwidth K	θ_D [c] K	ϕ^d K	$J/2\pi$ [e] MHz	M_2 10⁸ (rad/sec)²
20	3.51	2.03	1.1	29	14.5	1.0	5.67
21	3.56	1.84	1.5	27	11.3	2.2	5.13
22	3.62	1.69	1.7	24	9.5	4.6	4.67
23	3.67	1.55	2.0	22	7.8	8.6	4.27
24.7	3.76	1.32	2.3	18	5.5	25	3.71

[a] For the purposes of the numerical calculation which illustrate the application of the results in Appendix A we have calculated T_1 at $V = 20.0$ cm³/mole at all temperatures, Fig. 53. In this table we show the parameters that were used in that calculation. We also show the half bandwidth for vacancy waves using the undistorted single-particle wavefunctions of Sarkissian (1969). See Fig. 30.

[b] Sarkissian (1969).

[c] From the smooth curve on Fig. 28.

[d] From Fig. 29.

[e] From Figs. 31 and 32.

Here x_V is the concentration of vacancies, z is the number of near neighbors, and $\omega_3(V, 3)$ is the frequency for tunneling of a ³He atom into an adjacent empty lattice site in a pure ³He crystal. In Eq. (A1.21) the factors $x_V z$ are the probability that one of the z near neighbors of a ³He is empty (occupied by a vacancy). We estimate the frequency of tunneling of a ³He atom into a vacancy

$$\omega_3(V, 3) = \tfrac{3}{2} \int d\mathbf{x} \phi_R(\mathbf{x}) T(\mathbf{x}) \phi_{R'}(\mathbf{x}), \quad (A1.22)$$

where $\phi_R(\mathbf{x})$ is the wavefunction for a ³He atom at R with a vacant lattice site at R', $\phi_{R'}(\mathbf{x})$ is the wavefunction for a ³He atom at R' with a vacant lattice site at R, and $T(x)$ is the kinetic energy operator. The factor of $\tfrac{3}{2}$ comes from the fact that the potential energy has a similar off-diagonal matrix element but $\langle PE \rangle = \tfrac{1}{2}\langle KE \rangle$. The wavefunctions used to calculate $\omega_3(V, 3)$ should be slightly distorted ground-state wavefunctions. We ignore the distortion and calculate $\omega_3(V, 3)$ using the ground-state wavefunctions of Sarkissian (1969). The results of these calculations are shown in Table IV and on Fig. 30.

A.2 Zeeman–Tunneling Relaxation

We consider the relaxation of energy from the Zeeman system to the ³He tunneling system. The physics of this relaxation mechanism is the same as that of the Zeeman–vacancy wave relaxation mechanism. The energy in the Zeeman system is coupled to the motion of the ³He particles by the dipolar interaction. In this case the motion of the ³He particles is that due to tunneling instead of to the presence of vacancies.

We make the identifications

$$\mathcal{H}_1 \rightarrow \mathcal{H}_Z, \quad (A2.1)$$

$$\mathcal{H}_2 \rightarrow \mathcal{H}_T, \quad (A2.2)$$

and

$$\mathcal{H}_{12} \rightarrow \mathcal{H}_{ZT} = \mathcal{H}_d. \quad (A2.3)$$

Now the time evolution of $\mathcal{H}_{12}^*(t)$ is given by

$$\mathcal{H}_{12}(t) = \mathcal{H}_{ZT}(t) = \sum_{q=-2}^{+2} \sum_{i<j} \exp(i\mathcal{H}_0 t) B_{ij}{}^q S_{ij}{}^q$$

$$\times \exp(-i\mathcal{H}_0 t), \quad (A2.4)$$

where $H_0 = H_Z + H_T$. It is conventional at this stage to write

$$\exp(i\mathcal{H}_0 t) B^q(0) S^q(0) \exp(-i\mathcal{H}_0 t)$$

$$= B^q(0) \exp(i\mathcal{H}_0 t) S^q(0) \exp(-i\mathcal{H}_0 t), \quad (A2.5)$$

and use

$$\exp(i\mathcal{H}_0 t) S^q(0) \exp(-i\mathcal{H}_0 t) = \exp(i\mathcal{H}_T t) S^q(0)$$

$$\times \exp(-i\mathcal{H}_T t) \exp(-iq\omega_0 t). \quad (A2.6)$$

The time evolution of $S_{ij}{}^q$ due to H_Z is well known, $\exp(i\mathcal{H}_Z t) S^q(0) \exp(-i\mathcal{H}_Z t) = S^q(0) \exp(-iq\omega_0 t)$.

The curious feature of this procedure is noticed by comparison of Eqs. (A2.5) and (A2.6) with Eq. (A1.6) above. Above, when the motion of the ³He particles was due to vacancies this motion was assumed to be manifested in the time evolution of $B_{ij}{}^q$, the spatial part of $\mathcal{H}_{\text{dipolar}}$. Here, when the motion of the ³He particles is due to tunneling, the motion is assumed to be manifested in the time evolution of $S_{ij}{}^{-q}$ the spin part of $\mathcal{H}_{\text{dipolar}}$. The reason for this is simple. There is a useful pseudospin Hamiltonian which correctly describes the effect of the ³He tunneling motion. Thus that motion can be regarded as a motion of the spin operators only. No useful effective spin Hamiltonian has been written down which describes the motion of the ³He particles due to tunneling into vacancies. Thus in the treatment of the vacancy problem that motion has been taken to reside in $B_{ij}{}^q$.

This ambiguity in the treatment of the two processes can be resolved by returning to Eq. (A1.6) above and writing

$$\exp\,(i\mathcal{3C}_0 t) B^q(0) S^q(0)\,\exp\,(-i\mathcal{3C}_0 t)$$
$$= B^q(0) S^q(t)|_V \exp\,[-iq\omega_0(t)], \quad (A2.7)$$

where

$$S^q(t)|_V = \exp\,(i\mathcal{3C}_V t) S^q(0)\,\exp\,(-i\mathcal{3C}_V t). \quad (A2.8)$$

Then in Eq. (A1.10) one would have the factor

$$\sum_{i<j} B_{ij}{}^q(0) B_{ij}{}^{-q}(0) \langle S_{ij}{}^q(0) S_{ij}{}^{-q}(t)|_V\rangle. \quad (A2.9)$$

Results identical with those in Appendix A1 are achieved by the approximation

$$\langle S_{ij}{}^q(0) S_{ij}{}^{-q}(t) \mid _V\rangle = \langle S_{ij}{}^q(0) S_{ij}{}^{-q}(0)\rangle\, \exp\,(-t/\tau_V)$$
$$(A2.10)$$

[cf., Eq. (A0.15)]. It doesn't really matter where you put the time dependence due to the vacancy waves unless you are going to be serious about calculating the correlation functions.

Returning to the calculation of Zeeman–tunneling relaxation we can follow the results in Appendix A.1 through the steps leading to Eq. (A1.11). We have

$$T_{ZT}{}^{-1} = J_1(\omega_0)_T + J_2(\omega_0)_T, \quad (A2.7)$$

where

$$J_q(\omega)_T = \int_{-\infty}^{\infty} G_q(t)_T e^{-i\omega t}\,dt, \quad (A2.8)$$

$$G_1(t)_T = (\omega_0{}^2/k_Z)\sum_{i<j} B_{ij}{}^1(0) B_{ij}{}^{-1}(0)$$
$$\times\langle S_{ij}{}^1(0) S_{ij}{}^{-1}(t)|_T\rangle_T, \quad (A2.9)$$

and

$$G_2(t)_T = (4\omega_0{}^2/k_Z)\sum_{i<j} B_{ij}{}^2(0) B_{ij}{}^{-2}(0)$$
$$\times\langle S_{ij}{}^2(0) S_{ij}{}^{-2}(t)|_T\rangle_T. \quad (A2.10)$$

The time evolution of the S^q's is given by $\mathcal{3C}_T$. It is conventional at this stage to expand $S^q(t)$ in Taylor series for small t, i.e.,

$$S^q(t) = (1+i\mathcal{3C}_T t+\cdots) S^q(0) (1-i\mathcal{3C}_T t+\cdots).$$
$$(A2.11)$$

Then, Eq. (A2.9) for $G_1(t)_T$ can be put in the form

$$G_1(\tau)_T = \tfrac{1}{3}M_2 - (M_4/6)\tau^2+\cdots, \quad (A2.12)$$

where M_2 is the Van Vleck second moment defined in Eq. (A1.19), and M_4 is the Van Vleck fourth moment

given by (Van Vleck, 1948):

$$M_4 = (\gamma^4\hbar^4/N)\{ \sum_{j,k,l\neq} [3B_{jk}{}^2 B_{ji}{}^2 + 2A_{jk}{}^2(B_{jl}-B_{kl})^2$$
$$+2A_{jk}A_k(B_i-B_{jk})(B_{jl}-B_{kl})+2A_{jk}B_{jk}(B_{jl}-B_{kl})^2]$$
$$\times[\tfrac{1}{3}I(I+1)]^2+\sum_{k>j}[2B_{jk}{}^4\tfrac{41}{5}[I^2(I+1)^2-\tfrac{1}{3}I(I+1)]$$
$$+4B_{jk}{}^3 A_{jk}\tfrac{1}{5}[\tfrac{2}{3}I^2(I+1)^2-\tfrac{1}{2}I(I+1)]$$
$$+B_{jk}{}^2 A_{jk}{}^2[\tfrac{4}{5}I^2(I+1)^2-\tfrac{3}{5}I(I+1)]]\} \quad (A2.13)$$

in which the quantities A_{jk} and B_{jk} are

$$A_{jk} = -\tfrac{1}{2}(1-3\,\cos^2\theta_{jk})r_{jk}{}^{-3}$$

and

$$B_{jk} = \tfrac{3}{2}(1-3\,\cos^2\theta_{jk})r_{jk}{}^{-3}.$$

The second and fourth moments have been evaluated for bcc and hcp crystals, and are given by

$$M_2 = \begin{matrix} 22.796 & (bcc), \\ \times\,(10^{10}/V^2)\,\sec^{-2} & \\ 22.610 & (hcp), \end{matrix} \quad (A2.14)$$

and

$$M_4 = \begin{matrix} 517.76 & (bcc), \\ \times 10^{10}(J^2/V^2)\,\sec^{-4} & \\ 951.68 & (hcp), \end{matrix} \quad (A2.15)$$

where V is the molar volume in cm³/mole. In evaluating M_4, the exchange interaction is assumed to exist only between near neighbors, and only the terms of order J^2 in (A2.13) are retained. The lattice sums used to calculate (A2.13) and (A2.14) do not include the effects of the large-amplitude zero-point motion. A correct calculation of (A1.19) and (A2.12) would include the expectation value of $r_{ij}{}^{-6}$ in the sum $\sum_k r_{jk}{}^{-6}(t)$ and would be expected to decrease M_2 and M_4 in (A2.14) and (A2.15) by about $+10\%$ (Harris, 1971).

In order to evaluate (A2.8) and (A2.7), it is useful to approximate the series in (A2.12) with a simple function having the same Taylor series expansion for small values of τ. Two such functions appear to be useful, a Gaussian

$$G_1(\tau)_T = M_2/3\,\exp\,(-\tfrac{1}{2}\omega_T{}^2\tau^2), \quad (A2.16a)$$

where

$$\omega_T{}^2 = M_4/M_2,$$

and a Lorentzian (Richards, 1970)

$$G_1(\tau)_T = (M_2/3)(1+\omega_T{}^2\tau^2)^{-1}, \quad (A2.16b)$$

where $\omega_T{}^2 = \tfrac{1}{2}M_4/M_2$. (If the next higher order term of the series in (A2.12), $+(M_6/72)\tau^4$ were retained it would be possible to justify a prererence for one or the other of these expressions. However, evaluation of the sixth moment has proven too formidable a task for anyone to attempt. We will do the calculation including both possibilities and compare the results of each with the experiments.)

In the case of a powder of crystallites, we have that $G_2(\tau) = 4G_1(\tau)$ so that Eq. (A2.7) becomes

$$T_{ZT}^{-1} = J_1(\omega_0)_T + J_1(2\omega_0)_T. \qquad (A2.17)$$

Evaluation of (A2.8) then yields

$$J_1(\omega_0)_T = (\tfrac{1}{2}\pi)(M_2/3\omega_T)\exp(-\omega_0^2/2\omega_T^2);$$

$$\omega_T^2 = (M_4/M_2) \qquad (A2.18a)$$

for the Gaussian correlation function, and

$$J_1(\omega_0)_T = (\tfrac{1}{2}\pi)(M_2/3\omega_T)\exp[-(\omega_0/\omega_T)];$$

$$\omega_T^2 = M_4/2M_2 \qquad (A2.18b)$$

for the Lorentzian correlation function. The relation between ω_T and J for both correlation functions is

$$\omega_T = \begin{cases} 4.76J & \text{bcc} \\ \\ 6.48J & \text{hcp} \end{cases} \text{Gaussian} \qquad (A2.19)$$

$$\omega_T = \begin{cases} 3.36J & \text{bcc} \\ \\ 4.58J & \text{hcp} \end{cases} \text{Lorentzian} \qquad (A2.20)$$

The imaginary component of the Fourier transform of $G_1(\tau)$ gives rise to a slight shift to the central frequency of the resonant absorption and has been discussed in detail by Kubo and Tomita (1955).

A.3 Tunneling-Vacancy Wave Relaxation

We consider relaxation of energy from the ^{3}He tunneling system to the vacancy waves. The basic topology is shown in Fig. 37a. We make the identification

$$\mathcal{3C}_1 \to \mathcal{3C}_T \qquad (A3.1)$$

$$\mathcal{3C}_2 \to \mathcal{3C}_V \qquad (A3.2)$$

$$\mathcal{3C}_{12} \to \mathcal{3C}_{TV} = -\hbar J \sum_{RR'} \Delta\alpha(RR')\boldsymbol{\sigma}_R \cdot \boldsymbol{\sigma}_{R'}, \qquad (A3.3)$$

where $\Delta\alpha(RR') = \alpha(RR') - \langle \alpha(RR') \rangle$, and $\alpha_{RR'}$ is zero when a vacancy is at either R or R' and 1 for both R and R' occupied by ^{3}He atoms. To do this calculation it is most convenient to intercept the general development above at (A0.15). The integrand in Eq. (A0.15) is

$$\langle \mathcal{3C}_1(0)[\mathcal{3C}_{12}^*(0), [\mathcal{3C}_{12}^*(t), \mathcal{3C}_1(0)]]\rangle$$

$$= \langle \mathcal{3C}_{12}(0)[\mathcal{3C}_1(0), [\mathcal{3C}_1(0), \mathcal{3C}_{12}^*(t)]]\rangle$$

or from Eq. (A3.3)

$$(+i\hbar)^2\hbar^2 J^2 \sum_{RR'}\sum_{SS'} \langle \Delta\alpha_{RR'}(0)\Delta\alpha_{SS'}(t)|_V\rangle_V$$

$$\times (d^2/dt^2)\langle A_{RR'}(0)A_{SS'}(t)|_T\rangle_T, \qquad (A3.4)$$

where $A_{RR'} = \boldsymbol{\sigma}_R \cdot \boldsymbol{\sigma}_{R'}$. Substituting Eq. (A3.4) into

Eq. (A0.15) leads to

$$T_{TV}^{-1} = + \frac{\hbar^2 J^2}{k_T} \sum_P \int_0^\infty dt \langle \Delta\alpha_P(0)\Delta\alpha_P(t)|_V\rangle_V \frac{d^2}{dt^2}$$

$$\times \langle A_P(0)A_P(t)|_T\rangle_T, \qquad (A3.5)$$

where $\sum_P$ is a sum over neighboring pairs. Now we separate the pairs into 3-3 pairs, 3-V pairs, and VV pairs,

$$\Delta\alpha_P(0)\Delta\alpha_P(t) = (1-x)^2\Delta\alpha_{33}(0)\Delta\alpha_{33}(t)$$

$$+2x(1-x)\Delta\alpha_{3V}(0)\Delta\alpha_{3V}(t) + x^2\Delta\alpha_{VV}(t). \qquad (A3.6)$$

Using the definition of $\Delta\alpha_{33}$ and $\Delta\alpha_{3V}$, we have

$$\Delta\alpha_{33}(0) = \alpha_{33}(0) - \langle\alpha\rangle = 1 - (1-zx) = zx, \qquad (A3.7a)$$

$$\Delta\alpha_{3V}(0) = \alpha_{3V}(0) - \langle\alpha\rangle = 0 - (1-zx) = -(1-zx). \qquad (A3.7b)$$

$$\Delta\alpha_{VV}(0) = \alpha_{VV}(0) - \langle\alpha\rangle = -1+zx. \qquad (A3.7c)$$

Now for the correlation functions involving $\Delta\alpha_{33}(t)$, $\Delta\alpha_{3V}(t)$, and $\Delta\alpha_{VV}(t)$, we write

$$\langle \Delta\alpha_{33}(0)\Delta\alpha_{33}(t)\rangle = \langle \Delta\alpha_{33}(0)^2\rangle f_{33}(t), \qquad (A3.8a)$$

$$\langle \Delta\alpha_{3V}(0)\Delta\alpha_{3V}(t)\rangle = \langle \Delta\alpha_{3V}(0)^2\rangle f_{3V}(t), \qquad (A3.8b)$$

and

$$\langle \Delta\alpha_{VV}(0)\Delta\alpha_{VV}(t)\rangle = \langle \Delta\alpha_{VV}(0)^2\rangle f_{VV}(t), \qquad (A3.8c)$$

where $f_{33}(t)$, $f_{3V}(t)$, and $f_{VV}(t)$ are time decaying functions that have the general property that $f(0) = 1$ and $f(+\infty) = 0$. Putting Eqs. (A3.7a, 7b, 7c) and Eqs. (A3.8a, 8b, 8c) into Eq. (A3.6) leads to

$$\langle \Delta\alpha_P(0)\Delta\alpha_P(t)|_V\rangle_V = (1-x)^2(zx)^2 f_{33}(t)$$

$$+2x(1-x)(1-zx)^2 f_{3V}(t) + x^2(1-zx)^2 f_{VV}(t). \qquad (A3.9)$$

Keeping only the leading term in concentration, we get

$$\langle \Delta\alpha_P(0)\Delta\alpha_P(t)|_V\rangle_V = 2xf_{3V}(t). \qquad (A3.10)$$

The 3-V pair becomes uncorrelated after the vacancy has taken one step, where the mean time between steps is τ_V. For this physical process, we obtain for $f_{3V}(t)$

$$f_{3V}(t) = [1+(t/\tau_V)]\exp-(t/\tau_V). \qquad (A3.11)$$

The time dependence $\langle A_P(0)A_P(t)|_T\rangle_T$ is generated by the tunneling Hamiltonian and we write it as

$$\langle A_P(0)A_P(t)\rangle = \langle A^2(0)\rangle \exp(-\omega_T^2 t^2). \qquad (A3.12)$$

Putting (A3.10, 11 and 12) into (A3.5) leads to

$$T_{TV}^{-1} = 2x\frac{\hbar J^2}{k_T}\langle A_P^2(0)\rangle \int_0^\infty dt \left(1+\frac{t}{\tau_V}\right)$$

$$\times \exp-(t/\tau_V)\frac{d^2}{dt^2}\exp(-\omega_T^2 t^2). \qquad (A3.13)$$

The above integral can be done in the limit $\omega_T\tau_V \ll 1$,

which is indeed the physically relevant limit. That is, the motion of the vacancies is much faster than that of the tunneling ^{3}He's, i.e.,

$$T_{TV}^{-1} = -(\hbar^2 J^2/k_T)(2x/\tau_V)\sum_P \langle A^2 P(0)\rangle = 2x/\tau_V.$$

$$(A3.14)$$

The time τ_V called for to evaluate this equation is the time required for a vacancy to tunnel away from its lattice site. This time is

$$\tau_V^{-1} = z\omega_3(V, 3)x_V \qquad (A3.15)$$

for a vacancy in pure ^{3}He. Thus we have

$$T_{TV}^{-1} = 2zx_V\omega_3(V, 3). \qquad (A3.16)$$

A.4 Vacancy Wave–Phonon Relaxation

The vacancy wave–phonon relaxation process is the same as the mass fluctuation–phonon process which is discussed at length in Part 6 of this Appendix. In this case, the mass fluctuation associated with the vacancy motion is $\Delta m_R = -m_3$. Thus we may carry over most of the early results of Part 6 upon making the correspondence

$$\mathfrak{K}_1 \rightarrow \mathfrak{K}_P \qquad (A4.1)$$

$$\mathfrak{K}_2 \rightarrow \mathfrak{K}_V \qquad (A4.2)$$

$$\mathfrak{K}_{12} \rightarrow \mathfrak{K}_{PV} = \tfrac{1}{2}\sum_R \Delta m_R \dot{u}_R^2. \qquad (A4.3)$$

We may take over Eq. (A6.18) in the form

$$T_{VP}^{-1} = k_V^{-1}2600x_V(\Delta m/m)^2(\hbar/\tau_V)^2(k_B T/\hbar)(T/\theta_D)^6,$$

$$(A4.4)$$

where $x_V = \exp(-\beta\phi)$, $\tau_V^{-1} = z\omega_3(V, 3)$, and $\Delta m/m = -1$. We have taken the mass fluctuation correlation function for vacancy motion to have a Gaussian time dependence with characteristic time τ_V. At this point our picture of the vacancy–phonon coupling begins to differ from that of the ^{4}He–phonon coupling. We imagine here that at $t=0$, the vacancies and phonons are at the same temperature; the number of vacancies present is

$$x_V(\beta_P) = \exp(-\beta_P\phi). \qquad (A4.5)$$

The vacancy system is heated to $T_V > T_P$ by a mechanism which changes the energy per vacancy, but leaves the number of vacancies unchanged. Thus we have

$$E_V = Nx_V(T_P)(\phi + \tfrac{3}{2}k_B T_V), \qquad (A4.6)$$

where we take $k_B T_V \ll 2z\hbar\omega_3(V, 3)$, the vacancy bandwidth, about 6 K. The vacancies behave like classical particles. It is the energy $\tfrac{3}{2}k_B(T_V - T_P)$ that must be dumped into the lattice by $\mathfrak{K}_{VP}$. Thus we have

$$dE_V/dt = (d/d\beta_V)E_V = -\tfrac{3}{2}Nx_V(\beta_P)\beta_V^{-2}\dot{\beta}_V \quad (A4.7)$$

and

$$k_V = \tfrac{3}{2}Nx_V(\beta_P)\beta_P^{-2}. \qquad (A4.8)$$

Using Eq. (A4.8) in Eq. (A4.4) leads to

$$T_{VP}^{-1} = 1730x_V(\Delta m/m)^2(\tau_V^{-1})(\hbar/\tau_V k_B T)(T/\theta_D)^6.$$

$$(A4.9)$$

A.5 Tunneling–Mass Fluctuation Wave Relaxation

This relaxation process is exactly the same as the tunneling–vacancy relaxation process. In this case, the ^{4}He particle motion through the lattice accomplishes the same relaxation that the vacancy did above in Part 3. We may take our Eq. (A3.16) in the form

$$(T_{TMF})^{-1} = 2zx_4\omega_4(3, 3), \qquad (A5.1)$$

where $\omega_4(3, 3)$ is the tunneling frequency for a 3–4 pair in pure ^{3}He, and x_4 is the concentration of ^{4}He atoms.

A.6 Mass Fluctuation Wave–Phonon Relaxation

To do this calculation most easily within the framework discussed above, it is convenient to consider the rate at which energy is transferred from the phonons to the mass fluctuations. In the experimental observation of this process it goes in the opposite direction. We make the identification

$$\mathfrak{K}_1 \rightarrow \mathfrak{K}_P = \sum_q \hbar\omega(q)(N_q + \tfrac{1}{2}), \qquad (A6.1)$$

$$\mathfrak{K}_2 \rightarrow \mathfrak{K}_{MF}, \qquad (A6.2)$$

and

$$\mathfrak{K}_{12} = \mathfrak{K}_{PMF} = \tfrac{1}{2}\sum_R \Delta m_R \dot{u}_R^2, \qquad (A6.3)$$

where $\Delta m_R = m_R - m_3$. In terms of the phonon coordinates $\dot{u}_R$ is given by

$$\dot{u}_R = -i\sum_k [\hbar\omega(k)/2m_3 N]^{1/2}\hat{e}(k)$$
$$\times [a_k \exp(+i\mathbf{k}\cdot\mathbf{R}) - a_k^+ \exp(-i\mathbf{k}\cdot\mathbf{R})] \quad (A6.4)$$

and $p(0)$ of Eq. (A0.16) is given by

$$p(0) = \tfrac{1}{2}\sum_R \Delta m_R \sum_q \hbar\omega(q)[a_q^+ a_q, \dot{u}_R^2]. \quad (A6.5)$$

Upon using Eq. (A6.4) and the phonon commutation relations we find four contributions to the commutator. These are

$$p(0) = \tfrac{1}{2}\sum_R \Delta m_R C(kk')$$
$$\times \{\exp[i(\mathbf{k}-\mathbf{k}')\cdot\mathbf{R}][\hbar\omega(\mathbf{k}) - \hbar\omega(\mathbf{k}')]a_k^+ a_{k'}$$
$$- \exp[-i(\mathbf{k}+\mathbf{k}')\cdot\mathbf{R}][\hbar\omega(\mathbf{k}) + \hbar\omega(\mathbf{k}')]a_k^+ a_{k'}^+$$
$$+ \exp[-(\mathbf{k}+\mathbf{k}')\cdot\mathbf{R}][\hbar\omega(\mathbf{k}) + \hbar\omega(\mathbf{k}')]a_k a_{k'}$$
$$+ \exp[-(\mathbf{k}-\mathbf{k}')\cdot\mathbf{R}][\hbar\omega(\mathbf{k}) - \hbar\omega(\mathbf{k}')]a_k^+ a_{k'}\},$$

$$(A6.6)$$

where

$$C(kk') = \{\hbar[\omega(\mathbf{k})\omega(\mathbf{k}')]^{1/2}/2m_3N\}\hat{e}(\mathbf{k})\cdot\hat{e}(\mathbf{k}').$$

$$(A6.7)$$

We neglect the second and third terms (they correspond to a 2 phonon direct transition), and combine the first and fourth terms (they are Ramanlike terms). Thus we have

$$p(t) = \tfrac{1}{2}\sum_R \Delta m_R(t)|_{MF}\sum_{kk'} C(kk')\hbar[\omega(\mathbf{k})-\omega(\mathbf{k}')]$$

$$\times\{\exp-[(\mathbf{k}-\mathbf{k}')\cdot\mathbf{R}+i(\omega(\mathbf{k})-\omega(\mathbf{k}')t]+\text{C.C}\}a_k^+a_{k'}$$

$$(A6.8)$$

where $\Delta m_R(t)|_{MF}$, the time evolution of the mass at R due to the mass fluctuation waves, is the noise amplitude for this process. So we write

$$\langle p(0)p(t)\rangle = \sum_{RR'}\langle\Delta m_R(0)\Delta m_R(t)|_{MF}\rangle_{MF}\langle p_P(0)p_P(t)\rangle_P$$

$$(A6.9)$$

where

$$\langle p_P(0)p_P(t)\rangle = \sum_{kk'} A(kk')$$

$$\times\{\exp[i(\mathbf{k}-\mathbf{k}')\cdot(\mathbf{R}-\mathbf{R}')]\exp(-i\omega_{kk'}t)+\text{C.C.}$$

$$+\exp[i(\mathbf{k}-\mathbf{k}')(\mathbf{R}+\mathbf{R}')]\exp(+i\omega_{kk'}t)+\text{C.C.}\},$$

$$(A6.10)$$

$$A(kk') = -\tfrac{1}{4}C(kk')^2(\hbar\omega_{kk'})^2(n_k+1)n_{k'}, \quad (A6.11)$$

and

$$\omega_{kk'} = \omega(k)-\omega(k'). \quad (A6.12)$$

For a random distribution of the ^{4}He impurities, we have

$$\sum_{RR'}\langle\Delta m_R(0)m_{R'}(t)|_{MF}\rangle_{MF}\exp[+i(\mathbf{k}-\mathbf{k}')\cdot(\mathbf{R}-\mathbf{R}')]$$

$$= \sum_R\langle\Delta m_R(0)\Delta m_R(t)|_{MF}\rangle_{MF}, \quad (A6.13a)$$

$$\sum_{RR'}\langle\Delta m_R(0)\Delta m_{R'}(t)|_{MF}\rangle_{MF}\exp[i(\mathbf{k}-\mathbf{k}')\cdot(\mathbf{R}+\mathbf{R}')]$$

$$= \sum_R\langle\Delta m_R(0)\Delta m_R(t)|_{MF}\rangle_{MF}\exp[i2R(\mathbf{k}-\mathbf{k}')] = 0.$$

$$(A6.13b)$$

We assume the correlation function for Δm_R in Eq. (A6.13a) to have a Gaussian time dependence for purposes of computational ease. We write

$$\sum_R\langle\Delta m_R(0)\Delta m_R(t)|_{MF}\rangle_{MF} = x_4\Delta m^2\exp-(t/\tau_c)^2,$$

$$(A6.14)$$

where $\tau_c^{-1} = z\omega_4(3,3)$ $\omega_4(3,3)$ is the ^{3}He–^{4}He tunneling time and x_4 is the concentration of ^{4}He impurities. Thus

we have

$$T_{PMF}^{-1} = (\pi^{1/2}/\hbar^2k_p)x_4\sum_{kk'} A(kk')\tau_c\exp[-\tfrac{1}{4}(\omega_{kk'}\tau_c)^2].$$

$$(A6.15)$$

To do the sums on k and k', we use the following approximations:

(a) The phonon frequencies are assumed to be polarization independent; $\hbar\omega_\lambda(k) = \hbar\omega(k)$. Then, the polarization sums yield $\sum_{\lambda\lambda'}e_\lambda(k)e_{\lambda'}(k') = 1$.

(b) The acoustic approximation is made $\omega(\mathbf{k}) = c|\mathbf{k}|$.

(c) The sums on k and k' go to integrals with the replacement $\sum_k\to[V/(2\pi)^3]\int d\mathbf{k}$, and the integral over k' is converted to an integral on K through the transformation $\mathbf{k} = \mathbf{k}'+\mathbf{K}$.

(d) The occupation numbers for the states k and k' are

$$(n_k+1) = \exp(x_k)/[\exp(x_k)-1]$$

$$n_{k-K} = [\exp(x_k)-1]^{-1}+\Theta(K),$$

where $x_k = \beta\hbar ck$. We approximate $(n_k+1)n_{k'}$ by

$$(n_k+1)n_{k'} = \exp(x_k)/[\exp(x_k)-1]^2.$$

The combination of steps (a)–(d) leads to

$$\sum_{kk'} A(kk')\tau_c\exp[-\tfrac{1}{4}(\omega_{kk'}\tau_c)^2]$$

$$= -92\pi^{1/2}(V/2\pi^2)(\hbar^2c^4/m^2N^2)(\tau_c/\lambda^3)(k_BT/\hbar c)^7,$$

$$(A6.16)$$

where $\lambda = c\tau_c$, so that Eq. (A6.15) becomes

$$T_{PMF}^{-1} = -(2587/k_P)x_4(\Delta m/m)^2$$

$$\times(\hbar/\tau_c)^2(k_BT/\hbar)(T/\theta_D)^6, \quad (A6.17)$$

where $\hbar cq_D = k_B\theta_D$, and $N = [V/(2\pi)^3]\tfrac{4}{3}\pi q_D^3$. To find the rate at which energy is transferred from the mass fluctuation system to the phonons, we use Eq. (A0.22),

$$T_{MFP}^{-1} = T_{PMF}^{-1}(k_P/k_{MF})$$

$$= -k_{MF}^{-1}2600x(\Delta m/m)^2(\hbar/\tau_c)^2(k_BT/\hbar)(T/\theta_D)^6.$$

$$(A6.18)$$

For k_{MF}, we use the result from Eq. (D16)

$$E_{MF} = k_{MF}\beta = -(x_4)(\tfrac{7}{4})(z^2)[\hbar\omega_4(3,3)]^2\beta. \quad (A6.19)$$

Thus for $z = 8$, we have

$$T_{MFP}^{-1} = 1500(\Delta m/m)^2(k_BT/\hbar)(T/\theta_D)^6. \quad (A6.20)$$

A.7 Relaxation Topologies

There are seven distinct topologies for the energy baths which are involved in the relaxation processes in solid ^{3}He. Five of these topologies are associated with relaxation in pure ^{3}He, and two additional topologies are

associated with relaxation in dilute mixtures of ^{4}He in ^{3}He. In this part we will work out the formula for the experimentally observed long time in each of the topologies. The intrinsic relaxation times which enter into these formulae have been derived in detail in Parts 1–6 above.

We begin by stating the general results which are consequences of topology:

(1) When energy relaxes from the 1-system to the 2-system (which remains at the reservoir temperature), the *intrinsic relaxation time* for the relaxation of energy via the 1–2 linkage is defined by the equation

$$\dot{\beta}_1 = -T_{12}^{-1}(\beta_1 - \beta_2), \qquad (A7.1)$$

where β_1 is the inverse temperature of the 1-system, and $\beta_2 = \beta_R$, is the inverse temperature of the reservoir. See Fig. 52.

2. When energy relaxes from the combined 0, 1-system to the 2-system through the 1–2 linkage (see Fig. 52), the observed relaxation time is given by

$$T_1^{-1}\big|_{012} = T_{12}^{-1}[k_1/(k_1+k_0)], \qquad (A7.2)$$

where

$$k_n = dE_n/d\beta \qquad (A7.3)$$

and E_n is the energy of the n-system. We will call this time the *topological relaxation time* to contrast it with the intrinsic relaxation time defined above. This result is achieved by writing equations of motion for the temperatures of the three systems; i.e.

$$\dot{\beta}_0 = -T_{01}^{-1}(\beta_0 - \beta_1), \qquad (A7.4)$$

$$\dot{\beta}_1 = +(a/T_{01})(\beta_0 - \beta_1) - T_{12}^{-1}(\beta_1 - \beta_2), \quad (A7.5)$$

$$\dot{\beta}_2 = (b/T_{21})(\beta_1 - \beta_2). \qquad (A7.6)$$

We consider the following cases:

(A) $T_{12} \to +\infty$; energy conservation between 0 and 1 implies

$$k_0\dot{\beta}_0 + k_1\dot{\beta}_1 = 0 \quad \text{or} \quad a = k_0/k_1.$$

(B) $T_{01} \to +\infty$; energy conservation between 1 and 2 implies

$$k_1\dot{\beta}_1 + k_2\dot{\beta}_2 = 0 \quad \text{or} \quad b = k_1/k_2.$$

(C) For $T_{01} \ll T_{12}$ we can assume that 0 and 1 come to a common temperature quickly. We use Eq. (A7.4) in Eq. (A7.5) to write

$$\dot{\beta}_1 + (k_0/k_1)\dot{\beta}_0 = T_{12}^{-1}(\beta_1 - \beta_2).$$

Now since systems 0 and 1 are in equilibrium in a time fast compared to T_{12}, we have $\beta_0 = \beta_1$ and $\dot{\beta}_0 = \dot{\beta}_1$ or

$$\dot{\beta}_1 = [k_1/(k_1+k_0)]T_{12}^{-1}(\beta_1 - \beta_2).$$

3. When energy relaxes from the 0-system to the 1-system to the 2-system the observed long time is the longer of the two times associated with the two possible

topologies, i.e., the longer of

$$T_1^{-1}\big|_{01} = T_{01}^{-1},$$

or

$$T_1^{-1}\big|_{012} = T_{12}^{-1}[k_1/(k_1+k_0)].$$

for the topology in Fig. 52b. We make this observation to stress that the decision about long times and short times cannot be made without consideration of the relevant topologies. It is inappropriate in comparing 0–1 and 0, 1–2 to consider only the comparison of T_{01} with T_{12}.

In Table V, we list the seven topologies of interest and the appropriate intrinsic time and topological time for each. We denote the intrinsic time associated with each topology by the labeling above. We denote the various topologies by the letter sequence in Column (b). The bar in the letter sequence indicates where the long time occurs. In Row E, where the energy flow is $Z \to T \to V \to P$, the long time is due to the vacancy wave–phonon link, ZTV–P.

We complete this Appendix by writing out analytic formulas for the seven topological times of interest. We do this at $V = 20.0$ cm^3/mole and attempt to indicate (at least for this molar volume) the relative size of each of the seven times over the temperature range of experimental interest.

Topology Z–VP; Zeeman–Vacancy Relaxation. The *intrinsic* time is given by Eq. (A1.20)

$$T_{ZV}^{-1} = \tfrac{2}{3}(M_2/\omega_0)g(\eta), \qquad (A7.7)$$

where

$$g(\eta) = \eta/(1+\eta^2) + 4[\eta/(1+4\eta^2)], \qquad (A7.8)$$

and $\eta = \omega_0 \tau_V$. The *topological* time is equal to the intrinsic time. We do the calculations in terms of f defined by $\omega_0 = 2\pi \times 10^6 f$; f is the Zeeman frequency in megaHertz (MHz). For M_2 from Eq. (A1.19) we have

$$M_2 = 3 \times 10^8 \text{ sec}^{-2}. \qquad (A7.9)$$

Here M_2 has the dimensions $[T^{-2}]$; it is essentially the square of the precession frequency of a nuclear moment in the dipolar field of its neighbors. Define

$$\omega_d = \hbar^{-1}\mu H_{\text{loc}} \approx \hbar^{-1}\mu^2(z/\Delta^3) = 3 \times 10^4 \text{ sec}^{-1}, \quad (A7.10)$$
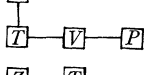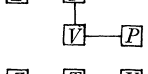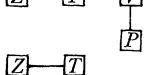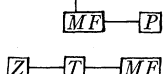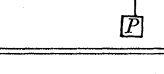
where $\mu = $ nuclear magnetic moment, $z = 8$, and $\Delta = 3.5 \times 10^{-8}$ cm. The microscopic time in Eq. (A7.8), τ_V, is given by Eq. (A1.21)

$$\tau_V^{-1} = x_V z \omega_3(V, 3) = 6 \times 10^{10} \exp[-14.5/T] \text{ sec}^{-1},$$

$$(A7.11)$$

where we have taken ϕ from Fig. 29. The T_1 minimum occurs at T such that $\omega_0 \tau_V \approx 1$ or at $T_{\text{min}} = 1.32$ K for Zeeman frequencies near 1 MHz. Note that the minimum is mildly frequency dependent. At $T = T_{\text{min}}$, $g(\eta) \approx 1$, and we find

$$T_1^{-1}(T_{\text{min}})\big|_{ZV} \approx M_2/\omega_0 \approx 5/f \text{ sec}^{-1} \qquad (A7.12)$$

TABLE V. Topologies. For each of the topologies discussed in Appendix A.7 we show the topological diagram (a), notation (b), intrinsic time (c), and topological time (d).

Topology	Notation	Intrinsic relaxation rate	Observable relaxation rate
	Z–VP	T_{ZV}^{-1}	$T_1^{-1}\mid_{ZV} = T_{ZV}^{-1}$
	ZV–P	T_{VP}^{-1}	$T_1^{-1}\mid_{VP} = [k_V/(k_Z+k_V)]T_{VP}^{-1}$
	Z–TVP	T_{ZT}^{-1}	$T_1^{-1}\mid_{ZT} = T_{ZT}^{-1}$
	ZT–VP	T_{TV}^{-1}	$T_1^{-1}\mid_{TV} = [k_T/(k_Z+k_T)]T_{TV}^{-1}$
	ZTV–P	T_{VP}^{-1}	$T_1^{-1}\mid_{VP} = [k_V/(k_Z+k_T+k_V)]T_{VP}^{-1}$
	ZT–MFP	T_{TMF}^{-1}	$T_1^{-1}\mid_{TMF} = [k_T/(k_Z+k_T)]T_{TMF}^{-1}$
	ZTMF–P	T_{MFP}^{-1}	$T_1^{-1}\mid_{MFP} = [k_{MF}/(k_Z+k_T+k_{MV})]T_{MFP}^{-1}$

At $T>T_{min}$, $\omega_0\tau_V\ll1$, T_1^{-1} is frequency independent, and given by

$$T_V^{-1}(T\gg T_{min}) = (10/3)M_2\tau_V = 10^{-3}\exp\ (14.5/T).$$
(A7.13)

At $T<T_{min}$, $\omega_0\tau_V\gg1$, T_1^{-1} is frequency dependent, and given by

$$T_V^{-1}(T\ll T_{min}) = \tfrac{4}{3}(M_2/\omega_0^2\tau_V)$$

$$= (10^5/f^2)\exp\ (-14.5/T).$$
(A7.14)

Topology Z–TVP; Zeeman–Tunneling Relaxation. The *intrinsic* time is given by Eq. (A2.17)

$$T_{ZT}^{-1} = [(2\pi)^{1/2}/3](M_2/\omega_T)h(x),$$
(A7.15)

where

$$h(x) = \exp\ (-\tfrac{1}{2}x^2)+4\exp\ (-2x^2)$$
(A7.16)

and

$$x=\omega_0/\omega_T\quad\text{and}\quad\omega_T=4.76J.$$

The *topological* time is equal to the intrinsic time. As above we do the calculations in terms of $\omega_0=2\pi\times10^6 f$. The value of M_2 is given by Eq. (A7.9). At $V=20.0$ cm^3/mole, the exchange frequency, J, is about 0.5 MHz. Thus we write $x=\omega_0/\omega_T=f/4.8$. For Eq. (A7.15) we have

$$T_{ZT}^{-1} = 16[\exp-(f^2/18)+4\exp-(f^2/4.5)]\ \text{sec}^{-1}.$$
(A7.17)

This relaxation time is temperature independent, since the time characterizing the microscopic motion is temperature independent. It is highly frequency dependent. For $f\to0$, we have

$$T_{ZT}^{-1}(f\to0) = 80\ \text{sec}^{-1}.$$
(A7.18)

For $f\to+\infty$, we have

$$T_{ZT}^{-1}(f\to+\infty) = 16\exp\ (-f^2/18)\ \text{sec}^{-1}.$$
(A7.19)

At $f=1$, we have $T_1\approx0.012$ sec. At $f=7$, we have $T_1\approx1.0$ sec.

Topology ZT–VP; Tunneling–Vacancy Relaxation. The *intrinsic* time is given by Eq. (A3.16)

$$T_{TV}^{-1} = 2zx_V\omega_V(3,3),$$
(A7.20)

where $\omega_V(3,3)$ is discussed in Part 2 above and in Sec. 4. The *topological* time is given in Table V as

$$T_1^{-1}\mid_{TV} = [k_T/(k_T+k_Z)]T_{TV}^{-1},$$
(A7.21)

where k_T and k_Z are given in Appendix D. Using Eqs. (D4, 8) for k_T and k_Z, we have

$$T_1^{-1}\mid_{TV} = [1+\tfrac{1}{12}(\omega_0/J)^2]^{-1}2x_Vz\omega_V(3,3).$$
(A7.22)

For $\omega_0=2\pi\times10^6 f$ and $J\approx0.5$ MHz, we have

$$T_1^{-1}\mid_{TV} = [1/(1+\tfrac{1}{3}f^2)]2x_Vz\omega_V(3,3).$$
(A7.23)

Using the numbers from Sec. 4, we find

$$T_1^{-1}\mid_{TV} = [10^{11}/(1+\tfrac{1}{3}f^2)]\exp\ (-14.5/T).$$
(A7.24)

This relaxation time is frequency dependent for $f > 2$, and is very strongly temperature dependent.

Topology ZTV–P; Vacancy–Phonon Relaxation. The *intrinsic* time is given by Eq. (A4.4)

$$T_{VP}^{-1} = k_V^{-1} 2600 x_V (\Delta m/m)^2 (\hbar/\tau_V)^2 (k_B T/\hbar)(T/\theta)^6,$$
(A7.25)

where $\tau_V^{-1} = z\omega_V(3,3)$. For the *topological* time we have from Table V

$$T_1^{-1}|_{VP} = [k_V/(k_Z + k_T + k_V)]T_{VP}^{-1},$$

where k_Z, k_T, and k_V are found in Appendix D. Using Eqs. (D4, 8, 12) for k_Z, k_T, and k_V we have

$$T_1^{-1}|_{VP} = 2600 x_V (k_B T/\hbar)(T/\theta)^6$$
$$\times (\tfrac{1}{4}\omega_0^2 + 3J^2 + \tfrac{3}{2}\omega_t^2 x_V)^{-1}(1/\tau_V^2), \quad (A7.26)$$

where $\hbar\omega_t = k_B T$. We have $\tau_V^{-1} = z\omega_V(3,3)$ which permits us to write

$$T_1^{-1}|_{VP} = 2600 x_V(k_B T/\hbar)(T/\theta)^6$$
$$\times [z^2\omega_V(3,3)/(\tfrac{1}{4}\omega_0^2 + 3J^2 + \tfrac{3}{2}\omega_t^2 x_V)]. \quad (A7.27)$$

Certainly the values of ω_0 and J of interest are in the vicinity of 1 MHz. In the denominator of the topological factor in Eq. (A7.27), we ignore the term proportional to x_V. At low temperatures, we have

$$T_1^{-1}(T \ll 1.0)|_{VP} = 10^4 x_V(k_B T/\hbar)(T/\theta)^6$$
$$\times \{[z\omega_V(3,3)]^2/(\omega_0^2 + 12J^2)\}. \quad (A7.28)$$

For $\omega_0/2\pi = J/2\pi = 1$ MHz, we have

$$T_1^{-1}(T \ll 1.0 \text{ K})|_{VP} = 8 \times 10^{14} T^7 \exp(-14.5/T).$$
(A7.29)

We take the transition to this low-temperature behavior to occur at T such that

$$x_V(k_B T/\hbar) \approx (1 \text{ MHz}), \quad \text{i.e., at } T < 0.6K.$$

This topology $(ZTV–P)$ for relaxation is competitive with topology ZT–VP for which the long time is given by Eq. (A7.24). Equating these two times we have

$$T_1^{-1}|_{TV} \gtrsim T_1^{-1}|_{VP} \quad (A7.30)$$

down to $T = 0.2K$.

Topology ZT–MFP; Tunneling–⁴He Relaxation. The *intrinsic* time is given by Eq. (A5.1)

$$T_{TMF}^{-1} = 2zx_4\omega_4(3,3). \quad (A7.31)$$

The topological time from Table V is

$$T_1^{-1}|_{TMF} = [k_T/(k_Z + k_T)]T_{TMF}^{-1}, \quad (A7.32)$$

where k_Z and k_T are given in Appendix D. From Eqs. (D4.8) with the replacements $J \approx 0.5$ MHz and $\omega_0 =$

$2\pi \times 10^6 f$, we have

$$T_1^{-1}|_{TMF} = [1/(1 + \tfrac{1}{3}f^2)]2zx\omega_4(3,3). \quad (A7.33)$$

This topology is competitive with the ³He–vacancy topology $(ZT–VP)$ at T, and x_4 determined by equating Eq. (A7.24) and Eq. (A7.33), i.e., at

$$2zx\omega_4(3,3) = 10^{11}\exp-(14.5/T). \quad (A7.34)$$

For $\omega_4(3,3) \approx J = 2\pi \times 10^6$, we have

$$x_4\exp(14.5/T) = 10.3. \quad (A7.35)$$

At $x_4 = 10^{-6}$, the transition from topology $ZT–VP$ to topology $ZT–MFP$ occurs at $T = 0.7K$; at $x_4 = 10^{-5}$ (10 ppm) it occurs at $T = 0.8K$, at $x_4 = 10^{-3}$ (1000 ppm) it occurs at $T = 1K$.

Topology ZTMF–P; Mass Fluctuation Wave–Phonon. The *intrinsic* time is given by Eq. (A6.20)

$$T_{MFP}^{-1} = 1500(\Delta m/m)^2(k_B T/\hbar)(T/\theta)^6. \quad (A7.36)$$

The topological time from Table V is

$$T_1^{-1}|_{MFP} = [k_{MF}/(k_Z + k_T + k_{MF})]T_{MFP}^{-1}, \quad (A7.37)$$

where k_Z, k_T, and k_{MF} are given in Appendix D. Using Eqs. (D4, 8, 16) for k_Z, k_T, and k_{MF}, we may write the topological factor as

$$\tfrac{14}{3}z(\omega_4(3,3)^2/\{\tfrac{1}{12}\omega_0^2 + J^2 + \tfrac{14}{3}zx_4[\omega_4(3,3)]^2\}). \quad (A7.38)$$

For $\omega_4(3,3) \approx J$ and x_4 small enough that the x_4 term in the denominator doesn't matter, again at 20.0 cm³/mole, we have

$$T_1^{-1}|_{MFP} = 5 \times 10^5 x_4 T^7 [1/(1 + \tfrac{1}{3}f^2)]. \quad (A7.39)$$

This topology is competitive with topology $ZT–MFP$. The two topologies give equally long times at T determined by equating Eq. (A7.33) with Eq. (A7.39), i.e., at

$$2z\omega_4(3,3) = 5 \times 10^5 T^7 \quad (A7.40)$$

or for $\omega_4(3,3) = J = 2\pi \times 10^6$ at $T \approx 2°K$. Thus at all temperatures of relevance the long time in the topology $ZTMF–P$ is much longer than the long time in the topology $ZT–MFP$.

Topology $ZTMF–P$ is also competitive with topology $ZT–VP$. We equate Eq. (A7.24) with Eq. (A7.39), and find

$$5 \times 10^5 T^7 x_4 = 10^{11}\exp-(14.5/T). \quad (A7.41)$$

For $x_4 = 10^{-6}$, the topologies give equally long times at $T \approx 0.5K$.

The notation used throughout this work is summarized in Table VI and VII.

The results of the numerical calculations in this Appendix are plotted in Fig. 53 of the text. On that figure representative data is also plotted. Recall that we have used no parameters in the theoretical expressions for the various times; (we have used J, θ_D, and ϕ

Table VI. Diffusion constants.

$D_Z(3,3)$	Diffusion of magnetization due to ^{3}He tunneling in a ^{3}He medium
$D_Z(V,3)$	Diffusion of magnetization due to the presence of vacancies in a ^{3}He medium
$D_Z(V,4)$	Diffusion of magnetization due to the presence of vacancies in a ^{4}He rich medium
$D_T(3,3)$	Diffusion of energy in the tunneling system due to ^{3}He–^{3}He tunneling
$D_3(V,3)$	Diffusion of ^{3}He due to vacancies in a ^{3}He medium
$D_3(V,4)$	Diffusion of ^{3}He due to vacancies in a ^{4}He medium
$D_4(3,3)$	Diffusion of a ^{4}He (mass fluctuation wave) in a ^{3}He medium
$D_3(4,4)$	Diffusion of a ^{3}He (mass fluctuation wave) in a ^{4}He medium
$D_V(3,3)$	$=D_Z(V,3)$

from experiment). The agreement between theory and experiment is truly remarkable.

APPENDIX B: EQUILIBRIUM TIMES; T_2, THE 10/3 EFFECT, ETC.

B.1 T_2

Consider the Zeeman system established by $\mathbf{H}_0$ and weakly coupled to the 1-system, a system of excitations described by H_1. Suppose that in the plane perpendicular to the z axis, the magnetization has a component

$$I_\perp(t) = I_x \cos \omega_0 t + I_y \sin \omega_0 t$$
$$= \exp(-\mathfrak{IC}_z t) I_x \exp(i\mathfrak{IC}_z t) \qquad (B1.1)$$

which is along the x axis at $t=0$. To prepare the system at $t=0$ so that it has this nonvanishing $\perp$ magnetization, we write

$$\sigma(t) = \sigma_0(t)\sigma_1$$
$$= \exp\{-[\beta_z(t)\mathfrak{IC}_z - \alpha(t)\omega_0 I_\perp]\} \exp(-\beta_1\mathfrak{IC}_1), \qquad (B1.2)$$

where $\sigma_0(t)$ has been arranged to describe the z component of the magnetization through $\beta_z(t)\mathfrak{IC}_z$ and the $\perp$ component through $\alpha(t)\omega_0 I_\perp$. The function $\alpha(t)$ describes the time evolution of $\langle I_\perp \rangle$. To see this we look at $\langle I_\perp \rangle$, where

$$\langle I_\perp \rangle = \text{Tr } I_\perp(t)\sigma(t)/\text{Tr } \sigma(t) = \text{Tr } I_x\sigma^*(t)/\text{Tr } \sigma^*(t), \qquad (B1.3)$$

where

$$\sigma^*(t) = \exp(i\mathfrak{IC}_z t)\sigma(t) \exp(-i\mathfrak{IC}_z t). \qquad (B1.4)$$

For $\alpha(t)\omega_0 I_\perp \ll 1$, we have

$$\langle I_x \rangle = -\alpha(t)\omega_0 \text{Tr } I_x{}^2/\text{Tr } 1, \qquad (B1.5)$$

where we have used Trace $\sigma^*(t) \simeq 1$, and the high-

temperature approximation, $\beta_z(t)\mathfrak{IC}_z \ll 1$. We define T_2 to be related to the rate of change of $\alpha(t)$, thus

$$d[\alpha(t)]/dt = -T_2{}^{-1}|_{Z1}\alpha(t). \qquad (B1.6)$$

Now we find T_2 in terms of the coupling of Z to 1 through $\mathfrak{IC}_d$ by computing $(d/dt)\langle I_\perp \rangle$ in direct analogy to the steps leading to Eq. (A0.16). We make the replacement

$$\mathfrak{IC}_1 \rightarrow \mathfrak{IC}_Z,$$
$$\mathfrak{IC}_2 \rightarrow \mathfrak{IC}_1,$$
$$\mathfrak{IC}_{12} \rightarrow \mathfrak{IC}_{Z1} = \mathfrak{IC}_d.$$

Then, analogous to Eq. (A0.8), we have

$$\langle \dot{I}_x \rangle = \left(\frac{i}{\hbar}\right)^2 \text{Re} \int_0^\infty dt' \langle I_x[\mathfrak{IC}_{Z1}{}^*(t), [\mathfrak{IC}_{Z1}{}^*(t'), \sigma^*(t)]]\rangle. \qquad (B1.7)$$

For $\sigma^*(t)$, we take $\sigma^*(t) = [1 - \alpha(t)\omega_0 I_x]\sigma_z(\beta_z)\sigma_1(\beta_1)$, where $\sigma_n(\beta) = \exp(-\beta_n\mathfrak{IC}_n)$. Thus Eq. (B1.7) becomes

$$\langle \dot{I}_x \rangle = -\omega_0\alpha(t)\left(\frac{i}{\hbar}\right)^2 \text{Re} \int_0^\infty dt'$$
$$\times \langle I_x[\mathfrak{IC}_{Z1}{}^*(t), [\mathfrak{IC}_{Z1}{}^*(t'), I_x]]\rangle. \qquad (B1.8)$$

Combining Eqs. (B1.5, 6, 8) leads to

$$T_2{}^{-1}|_{Z1} = \frac{1}{\hbar^2}$$
$$\times \left\{ \text{Re} \int_0^\infty dt' \langle I_x[\mathfrak{IC}_{Z1}{}^*(t), [\mathfrak{IC}_{Z1}(t'), I_x]]\rangle \Big/ \text{Tr } I_x{}^2 \right\}. \qquad (B1.9)$$

Of course this equation is recognized as being one which

Table VII. Fundamental Parameters and tunneling frequencies.

|	
θ_D	Debye temperature
ϕ	Vacancy excitation temperature
J	the 3–3 pair tunneling rate, exchange frequency
$\omega_3(V,3)$	Tunneling frequency for ^{3}He in ^{3}He due to vacancies
$\omega_3(V,4)$	Tunneling frequency for ^{3}He in ^{4}He due to vacancies
$\omega_3(V,M)$	Tunneling frequency for ^{3}He in a non-dilute mixture, M, due to vacancies
$\omega_3(4,3)$	Tunneling of a 3–4 pair in ^{3}He
$\omega_3(4,4)$	Tunneling of a 3–4 pair in ^{4}He
$\omega_3(4,M)$	Tunneling of a 3–4 pair in a mixture, M
$\omega_3(3,3)$	Tunneling of a 3–3 pair in ^{3}He
$\omega_3(3,4)$	Tunneling of a 3–3 pair in ^{4}He
$\omega_3(3,M)$	Tunneling of a 3–3 pair in a mixture, M
$\omega_V(3,3)[=\omega_3(V,3)]$	Tunneling of a vacancy in ^{3}He
$\omega_V(4,4)[=\omega_4(V,4)]$	Tunneling of a vacancy in ^{4}He
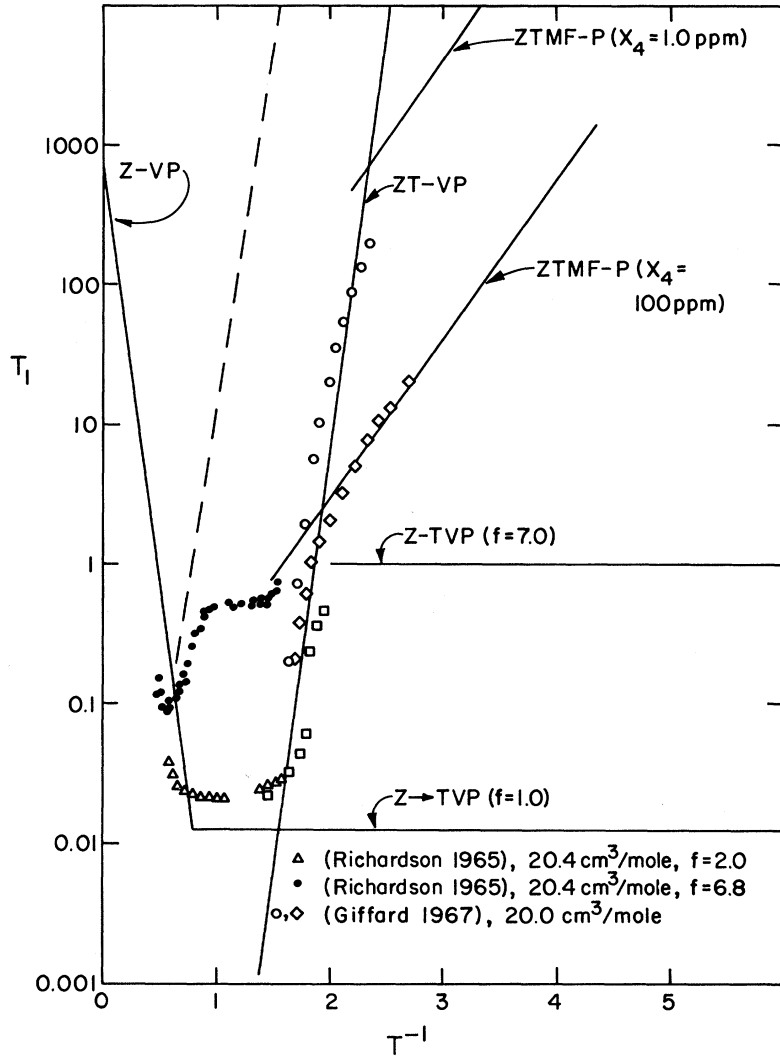
FIG. 53. Quantification of T_1. Here we have plotted the results of application of the formulas developed in A-7 for T_1 at V near 20.0 cm³/mole. We show the experimental T_1's of Richardson, Hunt, and Meyer (1965), and Giffard and Hatton (1967) for comparison.

we can write in the form

$$T_2^{-1}|_{Z1} = \frac{1}{\hbar^2} \operatorname{Re} \int_0^\infty d\tau \langle j(0)j(\tau)\rangle / \operatorname{Tr} I_x^2, \quad \text{(B1.10)}$$

where

$$j(\tau) = [I_x, \mathfrak{K}_{Z1}(\tau)].$$

A sequence of steps like those between (A1.10) and (A1.11) leads to

$$T_2^{-1}|_{Z1} = \tfrac{3}{2}J(0) + \tfrac{5}{2}J(\omega_0) + J(2\omega_0), \quad \text{(B1.11)}$$

where $J(\omega_0)$ is defined in Eq. (A1.12).

T_2; *Zeeman–Vacancy.* The coupled Zeeman–vacancy wave system is described by Eqs. (A1.1, 2, 3). To calculate T_2 we need $\mathfrak{K}_{ZV}(t)$ given by Eq. (A1.4). We

have

$$\mathfrak{K}_{Z1}^*(\tau) = \mathfrak{K}_{ZV}^*(\tau)$$

$$= \sum_{q=-2}^{+2} \sum_{i<j} B_{ij}{}^q(\tau) S_{ij}{}^q(0) \exp(-iq\omega_0\tau).$$

The correlation function called for in Eq. (B1.10) is

$$\langle j(0)j(\tau)\rangle = \sum_{qq'} \sum_{i<j} \exp(-iq\omega_0\tau) \exp[-i(q+q')\omega_0 t]$$

$$\times \langle B_{ij}{}^q(t) B_{ij}{}^{q'}(t+\tau)[I_x, S_{ij}{}^q(0)][I_x, S_{ij}{}^{q'}(0)]\rangle.$$

Now the spin commutations on the rhs of this equation lead to a relatively complicated result compared to the analogous commutations in Appendix A. Carrying out

the details of the calculation we obtain

$$T_2^{-1}|_{ZV} = \tfrac{2}{3}(M_2/\omega_0)$$

$$\times \{\tfrac{3}{2}\eta + \tfrac{5}{2}[\eta/(1+\eta^2)] + [\eta/(1+4\eta^2)]\} \quad (B1.12)$$

where $\eta = \omega_0 \tau_V$.

T_2; *Zeeman–Tunneling.* The coupled Zeeman–tunneling systems are described by Eqs. (A2.1, 2, 3). Using these Hamiltonians in the calculation of T_2 and the Gaussian approximation for the tunneling correlation function leads to

$$T_2^{-1}|_{ZT} = [(2\pi)^{1/2}/3](M_2/\omega_T)$$

$$\times \{\tfrac{3}{2} + \tfrac{5}{2}\exp[-\tfrac{1}{2}(\omega_0/\omega_T)^2] + \exp[-2(\omega_0/\omega_T)^2]\}.$$

$$(B1.13)$$

To get an idea of the numbers involved here, we calculate T_2 at $V = 20.0$ cm³/mole in the $\omega_0 \rightarrow 0$ limit; see the end of Appendix A. We have

$$[T_2(\omega_0 \rightarrow 0)]^{-1}|_{ZV} = (10/3)M_2\tau_V = [T_1(\omega_0 = 0)]^{-1}|_{ZV}$$

$$\simeq 10^{-3}\exp(14.5/T) \text{ sec}^{-1}$$

and

$$[T_2(\omega_0 \rightarrow 0)]^{-1}|_{ZT} = (10/3)(\tfrac{1}{2}\pi)^{1/2}(M_2/\omega_T)$$

$$= [T_1(\omega_0 \rightarrow 0)]^{-1} = 80 \text{ sec}^{-1}.$$

The Zeeman–tunneling process takes over from the Zeeman–vacancy process at $T = 1.3$K for $\omega_0 \rightarrow 0$.

B.2 10/3 Effect and Nonadiabatic Frequency Shift

The discussion of T_2 up to now considered only the real part of the Fourier components of the correlation function in Eq. (B1.10). The real part taken in Eq. (B1.10) gives the broadening of the spectral line in a cw experiment. We note that in the limit of large frequencies $\omega_0/\omega_T \gg 1$ the terms in $\exp - (\omega_0/\omega_T)^2$ in Eq. (B1.12) $\rightarrow 0$, and T_2^{-1} reaches a high-frequency limiting value which is three-tenths of the low-frequency value so that

$$1/T_2[(\omega_0/\omega_T) \gg 1] = (\tfrac{1}{2}\pi)^{1/2}(M_2/\omega_T)$$

$$= (3/10)[T_2(\omega_0 \rightarrow 0)]^{-1}.$$

An identical result is obtained in Eq. (B1.11) in the limit $\omega_0\tau_V \gg 1$. The physical interpretation of this is that the spectral linewidth becomes narrower by a ratio of 10/3 when the characteristic frequency of the higher-order terms in $\mathcal{H}_{Z1}*(\tau)$ (for which $q > 0$) at $\omega = \omega_p \pm q\omega_0$ are no longer coupled by the motion to the resonance line at $\omega = \omega_0$. An accompanying conjugate physical process is a small shift in the position of the center of the resonance line. This shift has a maximum displacement from the line center, ω_0, in the high- and low-field limits, when the motional frequency and precession frequency are comparable. This effect may be calculated by considering the contribution of the imaginary com-

ponents of the spectral function in (B1.11)

$$\delta\omega_q = \text{Im} \int_{-\infty}^{\infty} G_q(\tau)e^{-i\omega\tau}\,d\tau. \quad (B1.13)$$

When the powder assumption is used, the total shift, $\delta\omega$, is calculated to be given by

$$\delta\omega = \text{Im} \int_0^{\infty} [\exp(-i\omega_0\tau)G_1(\tau) + 2\exp(-2i\omega_0\tau)G_1(\tau)]\,d\tau.$$

$$(B1.14)$$

In the case of tunneling motion and the Gaussian approximation, the shift is given by (Kubo and Tomita, 1955)

$$+\delta\omega = \frac{M_2}{2\omega_T}\left\{\exp\left(-\frac{\omega_0^2}{2\omega_T^2}\right)\phi\left(\frac{\omega_0}{\omega_T}\right)\right.$$

$$\left. + 2\exp\left(-\frac{2\omega_0^2}{\omega_T^2}\right)\phi\left(\frac{2\omega_0}{\omega_T}\right)\right\}, \quad (B1.15)$$

where

$$\phi(u) = \int_0^u \exp(\tfrac{1}{2}x^2)\,dx. \quad (B1.16)$$

The shift has its maximum value when $\omega_0 \approx \omega_T$ and has the approximate value T_2^{-1} rad/sec.

APPENDIX C: DIFFUSION

C.1 Introduction

Suppose the components of the magnetization satisfy the macroscopic equations

$$\dot{M}_x = D_Z\nabla^2 M_x + \gamma H_0(z)M_y - (M_x/T_2), \quad (C1.1)$$

$$\dot{M}_y = D_Z\nabla^2 M_y - \gamma H_0(z)M_x - (M_y/T_2), \quad (C1.2)$$

and

$$\dot{M}_z = D_Z\nabla^2 M_z - T_{ZE}^{-1}[M_z - M_z(\beta_E)], \quad (C1.3)$$

where $H_0(x) = H_0 + Gx$ is the magnetic field along the z axis; it is made up of a constant field, H_0, and a field gradient pointing in the z direction and proportional to x; see Fig. 5. In the equation of motion for M_x and M_y, there is a decay term representing the intrinsic T_2 process acting among the spins, $M_\perp$ returns to zero after a 90° pulse in time T_2. In the equation of motion for M_z, there is a decay term representing the intrinsic T_1 process acting on the spins. This decay process returns M_z to the value it has when in equilibrium at temperature β_E^{-1}, $M_z(\beta_E)$. In each of these equations of motion there is a diffusion term, $D_Z\nabla^2 M_\alpha$, which incorporates the spin diffusion process into the description of the magnetization; it is characterized by the magnetization diffusion coefficient, D_Z.

The pulse sequence which is used in a typical diffusion experiment (90°–180°) looks at $M_\perp$. From Eqs. (C1.1, 2, 3) we see that $M_\perp$ and M_Z move independ-

ently. It is clear that a diffusion experiment carried out in this way measures the motion of $M_\perp$ and thus the magnetization diffusion coefficient. But a diffusion experiment which looks at the motion of M_z measures the energy diffusion. Because of the coupling of M_z through $\mathcal{K}_d$ to the various excitation systems in the solid, manifested in the T_1 term in Eq. (C1.3), the diffusion of energy can be quite complicated. We discuss energy diffusion and magnetization diffusion in detail in this Appendix. We want here to emphasize that there are two diffusion constants, the magnetization diffusion constant which is seen by looking at $M_\perp$, and the energy diffusion constant which is seen by looking at M_z.

D_Z; Magnetization Diffusion. Let us return to Eqs. (C1.1, 2, 3). We may use $m_\perp = M_x + iM_y$ to combine Eqs. (C1.1) and C1.2) in the form (Abragam, 1961)

$$(\partial m_\perp/\partial t) = \gamma H_0(x)m_\perp - (m_\perp/T_2) + D_x\nabla^2 m_\perp. \quad \text{(C1.4)}$$

The external field is a function of x so we write

$$m_\perp(x, t) = m^*(x, t)\exp(i\omega_0 t)\exp(-t/T_2) \quad \text{(C1.5)}$$

and find that m^* satisfies the equation

$$\partial m^*/\partial t = (-\gamma G)xm^* + D_x\nabla^2 m^*. \quad \text{(C1.6)}$$

If we ignore the diffusion term we have

$$m^*(x, t) = A\exp(-i\gamma \mathbf{G}\cdot \mathbf{x}t). \quad \text{(C1.7)}$$

By assuming that the diffusion term can be accounted for by making A depend upon t and substituting Eq. (C1.7) into Eq. (C1.6), we find

$$\partial[A(t)]/\partial t = -AD\gamma^2 G^2 t^2. \quad \text{(C1.8)}$$

Thus $A(t) = A(0)\exp(-D\gamma^2 G^2 t^3/3)$ and Eq. (C1.7) becomes

$$m^*(x, t) = A(0)\exp(-i\mathbf{G}\cdot \mathbf{x}t)\exp(-\tfrac{1}{3}D\gamma^2 G^2 t^3). \quad \text{(C1.9)}$$

Combining Eq. (C1.9) with Eq. (C1.5) leads to

$$m_\perp(\mathbf{x}, t) = A(0)\exp[-i\gamma H_0(\mathbf{x})t]$$
$$\times \exp[-(t/T_2)]\exp[-(D\gamma^2 G^2 t^3/3)]. \quad \text{(C1.10)}$$

The transverse magnetization given by Eq. (C1.10) at $\mathbf{x}$ and time t: (1) precesses at the local Larmor frequency, $\omega_0(\mathbf{x}) = \gamma H_0(\mathbf{x})$; (2) is damped by the particle motion coupling to $m_\perp$ through $\mathcal{K}_d$ as manifested in T_2; and (3) is damped by the spin diffusion which carries particles in the external field gradient. It is the last term, (3), which we want to understand. Assume that the external field gradient is along the $\mathbf{x}$ axis, $H_0(\mathbf{x})_z = H_0 + gx$. Then, in the absence of the diffusion process, the spins at $z = +a$ precess more rapidly than those at $z = -a$ by $\Delta\omega = 2\gamma Ga$. An x-dependent gradient in the transverse magnetization builds up, and when D is turned on the particles are driven in the x direction by the gradient. See Fig. 5. As time evolves, the y com-

ponent to the magnetization builds up as x and t increase, so that

$$M_y \propto \cos(\gamma Gxt) \quad \text{(C1.11)}$$

and the gradient which drives the magnetization increases,

$$\nabla^2 m_y = (d^2/dx^2)m_y = D(\gamma Gt)^2 m_y. \quad \text{(C1.12)}$$

Thus we have

$$\partial m_y/\partial t = D(\gamma Gt)^2 m_y \quad \text{(C1.13)}$$

and

$$m_y(t) \propto \exp[-(D\gamma^2 G^2 t^3/3)]. \quad \text{(C1.14)}$$

We have repeated the above calculation, Eqs. (C1.4–C1.10) in this way to emphasize the source of the dependence of the decay of transverse magnetization on t and G. As t increases, the magnetization gradient which drives the spins increases, $\nabla m_y = \gamma Gtm_y$. It is the time dependence of the gradient that appears in Eq. (C1.10) and leads to t^3 in the decay process.

D_E; Energy Diffusion. Consider the equation of motion for M_z, Eq. (C1.3). M_z is not coupled to $M_\perp$, but through the T_1 term M_z is coupled to the particle motion excitations in the system. Since, $M_z \propto \beta_Z$, we write Eq. (C1.1) in the form

$$\dot{\beta}_Z = +D_Z\nabla^2 \beta_Z - T_{Z1}^{-1}(\beta_Z - \beta_1). \quad \text{(C1.15)}$$

The second term in this equation couples β_Z to the temperature of the 1-system. The particle motion excitations that constitute the 1-system can diffuse. Thus β_1 obeys the equation of motion

$$\dot{\beta}_1 = D_1\nabla^2 \beta_1 + T_{1Z}^{-1}(k_Z/k_1)(\beta_Z - \beta_1). \quad \text{(C1.16)}$$

We look at the solution of Eqs. (C1.15) and (C1.16) when $T_{Z1} \to 0$. In this circumstance, the Zeeman system and the 1-system come rapidly to mutual equilibrium, $\beta_1 = \beta_Z$. Using Eq. (C1.16) in Eq. (C1.15), we have

$$\dot{\beta}_Z + (k_1/k_Z)\dot{\beta}_1 = D_Z\nabla^2 \beta_Z + (k_1/k_Z)\nabla^2 \beta_1. \quad \text{(C1.17)}$$

But since $\beta_1 = \beta_Z$ and $\dot{\beta}_1 = \dot{\beta}_Z$, we find

$$\dot{\beta}_Z = [(k_Z D_Z + k_1 D_1)/(k_Z + k_1)]\nabla^2 \beta_Z. \quad \text{(C1.18)}$$

Thus the z component of the magnetization diffuses in space with a diffusion constant D_E, called the *energy diffusion constant*, given by

$$D_E = (k_Z D_Z + k_1 D_1)/(k_Z + k_1). \quad \text{(C1.19)}$$

This result is easily understood. The energy in the system is transferred rapidly from the Zeeman system to the 1-system by T_{Z1}^{-1}. Thus the energy spends the fraction of its time $k_Z/(k_Z + k_1)$ in the Zeeman system where it moves with diffusion constant D_Z and the fraction of its time $k_1/(k_Z + k_1)$ in the 1-system where it moves with diffusion constant D_1.

C.2 Diffusion Constants

There are three particle motion excitations in solid ^{3}He which can carry energy by diffusive motion. These are the ^{3}He atoms, the vacancy waves, and the mass fluctuation waves. Here we estimate the diffusion constant for each of these excitations and discuss the dependence of the rate of energy diffusion on the topology of the energy baths.

$D_Z(3, 3)$; *Magnetization Diffusion due to Tunneling.* The diffusion constant for magnetization, D_Z, appears in both the motion of $M_\perp$ and M_z. D_Z is given by

$$D_Z(3, 3) = A_Z(3, 3)\Delta^2 J, \qquad (C1.20)$$

where Δ is the near neighbor distance, J is the tunneling frequency, and $A_Z(3, 3)$ is a constant of order 1. A calculation of D_Z from first principles requires first that a formal expression for D_Z be obtained. This is accomplished by placing the system in an external field and computing the response of the magnetization to the field. The magnetization diffusion constant has been calculated by several workers (Redfield and Yu, 1968, 1969). The results of these calculations are all similar and give

$$A_Z(3, 3) = 4.2/2\pi. \qquad (C1.21)$$

$D_Z(V, 3)$; *Magnetization Diffusion due to Vacancies.* At high temperature, the motion of a ^{3}He particle through the medium it is in is due to the presence of vacancies as near neighbors of the particle. The diffusion constant is

$$D_Z(V, 3) = A_Z(V, 3)\Delta^2\omega_3(V, 3), \qquad (C1.22)$$

where $\omega_3(V, 3)$ is the rate at which a ^{3}He particle tunnels into a neighboring vacancy site in a ^{3}He medium. For a ^{3}He particle in a ^{4}He medium, we have

$$D_Z(V, 4) = A_Z(V, 4)\Delta^2\omega_3(V, 4). \qquad (C1.23)$$

The constants $A_Z(V, 3)$ and $A_Z(V, 4)$ are of order 1.

$D_T(3, 3)$; *Energy Diffusion due to Tunneling.* The magnetization diffuses with magnetization diffusion constant D_Z in response to an external field perturbation because of the tunneling motion of the particles. The energy in the tunneling system also diffuses because of the tunneling motion of the particles. We define the *tunneling diffusion constant* to be the diffusion constant that measures the response of the *energy* of the tunneling system to an external perturbation. The tunneling diffusion constant is

$$D_T(3, 3) = A_T(3, 3)\Delta^2 J, \qquad (C1.24)$$

where $A_T(3, 3)$ is of order 1. Redfield and Yu (1968, 1969) have calculated $A_T(3, 3)$ and found $A_T(3, 3) \simeq A_Z(3, 3)$. Thus we have $D_Z \approx D_T$. This theoretical result disagrees with the results of two experiments. See the discussion in Sec. 6.

$D_V(3, 3)$ *and* $D_V(4, 4)$; *Diffusion of Vacancies.* A

suitable linear combination of vacancy waves will describe a localized propagating vacancy state. If this localized vacancy is in solid ^{4}He, it sees the medium it is in as an inert background. It interacts only with other localized vacancies. The mean free path for vacancy–vacancy scattering is

$$\lambda_{VV} = V/\sigma x_V, \qquad (C1.25)$$

where V is the molar volume, σ is the vacancy–vacancy cross section, $\sigma \approx \Delta^2$, and x_V is the vacancy concentration. For the vacancy diffusion constant we have

$$D_V(4, 4) = [A_V(4, 4)/S_V\lambda_{VV}], \qquad (C1.26)$$

where $A_V(4, 4)$ is of order 1, and S_V is the vacancy velocity. We estimate S_V to be

$$S_V = \omega_V(4, 4)\Delta, \qquad (C1.27)$$

where $\omega_V(4, 4)$ is the frequency for tunneling of the ^{4}He neighbor of a vacancy site into the vacancy site. Using $V/N = \Delta^3$, $\sigma \approx \Delta^2$ and Eqs. (C1.25, 26, 27), we have

$$D_V(4, 4) \approx A_V(4, 4)[\Delta^2\omega_V(4, 4)/x_V]. \qquad (C1.28)$$

If the localized vacancy is in solid ^{3}He, it does not see the medium it is in as an inert background. The vacancy in moving through the ^{3}He medium must disarrange the spins. It has a diffusion constant given by

$$D_V(3, 3) = A_V(3, 3)\Delta^2\omega_V(3, 3). \qquad (C1.29)$$

The physical situation is exactly analogous to that of a hole in a magnetic insulator. This latter problem has been dealt with by Brinkman and Rice (1970).

Note $D_V(4, 4)$ and $D_V(3, 3)$ differ by orders of magnitude. The vacancy diffusion coefficients $D_V(3, 3)$ and $D_V(4, 4)$ are not directly observable in NMR experiments. Such experiments see the motion of ^{3}He atoms. These diffusion constants are observable in a light scattering experiment.

$D_4(3, 3)$ *and* $D_3(4, 4)$; *Diffusion of Mass Fluctuation Waves.* For a ^{4}He particle in a ^{3}He medium, the diffusion constant is

$$D_4(3, 3) = A_4(3, 3)[\Delta^2\omega_4(3, 3)/x_3], \qquad (C1.30)$$

where $\omega_4(3, 3)$ is the rate of tunneling of a 3, 4 pair in a ^{3}He medium. For a ^{3}He particle in a ^{4}He medium, the diffusion constant is

$$D_3(4, 4) = A_3(4, 4)\Delta^2\omega_4(3, 3), \qquad (C1.31)$$

where $\omega_3(4, 4)$ is the rate of tunneling of a 3, 4 pair in a ^{4}He medium. $D_3(4, 4)$ and $D_4(3, 3)$ are analogous to $D_V(4, 4)$ and $D_V(3, 3)$, respectively as far as their dependence on the medium is concerned.

APPENDIX D. SPECIFIC HEATS, Etc.

In this Appendix we tabulate the specific heats and the constants k_n which enter the calculations of the relaxation times for the various baths.

D.1 Zeeman System

$$\mathcal{H}_Z = -\mathbf{H}_0 \cdot \sum_R \mathbf{u}_R. \qquad (D1.1)$$

At $k_B T \gg \hbar\omega_0$ the energy of the Zeeman system is

$$E_Z = -(N/4)[\hbar\omega_0/k_B T]^2, \qquad (D1.2)$$

where $\omega_0 = \gamma H_0$ is the Zeeman frequency; the specific heat of the Zeeman system is

$$C_Z = k_B(N/4)[\hbar\omega_0/k_B T]^2, \qquad (D1.3)$$

the energy constant k_Z is

$$k_Z = -(N/4)[(\hbar\omega_0)^2]. \qquad (D1.4)$$

D.2 Tunneling System

$$\mathcal{H}_T = -\hbar J \sum_{RR'} \sigma_R \cdot \sigma_{R'}. \qquad (D1.5)$$

At $k_B T \gg \hbar J$, the energy of the tunneling system is

$$E_T = -\tfrac{3}{8} Nz[(\hbar J^2) k_B T]; \qquad (D1.6)$$

the specific heat is

$$C_T = \tfrac{3}{8} N k_B z[\hbar J/k_B T)^2]; \qquad (D1.7)$$

the energy constant k_T is

$$k_T = -\tfrac{3}{8}(Nz/k_B)(\hbar J)^2. \qquad (D1.8)$$

D.3 Vacancy Excitations

$$\mathcal{H}_V = \sum_k \epsilon(k) C_k^+ C_k, \qquad (D1.9)$$

where $\epsilon_V(k) = \phi_0 + zt \cos k\Delta$ from Eq. (15). Experimental temperatures are much less than ϕ_0 or the bandwidth $2zt \approx 6K$. Thus the energy of the vacancies is

$$E_V = (\phi_0 + \tfrac{3}{2} k_B T) n_V, \qquad (D1.10)$$

where $n_V = \exp(-\beta\phi)$ is the number of vacancies; here ϕ is the experimentally observed vacancy excitation temperature, $\phi \approx \phi_0 - zt$. The specific heat of the vacancies is

$$C_V = dE_V/dt \approx k_B(\phi/T)^2 n_V. \qquad (D1.11)$$

The energy constant of the vacancies calculated at constant vacancy number, n_V, is

$$k_V = (dE_V/d\beta)_{n_V} = -\tfrac{3}{2}(k_B T)^2 n_V. \qquad (D1.12)$$

D.4 Mass Fluctuation Wave System

$$\mathcal{H}_{MF} = \sum_k \epsilon_{MF}(k) d_k^+ d_k, \qquad (D1.13)$$

where $\epsilon_{MF}(k) = 2z\hbar\omega_{34}(3,3)(1 - \cos k\Delta)$. The energy of the ^{4}He system is (for $z = 8$)

$$E_{MF} = (14/3) z \tfrac{3}{8} N\{[\hbar\omega_{34}(3)]^2/k_B T\} \qquad (D1.14)$$

the specific heat is

$$C_{MF} = [(14/3)z]\tfrac{3}{8} N z k_B[\hbar\omega_3(4,3)/k_B T]; \qquad (D1.15)$$

the constant k_{MF} is

$$k_{MF} = -(14/3)z\tfrac{3}{8}Nz[\hbar\omega_3(4,3)]^2. \qquad (D1.16)$$

D.5 Phonon System

$$\mathcal{H}_P = \sum_k \hbar\omega(k)[n(k) + \tfrac{3}{2}], \qquad (D1.17)$$

where the $\omega(k)$ are the phonon frequencies. The energy of the phonon system is given by

$$E_P = (3\pi^4/5)(N/V)k_B T(T/\theta_D)^3, \qquad (D1.18)$$

where θ_D is taken to be the experimentally observed Debye temperature. The specific heat of the phonon system is

$$C_P = (12\pi^4/5)(N/V)k_B(T/\theta_D)^3 \qquad (D1.19)$$

and the energy constant is

$$k_P = dE_P/d\beta = -5(E_P/\beta) = 3\pi^4(N/V)(k_B T)^2(T/\theta_D)^3. \qquad (D1.20)$$

REFERENCES

Abragam, A., 1961, "The Principles of Nuclear Magnetism" (Oxford U. P. Oxford, England).

Ackerman, C. C., and R. A. Guyer, 1968, Ann. of Phys. **50**, 128.

Adams, E. D., M. F. Panczyk, R. A. Scribner, and J. R. Gonano, 1968, Eleventh Intern. Conf. on Low Temp. Phys. **1**, 413.

Anderson, A. C., W. Reese, and J. C. Wheatley, 1962, Phys. Rev. **127**, 671.

Anderson, P. W., 1963, *Concepts in Solids*, (Benjamin, New York).

Andreev, A. F., and L. M. Lifshitz, 1969, Zh. Eksp. Teor. Fiz. **56**, 2057 [Sov. Phys.—JETP **29**, 1107].

Baker, G., H. E. Gilbert, J. Eve, and G. S. Rushbrooke, 1967, Phys. Rev. **164**, 800.

Balakrishnan, R., and R. V. Lange, 1971, Phys. Rev. **3A**, 496.

Bitter, F., 1931, Phys. Rev. **39**, 1540.

Bernier, M., 1970a, Solid State Comm. **8**, 2151.

——, 1970b, J. of Low Temp. Phys. **3**, 29.

——, and A. Landesman, 1969, Solid State Comm. **7**, 529.

Brenig, W., 1963, Z. Physik **171**, 60.

Brinkman, Wm., and M. Rice, 1970, Phys. Rev. B, **1**, 1324.

Brueckner, K. A., and J. Froberg, 1965, Prog. Theoret. Phys. (Kyoto) Suppl.

——, and R. Thieberger, 1969, Phys. Rev. **178**, 362.

Carruthers, P. C., 1961, Rev. Mod. Phys. **33**, 92.

Chester, G. V., 1970, Phys. Rev. A, **2**, 256.

deWette, F. W., L. H. Nosanow, and N. R. Werthamer, 1967, Phys. Rev. **162**, 824.

Edwards, D. O., A. S. McWilliams, and J. G. Daunt, 1962, Phys. Letters **8**, 195.

——, and R. C. Pandorf, 1965, Phys. Rev. **140**, A816.

——, and R. C. Pandorf, 1966, Phys. Rev. **144**, 143.

——, and R. C. Pandorf, 1968, Phys. Rev. **169**, 222.

Fernandez, J. F., and H. A. Gersch, 1966, Phys. Rev. **149**, 514.

Fredkin, D. R., and N. R. Werthamer, 1965, Phys. Rev. **138**, A1527.

Garwin, R. L., and H. A. Reich, 1964a, Phys. Rev. Letters **12**, 354.

——, and A. Landesman, 1964b, Phys. Rev. **133**, A1503.

——, and A. Landesman, 1965, Physics **2**, 107.

Giffard, R. P., 1968a, thesis, Oxford University.

——, 1968b, remarks made at *LT*-11, St. Andrews (unpublished).

——, and J. Hatton, 1967, Phys. Rev. Letters **18**, 1106.

——, J. Hatton, and W. Truscott, 1971, J. Low Temp. Phys. **4**, 153.

Gillis, N. S., T. R. Koehler, and N. R. Werthamer, 1968, Phys. Rev. **175**, 1110.

Glyde, H. R., 1969, Phys. Rev. **177**, 202.

Goodkind, J. M., and W. M. Fairbank, 1960a, Phys. Rev. Letters, 4, 458.

Goodkind, J., and W. M. Fairbank, 1960b, Helium Three, J. G. Daunt, editor, Ohio Univ. Press, Columbus Ohio.

Grilly, E. R., and R. L. Mills, 1959, Ann. Phys. (NY) 8, 1.

Guyer, R. A., 1968a, Phys. Letters 27a, 452.

——, 1968b, Solid State Comm. 7, 315.

——, 1969, Solid State Physics 23, 412.

——, and L. I. Zane, 1969, Phys. Rev. 188, 445.

——, and L. I. Zane, 1970, Phys. Rev. Letters 24, 660.

Hansen, J. P., and D. Levesque, 1968, Phys. Rev. 165, 293.

Harris, A. B., 1971 (to be published).

Hartmann, S. R., 1964, Phys. Rev. 133, A17.

Herring, C., 1966, Magnetism IV, edited by Rado and Suhl, (Academic, New York).

Hetherington, J. H., 1968, Phys. Rev. 176, 231.

——, W. J. Mullin, and J. H. Nosanow, 1967, Phys. Rev. 154, 175.

Hoerner, H., 1967, Z. Physik 205, 72.

Hogan, N. R., R. A. Guyer, and H. A. Fairbank, 1969, Phys. Rev. 185, 356.

Homer, J. M., and M. G. Richards, 1969a, Phys. Rev. Letters 22, 273.

——, and M. G. Richards, 1969b, Phys. Rev. 182, 318

Hunt, E. R., R. C. Richardson, J. R. Thompson, R. A. Guyer, and H. Meyer, 1967, Phys. Rev. 163, 181.

——, and J. R. Thompson, 1968, Phys. Rev. Letters 20, 249.

Iwanoto, F., and H. Hamaizawa, 1966, to Prog. Theor. Phys. 37/38, 234.

Koehler, T. R., 1966, Phys. Rev. Letters 17, 89.

——, 1967, Phys. Rev. Letters, 18, 654.

Kirk, W. P., E. B. Osgood, and M. C. Garber, 1969, Phys. Rev. Letters 23, 833.

Krumhansl, J. A., and S. Y. Wu, 1968, Phys. Letters 28A, 263.

Kubo, R., and K. Tomita, 1954, J. Phys. Soc. Japan 9, 888.

Landesman, A., and Bernier, M. (1971) J. Low Temp. Phys. (to be published).

Leggett, A. J., 1970, Phys. Rev. Letters, 25, 1543.

McMahan, A. K., and L. H. Nosanow, 1970, preprint.

Meyer, H., 1968, J. Appl. Phys. 39, 390.

Mills, R. L., E. R. Grilly, and S. G. Sydoriak, 1961, Ann. Phys. (N.Y.) 12, 41.

Miyoshi, D. S., R. M. Cotts, A. S. Greenberg, and R. C. Richardson, 1970a, Phys. Rev. A 2, 870.

——, R. M. Cotts, A. S. Greenberg, and R. C. Richardson, 1970b, unpublished.

Mueller, K. H., 1970, Duke University, private communication.

Mullin, W. J., 1971, Phys. Rev. Letters, 26, 611.

——, 1968, Phys. Rev. Letters 20, 254.

Nosanow, L. H., 1966, Phys. Rev. 146, 120.

——, and C. M. Varma, 1968, Phys. Rev. Letters 20, 912.

——, and N. R. Werthamer, 1965, Phys. Rev. Letters, 15, 618.

Panczyk, M. F., R. A. Scribner, J. R. Gonano, and E. D. Adams, 1968, Phys. Rev. Letters 21, 594.

——, R. A. Scribner, G. C. Straty, and E. D. Adams, 1967, Phys. Rev. Letters, 19, 1102.

——, and E. D. Adams, 1969, Phys. Rev. 187, 321.

Pipes, B., and W. M. Fairbank, 1969, Phys. Rev. Letters, 23, 520.

Pollack, G. L., 1969, Rev. Mod. Phys. 41, 48.

Redfield, A., and W. N. Yu, 1968, Phys. Rev. 169, 443.

——, and W. N. Yu, 1969, Phys. Rev. 177, 1018.

Reich, H. A., and W. N. Yu, 1963, Phys. Rev. 129, 630.

——, 1969, Solid State Comm. 7, 529.

Richards, M. G., J. Hatton, and R. Giffard, 1965, Phys. Rev. 139, A19.

——, 1970, Advan. Mag. Res. 5.

Richards, P. M., 1965, Phys. Rev. 137, A1327.

Richardson, R. C., E. Hunt, and H. Meyer, 1965, Phys. Rev. 138, A1326.

——, A. Landesman, E. R. Hunt, and H. Meyer, 1966, Phys. Rev. 146, 244.

Sample, H. H., and C. A. Swenson, 1967, Phys. Rev. 158, 188.

Sarkissian, B., 1969, thesis, Duke University (unpublished).

Scribner, R. A., M. F. Panczyk, and E. D. Adams, 1969, J. Low Temp. Phys. 1, 313.

Schuck, A. F., and R. L. Mills, 1961, Phys. Rev. Letters 6, 596.

Senghaphan, W., and G. O. Zimmerman, 1968, Phys. Rev. Letters, 20, 371.

Sites, J., D. Osheroff, R. C. Richardson, and D. M. Lee, 1969, Phys. Rev. Letters. 23, 835.

Slichter, C. P., 1963, Principles of Magnetic Resonance (Harper, New York).

Straty, G. C., and E. D. Adams, 1966, Phys. Rev. 150, 123.

——, and E. D. Adams, 1968, Phys. Rev. 169, 232.

Tedrow, P. M., and D. M. Lee, 1969, Phys. Rev. 187, 398; and 181, 399.

Thompson, J. R., E. R. Hunt, and H. Meyer, 1967, Phys. Letters 25A, 313.

Thouless, D. J., 1965, Proc. Phys. Soc. 86, 893.

Van Vleck, J. H., 1948, Phys. Rev. 74, 1168.

Varma, C. M., 1969, Phys. Rev. Letters, 23, 778.

Werthamer, N. R., 1969, Am. J. Physics, 37, 763.

Zane, L. I., 1970, thesis, Duke University (unpublished).